Automotive Cooling Systems based on Metal Hydrides

A thesis accepted by the Faculty of Energy Technology, Process Engineering and Biological Engineering of the University of Stuttgart in partial fulfillment of the requirements for the degree of Doctor of Engineering Sciences (Dr.-Ing.)

by

Marc Linder

born in Ulm

Main referee:	Prof. Dr.-Ing. habil. Eckart Laurien
Co-referee:	Prof. Dr.-Ing. habil. Hans Müller-Steinhagen
Date of defense:	July 9th, 2010

Institute of Nuclear Technology and Energy Systems

University of Stuttgart

2010

Acknowledgement

Herewith, I would like to thank all colleagues and students of the Institute of Nuclear Technology and Energy Systems at the University of Stuttgart that have contributed to this work. I am especially grateful to Prof. Dr.-Ing. Eckart Laurien, Dr.-Ing. Rudi Kulenovic, Dr.-Ing. Patrick Schäfer, Dr.-Ing. Rainer Mertz and Ms. Jacqueline Edwards for their great assistance in their respective fields.

However, I owe my deepest gratitude to my family and to Marie-Louise Lemloh whose continuous support made this thesis possible.

Marc Linder

Abstract

The present work focuses on metal hydride sorption systems as an alternative technology for automotive air-conditioning systems. Although this technology offers the possibility to increase the energy efficiency of a car (by utilising waste heat) and consequently reduces the CO_2 emissions, its weight specific cooling power has so far been the main obstacle for an automotive application. Based on investigations of various metal hydrides, two alloys ($LmNi_{4.91}Sn_{0.15}$ and $Ti_{0.99}Zr_{0.01}V_{0.43}Fe_{0.09}Cr_{0.05}Mn_{1.5}$) were chosen for further investigations on different laboratory test benches. A capillary tube bundle reaction bed was applied due to its large heat transfer surface and consequently expected short cycle times. The experimental investigations were carried out systematically starting with material characterisation of each individual metal hydride (Pressure-concentration isotherm measurements, intrinsic absorption/desorption kinetics), followed by the measurement of individual reaction bed dynamics (for both alloys) and the analysis of the coupled metal hydrides (sorption system).

One important result obtained from the measurements of individual reaction bed dynamics is the limitation of the fast metal hydride sorption system due to slow intrinsic desorption kinetics of the alloy working at low temperatures (cooling temperature). Therefore, the very fast AB_2-type alloy ($Ti_{0.99}Zr_{0.01}V_{0.43}Fe_{0.09}Cr_{0.05}Mn_{1.5}$) was applied at the high-pressure side (low temperatures) which allows half-cycle times of the sorption system in the range of 100 to 120 s. The corresponding specific cooling power of the sorption system is therefore around 640 W/kg related to the desorbing alloy. In comparison to the state of the art metal hydride based cooling system, the specific power of the sorption system is more than tripled which leads to a clearly reduced necessary mass of metal hydride.

Based on the experimental investigations, two different metal hydride sorption systems for automotive cooling were investigated: The thermally driven sorption system (closed system) and an open system for hydrogen-fueled cars that is conceptually proposed in this work. This new metal hydride sorption system utilizes the hydrogen pressure difference between a high-pressure storage tank and the fuel cell or combustion engine. Its main advantage in comparison to the closed sorption system is the clearly reduced system complexity that is especially necessary for automotive cooling.

Kurzfassung

Die vorliegende Arbeit untersucht Metallhydrid-Sorptionssysteme als eine Alternative zu konventionellen Fahrzeug-Klimaanlagen. Mit Hilfe dieser Technologie ist sowohl eine Effizienzsteigerung des Fahrzeugs als auch eine damit einhergehende Reduzierung der CO_2-Emissionen möglich (durch Nutzung der Abwärme). Bisher ist allerdings die gewichtsspezifische Leistung der maßgebliche Hinderungsgrund für eine Anwendung im Fahrzeugbereich. Anhand der Untersuchung zahlreicher Metallhydride wurden zwei Legierungen ($LmNi_{4.91}Sn_{0.15}$ und $Ti_{0.99}Zr_{0.01}V_{0.43}Fe_{0.09}Cr_{0.05}Mn_{1.5}$) für weitergehende Experimente an verschiedenen Teststänlden im Labor ausgewählt. Auf Grund der großen Wärmeübertragungsoberfläche und der damit verbundenen erwarteten kurzen Zykluszeit wurde ein Kapillarrohrbündel-Reaktionsbett verwendet. In systematischen, experimentellen Untersuchungen wurden zunächst die Materialeigenschaften beider Metallhydride getrennt voneinander bestimmt (Konzentrations-Druck Isothermen, intrinsische Absorptions- und Desorptionskinetik), gefolgt von Messungen der Reaktionsdynamik des einzelnen Reaktionsbetts (für beide Legierungen) und der Untersuchung von gekoppelten Metallhydriden (Sorptionssystem).

Ein wichtiges Ergebnis der Dynamikmessungen mit einzelnen Reaktionsbetten ist die Leistungsbeschränkung des schnellen Sorptionssystems auf Grund der langsamen intrinsischen Desorptionskinetik der Legierung bei tiefen Temperaturen (Kühltemperatur). Daher wurde die sehr schnelle AB_2-Legierung ($Ti_{0.99}Zr_{0.01}V_{0.43}Fe_{0.09}Cr_{0.05}Mn_{1.5}$) auf der Hochdruckseite (tiefe Temperaturen) verwendet, was eine Halbzykluszeit des Sorptionssystems in der Größenordnung von 100 bis 120 s ermöglichte. Die entsprechende spezifische Kühlleistung beträgt damit ca. 640 W/kg bezogen auf das desorbierende Metallhydrid. Im Vergleich zum aktuellen Stand der Technik der Metallhydrid-Sorptionssysteme konnte die spezifische Leistung des Systems damit mehr als verdreifacht werden, wodurch sich die benötigte Masse an Metallhydrid deutlich reduziert.

Anhand der experimentellen Untersuchungen wurden zwei unterschiedliche Metallhydrid-Sorptionssysteme zur Fahrzeugkühlung untersucht: Das thermisch betriebene Sorptionssystem (geschlossenes System) sowie ein offenes System für wasserstoffbetriebene Fahrzeuge, das konzeptionell in dieser Arbeit vorgeschlagen wird. Dieses neue System nutzt die Wasserstoffdruckdifferenz zwischen einem Hochdruckspeicher und der Brennstoffzelle oder einem Verbrennungsmotor. Der größte Vorteil im Vergleich zu dem geschlossenen Sorptionssystem liegt in einem deutlich einfacheren Aufbau, der gerade für eine Anwendung im Automobilbereich notwendig ist.

Contents

Nomenclature, abbreviations and indices

Nomenclature

A	Reaction bed surface	m^2
c_p	Specific heat capacity	J/(kg K)
C_a	Kinetics constant (material dependent)	1/s
d	Diameter	m
D_{eff}	Effective diffusion coefficient	
E_a	Activation energy	kJ/mol
f_{Hys}	Hysteresis factor	-
f(t)	Exponential function (reacted fraction)	%
g(t)	Exponential function (heat transfer)	-
G	Molar free enthalpy	J/mol
h(t)	Exponential function (coupled reaction beds)	-
Δh	Specific enthalpy	J/kg
ΔH	Molar enthalpy of reaction	J/mol
K	Permeability	m^2
l	Length of capillary tubes	m
m	Mass	kg
m_{Pl}	Plateau factor	-
n_{H2}	Exchanged hydrogen	mol
p	Pressure	bar
p^0	Standard pressure (1.013)	bar
P	Power	W
P_{spec}	Specific power	W/kg
P_{char}	Characteristic power	W/kg
Q	Heat	J
r	Radius	m

R	Universal gas constant (8.314)	J/(mol K)
R_c	Ratio of the generated cooling effect	-
ΔS	Molar entropy of reaction	J/(mol K)
ΔT	Temperature difference	K
$t_{half\text{-}cycle}$	Half-cycle time	s
T	Temperature	K, °C
v	Flow velocity	
$\dot{V}$	Water flow rate	l/min
x	Hydrogen uptake/storage capacity	%
Z(p,T)	Real gas factor	-

Greek letters

α	Solution phase of hydrogen in metal	-
β	Hydride phase	-
ϵ	Porosity	-
η_{FC}	Efficiency of the fuel cell	-
λ_{eff}	Effective thermal conductivity	W/(m K)
ρ	Density	kg/m^3
τ	Characteristic time	
ϕ	Reaction rate	$kg/(m^3 s)$
φ	Hydrogen flow rate	mol/min

Abbreviations

A	High-pressure alloy in sorption systems/ Strong hydride former
B	Low-pressure alloy in sorption systems/ Weak hydride former
CHP	Combined heat and power generation
EMV	Electromagnetic valve
F.S.	Full scale
IKE	Institut für Kernenergetik und Energiesysteme
LHV	Lower heating value
Lm	Lanthanum-rich misch metal
Me	Metal
MeH	Metal hydride
MFC	Mass flow controller
MFM	Mass flow meter
PCI	Pressure-concentration isotherm
PnV	Pneumatically actuated valve
RB	Reaction bed
V	Valve
VCR	Connection type with gasket

Indices

^{0}	At standard pressure (1.013 bar)
Abs	Absorption
Amb	Ambient temperature
coupled	Coupled reaction beds
cr	Critical
Cool	Cooling temperature
Des	Desorption
dyn	Reaction bed dynamics

eff	Effective
eq	Equilibrium
g	Gas phase
H_2	Hydrogen
Heat	Heating temperature
ht	Heat transfer process
Hys	Hysteresis
in	Inlet
intr	Intrinsic reaction kinetics
mid	Middle of plateau region
norm	Normalized value
out	Outlet
pl	Plateau
s	Solid
sat	Saturated
water	Water side

1 Introduction

1.1 Motivation

Constantly increasing prices for energy supply on the one hand and expected global warming due to carbon dioxide emissions on the other hand, are heavily discussed issues about our future energy system and its economic and ecologic price. The constant economic growth of industrial and especially of developing countries combined with the fast increasing population in these areas are crucial facts that increase the necessity for a rational use of all available forms of energy.

Beside the special part of the renewable energies in their respective field, energy efficiency is seen as an additional important path on the way to a sustainable and payable future energy supply. The ratio of useful energy output to total energy input gives an idea of the energy efficiency of the respective conversion technology. Scaling this up to a national energy economy, the total energy demand can be reduced if the over-all energy efficiency is growing faster than the energy consumption, e.g. due to a growing economy or population. Therefore, increased energy efficiency could tackle national emission or consumption targets without fearing the loss or reduction of living and comfort standards.

The energy efficiency value is highly depending on the useful energy output. In CHP (combined heat and power generation) systems, unavoidable waste heat is used, e.g. in heating systems. Depending on the technology, waste heat recovery might demand an increase of the waste heat temperature that reduces the power output [1]. Even if the waste heat recovery is not affecting the power output, the overall efficiency of the CHP system is only higher than the efficiency of the stand-alone power generation system as long as the recovered waste heat is useful (e.g. in winter time). The same holds true for the energy conversion in automotive internal combustion engines (see Figure 1-1). In this case, released heat is around 68 % of the total energy input; only 32 % is available for mechanical propulsion [2].

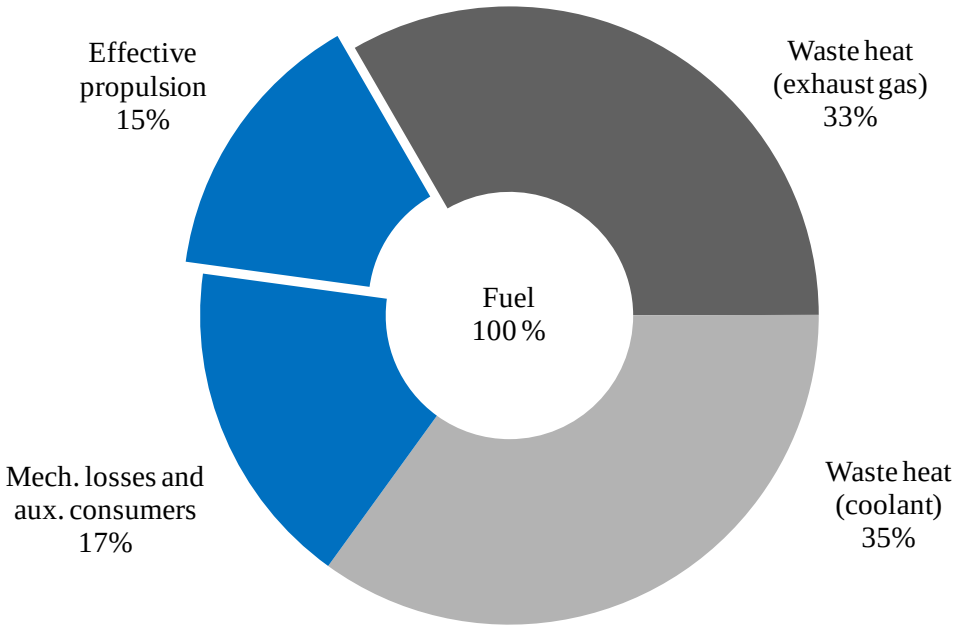

Figure 1-1: Energy distribution of internal combustion engine (driving speed: 80 km/h) [2]

However, as soon as heating of the cabin is required, the waste heat (coolant) turns into useful energy and the overall efficiency is increased. If a more effective engine is not able to achieve the necessary thermal comfort level, additional heating measures must provide the missing thermal power [3]. Consequently, the overall efficiency of the car depends on the boundary conditions, e.g. ambient temperature.

The European research project TOPMACS [4] that targeted to extend the CHP period of automotive combustion engines, gave the background for this work. The aim of the project was the development and built-up of **T**hermally **Op**erated **M**obile **A**ir-**C**onditioning **S**ystems in order to use the engines' waste heat as main driving energy source for the refrigeration system.

The state of the art mobile air-conditioning system is a vapor compression system, where the evaporation of a refrigerant generates the cooling effect. After a mechanically driven compression of the refrigerant vapor, a condensation at ambient temperature is possible and heat absorbed during evaporation is released to the ambient. A reduction of the refrigerant pressure by means of an expansion valve completes the refrigeration cycle.

Although this mature technology offers high cooling performance with reasonable weight and volume constraints, two main drawbacks cannot be neglected:

1. The compression of refrigerant vapor demands mechanical energy from the engine and consequently increases the overall fuel consumption along with the corresponding CO_2 emissions of the vehicle. According to Onanda *et al.* [5], mobile air conditioning systems (when in use) are responsible for around 15 % of the fuel used by modern cars. This value can even rise up to 30 %, depending on the vehicle and driving conditions (e.g. during congestion).
2. Even during regular operation, the state of the art mobile air conditioning system is not fully leak-tight. Taking the losses of refrigerant during maintenance and at the end of the vehicle's lifetime into account, the minimum yearly refrigerant emissions are in the order of 90 g or 10-15 % of the initial charge [6]. Due to the high global warming potential (GWP=1300) of the state of the art refrigerant (R134a), this value corresponds to around 10 g/km equivalent CO_2 emissions for a vehicle traveling 12,000 km/year.

Therefore, due to the climate-damaging effect of the current refrigerant on the one hand and the increased fuel consumption of the vehicle on the other hand, new, innovative solutions for mobile air conditioning systems are necessary.

The metal hydride sorption technology has so far been investigated for different applications like stationary heat pumps, cooling systems or heat transformers. However, the interesting application as thermally driven cooling system for cars could not have been seriously taken into account as the specific power of the state of the art metal hydride sorption system was clearly too low (~ 170 W/kg related to the desorbing metal hydride). Therefore, in this work a new combination of capillary tube bundle reaction bed and metal hydride working pair was utilized to investigate the possibility of increasing the specific cooling power of this technology. The general operation principle of metal hydride based sorption system is a closed operation cycle that utilizes hydrogen as working fluid (comparable to R143a in conventional air-conditioning systems). The underlying principle is the thermally driven compression of the working fluid (hydrogen) and its reaction with the metal hydride at different pressures. This system was mainly investigated in the frame of the 'TOPMACS' project.

The utilisation of hydrogen as fuel for future vehicles and its storage in compressed state, offers the possibility to use the pressure difference between the hydrogen storage tank and the fuel cell or combustion engine (instead of the thermally driven compression) as main driving energy for an open metal hydride based cooling system. With this new proposed working principle, the potential energy (stored compression work) of the pressurized hydrogen storage tank can be re-used for onboard cooling to increase the overall efficiency of the vehicle. As the thermally driven compression of hydrogen is not necessary for the operation of this system, the amount of system components (e. g. heat exchangers, pumps, reaction beds) is drastically reduced in comparison to the closed sorption system.

1.2 Literature review

1.2.1 Metal hydrides

The chemical reaction of hydrogen and metal powder to form a metal hydride is given by the overall equation (1-1) where Me denotes any kind of metal or alloy able to absorb hydrogen (H_2), MeH the corresponding metal hydride and ΔH the enthalpy of the reaction. It can be regarded as a reversible process and according to the principle of *Le Chatelier-Braun*, a pressure increase shifts the equilibrium to the right (hydrogen is absorbed), whereas a temperature increase shifts it to the left [7, 8]. A release of hydrogen (desorption) from the metal hydride is therefore possible by either reducing the hydrogen pressure or increasing the temperature. As the hydrogen absorption is generally exothermic, the endothermic desorption tends to cool the metal powder.

$$Me + \frac{y}{2} H_2 + \Delta H \quad \leftrightarrow \quad MeH_y \qquad (\Delta H < 0) \tag{1-1}$$

The stability (dissociation pressure) of the metal hydride phase is one important issue for its applicability. Technically relevant pressure and temperature conditions of the metal-hydrogen reaction depend on the desired application but can be typically assumed as $p \approx 1 - 100$ bar and $T \approx 240 - 750$ K, respectively [7]. Pure, low electro-negative metals (so called A-metals, e.g. Li, Na, K, Cs, Mg, Ca, La Ti or Zr), form stable hydrides with either too high dissociation temperatures and/or too low equilibrium pressures. Therefore only a few, e.g. Mg (with a desorption pressure of 1 bar at around 300 °C), seem interesting for technical applications. More electro-negative metals (so called B-metals, e.g. Cu, Ni, Co, Fe, Mn, Cr, or Mo) do not form hydrides (very unstable) at technical relevant temperatures and pressures [9]. Since van Vucht *et al.* [10] published the possibility of alloying A- and B-metals to intermetallic compounds in order to produce alloys with practicable (intermediate) metal hydride phase stability, different A/B-metal combinations were investigated and lead to a variety of intermetallic compounds mostly belonging to one of the metal hydride types summarized in Table 1-1 [11].

Although the expression ‘metal hydride’ refers originally to the metal hydride phase of the reaction, it is generally simplified in literature and used for any alloy able to react with hydrogen forming a metal hydride phase.

Table 1-1: Classification of metal hydrides

Structure	Examples
A_2B	Zr_2Cu, Ti_2Pd, Mg_2Ni
AB	LaNi, MgNi, TiFe, ZrCo
AB_2	$TiMn_2$, $CaNi_2$, $GdCo_2$, $ZrMn_2$, $ZrCr_2$, $TiCr_2$
AB_5	$LaNi_5$, YCo_5, $EuNi_5$, $CaNi_5$, $LaCo_5$

The absorption and desorption characteristics of the metal hydride can be varied by partial substitution of alloy elements. Therefore, an adaptation of the metal hydride to the respective application is possible. In this work, the alloys $LmNi_{4.91}Sn_{0.15}$ (AB_5, based on $LaNi_5$ but non-stoichiometric) and $Ti_{0.99}Zr_{0.01}V_{0.43}Fe_{0.09}Cr_{0.05}Mn_{1.5}$ (AB_2, based on $TiMn_2$) are used.

Activation

As the density of the metal hydride is smaller than the density of the respective metal, a hydrogenation leads to stresses within the lattice and therefore to a smashing of the commonly brittle metal hydride bulk. During the first several ab- and desorption cycles (activation process), the particle size is enormously reduced and stabilizes generally in the order of 1 to 20 µm [12], depending on the metal hydride.

A smaller particle size offers two main advantages: The surface area is increased and the diffusion distance for dissolved hydrogen in the metal hydride bulk is decreased.

Pressure-Concentration Isotherms (PCI)

A commonly used method to characterize metal hydrides is the Pressure-Concentration Isotherm (PCI) measurement. Figure 1-2 shows a schematic PCI of a metal hydride that is exposed to an increasing hydrogen pressure under equilibrium conditions. The pressure (p, logarithmic scale, y-axis) of the system is shown versus the hydrogen uptake (x, x-axis) of the metal hydride. The hydrogen uptake is generally given as storage capacity of the metal hydride, which is the quotient of absorbed hydrogen mass divided by the metal mass [%]. Detailed descriptions of metal hydride PCI

analysis and measurement procedures can be found in various references [9, 11, 13, 14].

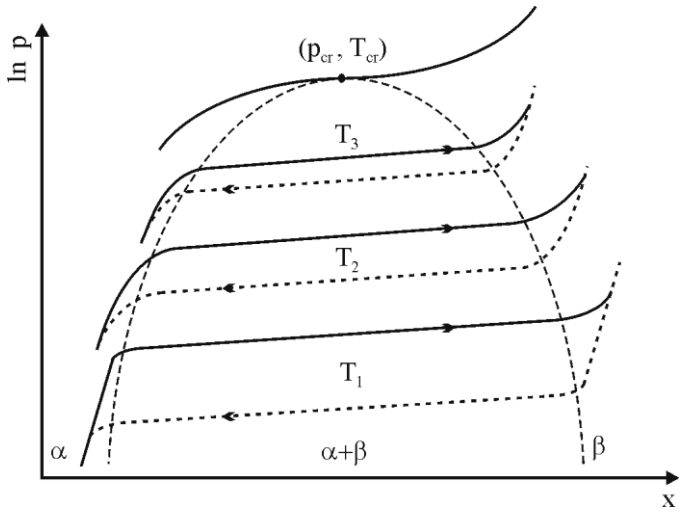

Figure 1-2: Schematic pressure-concentration isotherms of one metal hydride

Following three important parameters for the applicability of metal hydrides in sorption systems, e.g. cooling systems, are directly derived from the PCI measurement:

Effective storage capacity for sorption systems

The effective storage capacity for sorption systems can be defined as the storage capacity of the metal hydride within the plateau region (dashed line in Figure 1-2). Outside of this region, hydrogen is dissolved stochastically within the metal lattice (α-phase) or within the metal hydride lattice (β-phase). Therefore, the chemical reaction (phase transformation, α => β-phase) correlated with the enthalpy of the reaction takes place within the plateau region only. As the enthalpy of the reaction generates the intended effect, e.g. cooling effect, the areas outside of the plateau region are not useful for sorption systems.

Hysteresis

The absorption pressure is always higher than the desorption pressure. A commonly used explanation for this hysteresis effect is based on the idea of consumed free enthalpy: During the

formation of the hydride phase, the lattice is expanded up to 30 %. The induced stresses and deformations lead to a consumption of free enthalpy and contribute to the pressure hysteresis [9]. This hysteresis effect can be quantified by the hysteresis factor (f_{hys}) based on equation (1-2):

$$\Delta G_{Hys}\left[\frac{J}{mol_{H_2}}\right] = R \cdot T \cdot f_{Hys} = R \cdot T \cdot \ln\left(\frac{p_{Pl}^{Abs}}{p_{Pl}^{Des}}\right) \qquad (1\text{-}2)$$

The hysteresis is an important characteristic that determines the applicability of the alloy. Especially in sorption systems, a small as possible hysteresis is necessary as it generally reduces the efficiency of the system.

Plateau slope

Real PCI show a sloping plateau region. Therefore, the plateau pressure is commonly defined as the equilibrium pressure in the middle of the plateau. Although the slope may not be constant over the whole plateau region, one plateau slope factor (m_{Pl}) for absorption and one for desorption are generally sufficient to describe the plateau characteristics of the alloy:

$$m_{Pl} = \left.\frac{d\left(\ln\frac{p_{eq}}{p^0}\right)}{dx}\right|_{x_{mid}} \qquad (1\text{-}3)$$

For sorption systems a small plateau factor is important as the change of the equilibrium pressure during the reaction should be as small as possible. If a distinct desorption pressure is necessary, a steep plateau reduces either the useful hydrogen storage capacity or increases the necessary metal hydride temperature. Both effects reduce the efficiency of the sorption system.

PCI measurement set-up

High reaction enthalpy combined with high density and low thermal conductivity of metal hydride powders complicate experimental investigations of metal-hydrogen systems under isothermal conditions. A frequently used technique for PCI investigations is the *static* measurement method,

where a slow stepwise increase of the hydrogen content enables the system to reach its equilibrium. Another measurement method, which is more representative for technical applications, is to control the hydrogen flow rate [15]. The hydrogen uptake of a metal hydride can be determined either on a gravimetric or on a volumetric working test-bench. Applying the gravimetric method, a high-precision balance is necessary to observe the absorption and desorption, respectively, whereas the volumetric method is based on the conservation of mass in a closed system with known volume. If the system is fully sealed, the hydrogen uptake is proportional to the measured pressure loss in the system. Both principles and their respective advantages are described and compared in detail in [9].

The set-up shown in Figure 1-3 is based on the volumetric method and was constructed within the dissertation of Friedlmeier in 1997 [9]. It is generally applied for metal hydride characterisation at the Institute of Nuclear Energy and Energy Systems (IKE) and consists mainly of a hydrogen mass flow controller (MFC), a differential pressure sensor (Δp), hydrogen volumes, a sample reactor and several pressure and temperature sensors. As the test-bench is measuring by means of the volumetric method, volumes of all relevant system parts are known. Several authors give a detailed description of the measurement procedure of PCI measurements, the hydrogen uptake calculation procedure as well as the achievable accuracies of this type of measurement system [7, 9, 15, 16]. The underlying principle (for absorption) is based on the idea that at the beginning of the measurement the complete amount of hydrogen is in the grey part of the system and the blue part containing the metal hydride in the sample reactor is evacuated. During the measurement, the mass flow controller (MFC) limits the hydrogen flow rate from the grey to the blue part of the system. Therefore, the pressure increase in the sample reactor (blue part) can be adjusted to the intrinsic kinetics of the sample. As long as the absorption rate of hydrogen of the metal hydride sample is higher than the hydrogen supply rate through the MFC the metal-hydrogen system is in equilibrium state.

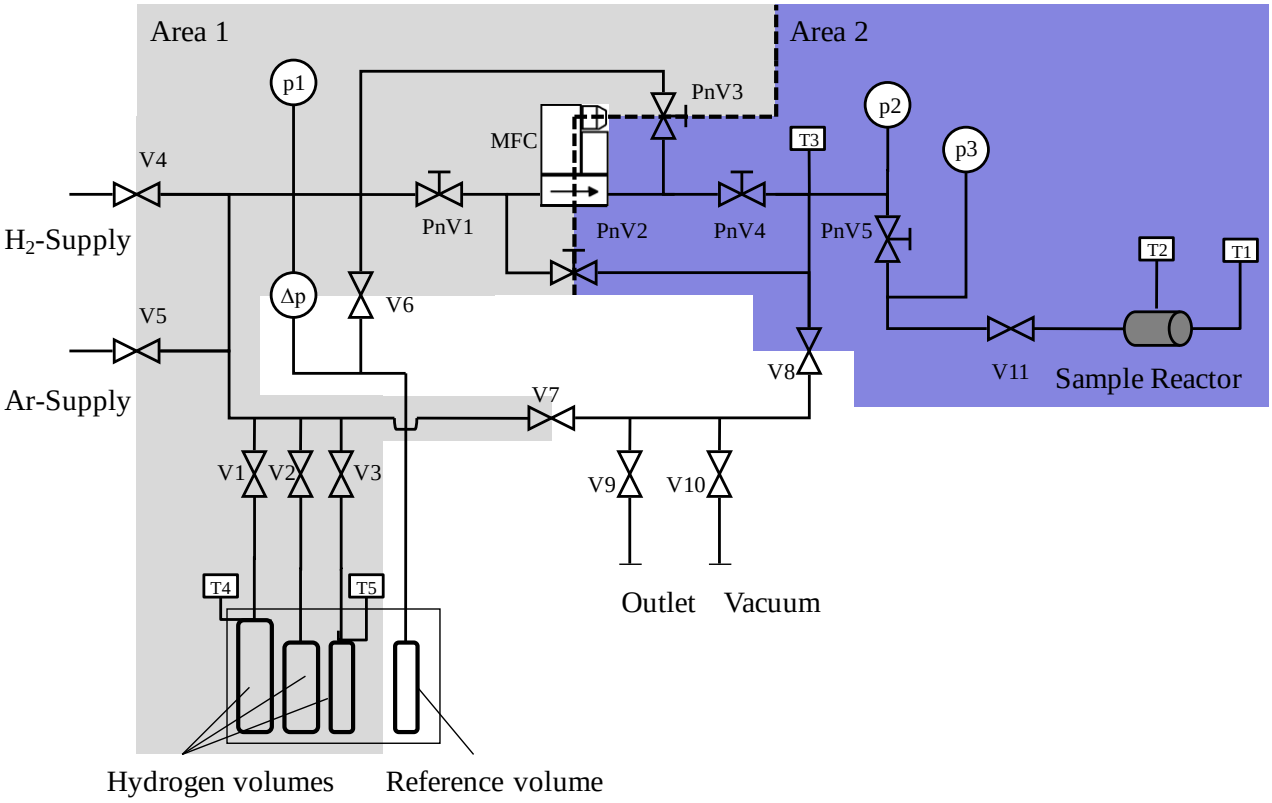

Figure 1-3: Schematic flow diagram test bench for PCI/kinetics measurements

As the hydrogen mass flow rate during the PCI measurement is controlled, an excessive heat generation can be avoided even with simple sample reactor designs. In Figure 1-4, the sample reactor used at IKE for PCI measurements is shown. It consists mainly of a stainless steel tube that is connected to the PCI measurement set-up with a VCR connection (left side). The VCR sealing contains a filter plate (0.5 µm) to prevent the discharge of metal powder. The sample mass is loosely filled into the stainless steel tube from the opposite side. A VCR blind plug that contains a small tube for temperature measurement (right side) closes the sample reactor. By means of a cladding tube (not shown in Figure 1-4) which is connected from the right side to the two flanges of the stainless steel tube, the temperature of the sample reactor can be adjusted by a water flow from a connected thermostat.

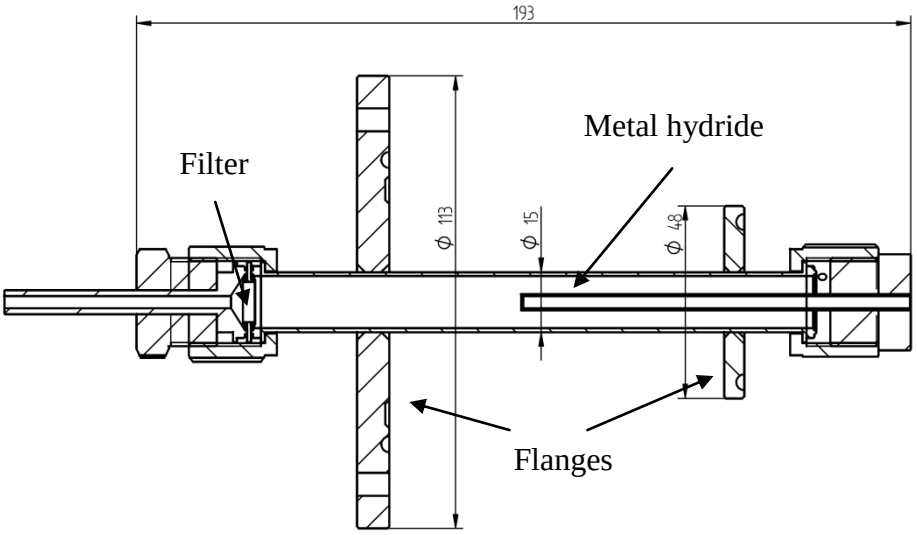

Figure 1-4: Sample reactor for PCI measurements

Van't Hoff plot and mathematical description of metal hydride properties

For the ideal case (no hysteresis and plateau slope), the logarithmic equilibrium pressure can be drawn versus the reciprocal temperature of the metal hydride and the resulting straight line is called van't Hoff plot. The slope of the van't Hoff plot is proportional to the enthalpy change of hydriding (ΔH) and the point of intersection between van't Hoff plot and ordinate (for $T \rightarrow \infty$) corresponds to the entropy change ΔS divided by the universal gas constant R [9, 14]. However, due to the hysteresis and plateau slope effect, a simple van't Hoff equation is not applicable for accurate description of metal hydrides. Figure 1-5 shows schematically the 'van't Hoff' coherences of the more realistic case: Here, two areas, one for absorption and one for desorption, are necessary to describe all possible states within the plateau region.

A sufficiently accurate mathematical description (equation (1-4)) of the metal hydride properties is based on the van't Hoff plot of the ideal case using different values of reaction enthalpy and entropy for ab- and desorption and the plateau factor m_{Pl} [17, 18].

$$\ln\left(\frac{p_{Pl}}{p^0}\right) = \frac{\Delta H}{R \cdot T} - \frac{\Delta S}{R} + m_{Pl} \cdot (x - x_{mid}) \qquad (1\text{-}4)$$

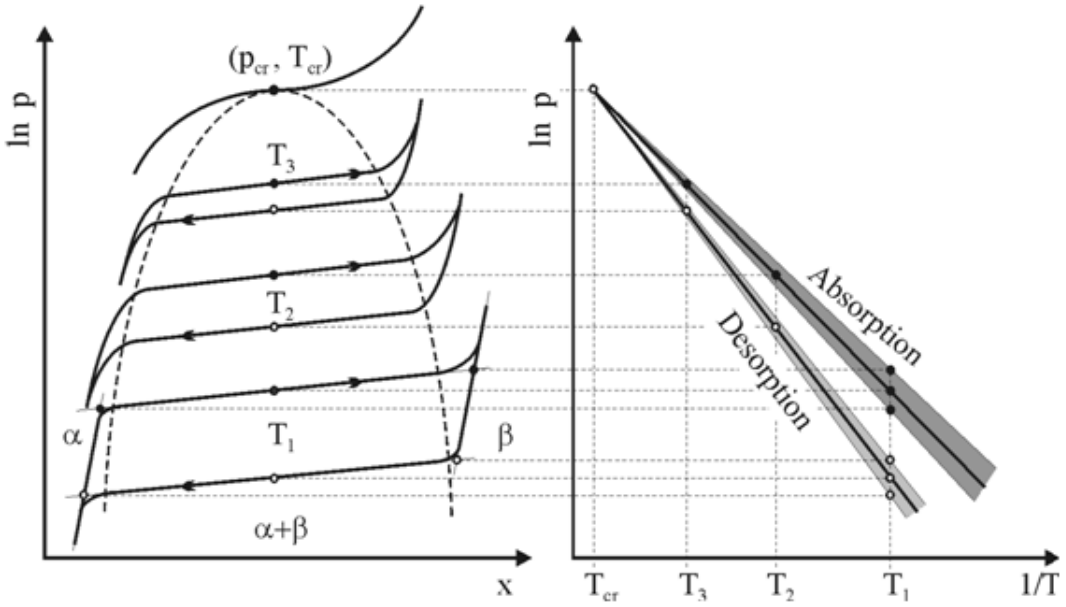

Figure 1-5: Schematic Pressure-concentration isotherms and adapted van't Hoff plots

Intrinsic reaction kinetics of the metal-hydrogen reaction

Whereas the chemical thermodynamics describes chemical states and equilibriums, the chemical reaction kinetics deals with the rate of the respective chemical reaction. *Stability* can therefore describe either the equilibrium state of the reaction (chemical thermodynamics) or a very slow reaction towards this equilibrium (chemical kinetics) [19]. As the reaction of the metal powder with hydrogen is generally an exothermic process, the temperature of the metal powder increases during the absorption. According to the van't Hoff equation, a temperature increase leads to an increasing equilibrium pressure. As soon as the equilibrium pressure of the metal hydride approaches the available hydrogen pressure the reaction decelerates. Therefore, it is necessary to distinguish between the pure (intrinsic) reaction kinetics of the metal hydride and the reaction bed dynamics, where heat and mass transfer co-determine the kinetics of the reaction.

The intrinsic reaction kinetics depends on external factors like temperature and applied hydrogen pressure as well as on internal factors, e.g. hydrogen concentration and particle size. Additionally, the previous history of the material determines the surface quality (adsorbed impurities, e.g. oxygen) and influences the reaction kinetics of the alloy [9, 20, 21]. Wang *et al.* [22] divided the hydriding process into three separated steps and developed a single equation for:

(1) Dissolution of hydrogen on the surface,
(2) Diffusion of hydrogen through the lattice and
(3) Phase transformation or nucleation and growth.

In order to identify the rate-controlling step, the mathematical model of each step was compared with experimental results obtained from $LmNi_5$ [23]. For the first hydriding process, 'nucleation and growth' of the β-phase was identified as controlling step. After the activation of the metal hydride, the authors were not able to identify clearly the hydriding controlling step as it varies with experimental conditions.

However, if the slowest reaction step is thermally activated, the overall reaction is also temperature dependent. Therefore, the activation energy of this step determines the kinetics of the total reaction [9]. This general approach leads to the commonly used kinetics equation (1-5) for the absorption rate ϕ based on the Arrhenius correlation [17, 18, 24-26]:

$$\phi = -C_a e^{(-\frac{E_a}{RT})} \ln(\frac{p}{p_{eq}})(\rho_{sat} - \rho_s) \qquad (1\text{-}5)$$

with the activation energy E_a and the constant C_a as material specific values. The Arrhenius term represents the temperature dependency of the overall reaction whereas the logarithmic term includes the dependency on the hydrogen gas pressure p related to the equilibrium pressure p_{eq} according to the van't Hoff plot. ρ_{sat} represents the density of the fully saturated metal hydride and ρ_s its density for the respective hydrogen load situation.

Intrinsic reaction kinetics measurement and determination of the characteristic time

The PCI measurement set-up shown in Figure 1-3 can be adapted for intrinsic reaction kinetics measurements. Whereas during the PCI measurement, the mass flow controller (MFC) limits the hydrogen flow rate, the kinetics measurement starts with the opening of all possible connections (PnV2 and PnV3) in order to increase the hydrogen pressure in the sample reactor as fast as possible. The underlying principle is the measurement of the time that is necessary for the metal-hydrogen system to readjust to the new equilibrium (relaxation time). The original equilibrium (uncharged metal) is disturbed by a sudden hydrogen pressure increase that leads to an absorption until the new equilibrium (metal hydride load situation for a given temperature and pressure) is reached. These coherences are schematically shown in Figure 1-6 where the hydrogen pressure

increase is plotted as dashed step function. The intrinsic reaction kinetics is plotted as reacted fraction f(t) according to equation (1-6):

$$f(t) = \frac{m_{H_2}(t)}{m_{H_2,\infty}} \cdot 100 \quad [\%] \qquad (1\text{-}6)$$

Assuming a first-order reaction, the characteristic time τ of the absorption (relaxation time) can be derived from equation (1-7) based on the measured reacted fraction. It is generally defined as the necessary time to reach around 63.2 % of the final value.

$$f(t) = 100 \cdot (1 - e^{\frac{-t}{\tau}}) \qquad (1\text{-}7)$$

Due to the exponential behavior of the system, a doubling of the characteristic time (2τ) leads to a reacted fraction of 86.5 % whereas 95 % of the final value is reached after a tripling of the characteristic time (3τ). The experimentally derived characteristic time value corresponds to one distinct measurement with defined parameters like hydrogen pressure increase, load situation and metal hydride temperature.

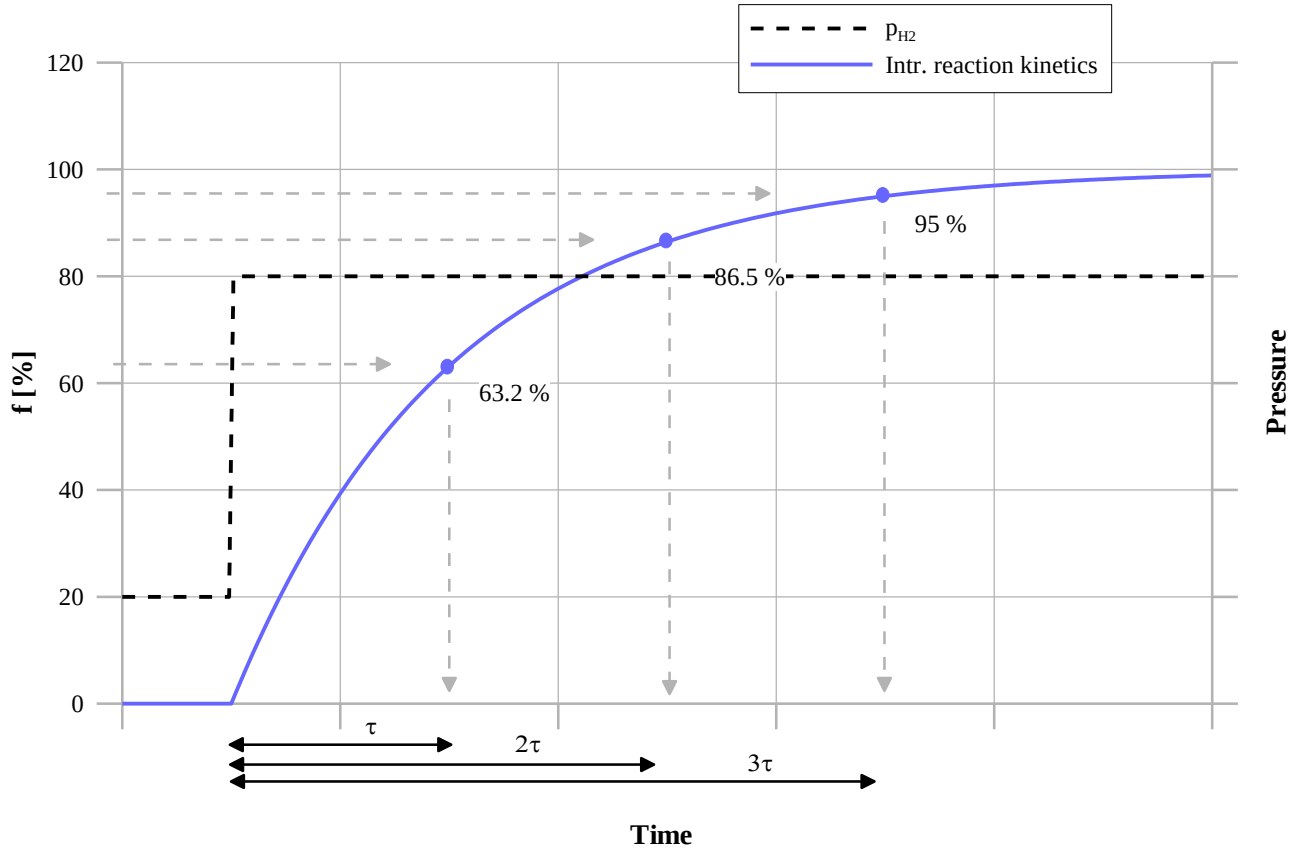

Figure 1-6: Characteristic time (relaxation time) of intrinsic reaction kinetics

1.2.2 Metal hydride reaction beds

The reaction bed is the crucial component for all types of metal hydride sorption systems (Figure 1-7). It has to guarantee a very good transfer of heat (heat of reaction) and of the working gas (hydrogen) into and from the metal powder bulk.

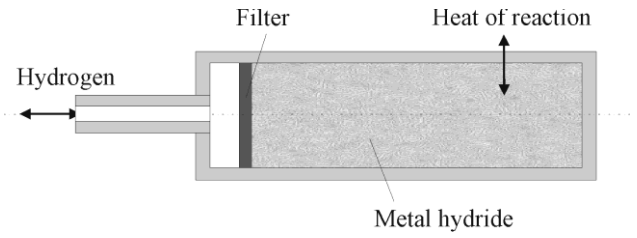

Figure 1-7: Schematic drawing of metal hydride reaction bed

As the significant volume expansion of the powder during the hydriding process may lead to unacceptable high stresses on the reaction bed construction, the necessary additional space must be provided. Therefore, the inner volume is generally filled up to 50 % only [27]. Additionally, the decrease of the metal powder grain size during the first operation cycles (activation) demands a finely pored filter inside the reaction bed to prevent the discharge of metal powder.

Power density

Based on the reaction enthalpy of the metal hydride [kJ/mol], a given metal hydride inventory defines the maximum hydrogen uptake and consequently its stored energy. The specific storage capacity (energy density) of a system can be calculated by the amount of stored energy divided by the necessary mass of alloy (or total mass of the system). This specific value is also used for the characterisation of different methods for hydrogen storage. As the maximum storage capacity of metal hydrides working at room temperature is around 2 %, the necessary metal hydride inventory to store 4 kg of hydrogen (necessary to reach 400 km driving distance with a fuel cell engine) is around 200 kg, which is especially for automotive applications not acceptable. Therefore, the metal hydride storage method is not reasonable for automotive applications as long as the storage capacity is not clearly improved.

However, the important value for sorption systems is the power density, namely, the achievable cooling power divided by the necessary mass of alloy, which is determined by the necessary time for charging or discharging of the reaction beds (reaction bed dynamics). Comparable to the intrinsic reaction kinetics measurements, the reaction bed dynamics of one type of reaction bed can also be characterized by a relaxation time measurement (see chapter 1.2.1). For given boundary conditions, like initial reaction bed temperature, metal hydride load situation and hydrogen pressure increase (step function), the time necessary to reach to new equilibrium can be measured. As the intrinsic reaction kinetics of commonly used metal hydrides are generally very fast, all applicable alloys in sorption systems are so far assumed to be fast enough and their influence on the operation of the system to be negligible [7, 9, 11, 25]. These coherences are schematically shown in Figure 1-8 where the intrinsic reaction kinetics is assumed to be clearly faster than the reaction bed dynamics. Due to the short characteristic time of the intrinsic reaction kinetics, the reaction bed dynamics is limited by, e.g. heat and mass transfer limitations and not by the intrinsic chemical reaction. Therefore, the characteristic time of the reaction bed dynamics can be reduced with improved reaction bed designs. However, if the characteristic times of the reaction bed dynamics and the intrinsic reaction kinetics are identical, the process is limited by the kinetics of the chemical reaction and therefore not affected by an optimized reaction bed design.

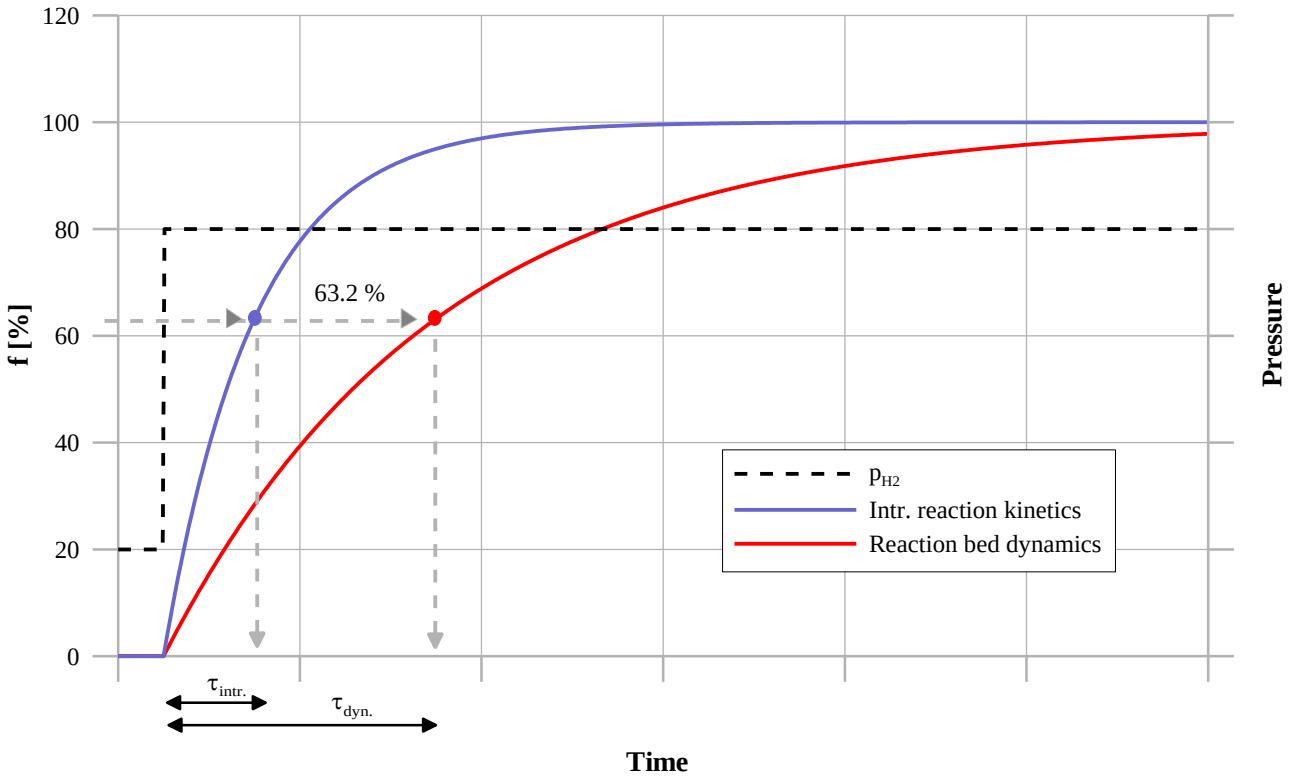

Figure 1-8: Schematic comparison of reaction bed dynamics and intrinsic reaction kinetics

The resulting effect on the characteristic cooling power P_{char} can be expressed according to equation (1-8):

$$P_{char} = \frac{\dot{Q}}{m_{MeH}} = \frac{\frac{Q_{cool}}{m_{MeH}}}{\tau} = \frac{\Delta h}{\tau} \qquad \left[\frac{W}{kg}\right] \tag{1-8}$$

with the mass of metal hydride m_{MeH}, the specific enthalpy of reaction Δh and the characteristic time for the reaction process τ. As the specific enthalpy of reaction (Δh) is identical (identical metal hydride), the characteristic power depends on the characteristic time, only. Hence, the fast intrinsic reaction kinetics of metal hydrides (τ_{intr}) offer the possibility to increase to specific power of sorption systems drastically if optimized reaction bed designs allowing fast reaction bed dynamics (τ_{dyn}) are used.

Reaction bed dynamics

Whereas the intrinsic reaction kinetics is based on chemical and physical properties of the respective metal hydride, the reaction bed dynamics depends on global parameters like temperature and pressure distribution in the reaction bed. In the case of hydrogen absorption, the released reaction enthalpy (heat of reaction, Figure 1-7) increases the temperature of the metal hydride bulk and consequently the equilibrium pressure of the reaction. As soon as the local equilibrium pressure of the metal hydride (corresponding to local metal hydride temperature) reaches the hydrogen supply pressure, a further hydrogen uptake is directly proportional to the heat transfer characteristics of the reaction bed (assuming ideal mass transfer). Therefore, hydrogen distribution and heat transfer are the main factors that influence the reaction bed dynamics and consequently the power density of the reaction bed.

Hydrogen distribution

The hydrogen transport inside the reaction bed is limited and depends on the effective permeability of the powder bulk. Additionally, the necessary filter (to prevent powder discharge) increases the hydrogen flow resistance. A common method to improve the hydrogen transport inside the reaction bed is the application of sintered-metal filter arteries or surrounding tubes that offer two main advantages:

1. A low flow resistance path along the axial direction of the reaction bed (e.g. inside the artery) and consequently a short diffusion way through the more compact structure (metal powder bulk) in radial direction facilitate the hydrogen distribution.

2. The increased filter surface (the artery itself) reduces hydrogen pressure loss through the filter as the hydrogen velocity decreases with increasing filter surface.

An exact mathematical description of the hydrogen transport mechanism is complicated due to the random nature of the bulk material [28]. The hydrogen mass balance is given in equation (1-9) where ε is the porosity of the metal bulk, ρ_g the gas density, v_g the gas velocity and ϕ the rate of hydrogen sorption reaction according to the intrinsic reaction kinetics equation (1-5):

$$\varepsilon \frac{\partial \rho_g}{\partial t} = -\nabla\left(\rho_g v_g\right) - (1-\varepsilon)\cdot\phi \qquad (1\text{-}9)$$

Heat transfer

A simple metal hydride powder bulk can be seen as porous medium consisting of small particles with widespread grain and pore sizes. The mathematical description of the heat transfer process inside the metal hydride bulk is generally simplified by following assumptions [29-32]:

- Convective heat transfer (by convection of hydrogen) is negligibly small compared to conductive heat transfer.
- Heat transfer by radiation is neglected.

Taking these assumptions into account, the energy equation inside the powder bulk is given as:

$$(1-\varepsilon)\cdot\left(\rho_S\cdot c_{P,S}\right)\cdot\frac{\partial T}{\partial t}=-\nabla\left(\lambda_{eff}\nabla T_S\right)-(1-\varepsilon)\cdot\phi\cdot\left(\frac{\Delta H}{M_{H_2}}-c_{P,S}\cdot T\right) \qquad (1\text{-}10)$$

where ρ_S and $c_{P,S}$ denotes the bulk density and specific heat, M_{H2} is the mol mass of hydrogen, ϕ the rate of the chemical reaction based on equation (1-5) and ΔH denotes the reaction enthalpy of the respective metal hydride. The thermal conductivity of the powder bulk is described by an isotropic effective coefficient λ_{eff}. Its value for a simple metal hydride powder bed depends primarily on the hydrogen pressure [33-36]: The plot of 'effective conductivity versus pressure' shows a tilted S-shaped characteristic with a very low and almost constant (< 0.1 W/(m K)) effective conductivity for small pressures (< 0.001 bar). During the intermediate phase the conductivity is increasing constantly with increasing pressure until it stabilizes again at around 1 W/(m K) for higher pressures (> 1 bar). For activated Mg powder, an additional dependency of the thermal conductivity on the hydrogen content has been published [37, 38]. It increases from around 2 W/(m K) to around 8 W/(m K) with increasing hydrogen content. However, as the storage capacity of Mg is with around 7 wt-% very high and its working temperature is above 300 °C, it can be seen as an exception.

As sorption systems are mainly working above atmospheric pressure, clearly below 300 °C and with around 1.5 % storage capacities, an effective thermal conductivity of around 1 W/(m K) can be reasonably assumed. However, the heat transfer from the reacting metal powder to the heat carrier determines mainly the reaction bed dynamics of the absorption (vice versa for desorption). An improvement of the effective conductivity of the metal hydride bulk leads directly to a higher flux and therefore to faster reaction bed dynamics. As simple reaction beds are not sufficient to meet reasonable reaction rates [39], different measures to improve the effective thermal conductivity have been investigated and lead to different designs of metal hydride reaction beds.

Realized reaction bed designs

The following figures show different schematic drawings of selected experimentally investigated reaction beds and summarize the practical state of the art. In general, a comparison between two reaction bed designs is difficult as long as different hydrides with different boundary conditions are applied. Especially, the applied hydrogen pressure increase (step function) is directly correlated to the reaction bed dynamics. Therefore, a quantitative comparison of the different reaction bed dynamics is not reasonable.

Tubular reaction beds with central filter artery

The reaction bed shown in Figure 1-9 is a kind of standard solution and was applied in various sorption system prototypes [11, 40-42]. Hydrogen enters the reaction bed from one end and is easily distributed in axial direction due to the central porous tube (artery). The radial hydrogen distribution characteristic depends on the consistency of the bulk material. In the case of a liquid heat carrier, a coaxial surrounding tube and the reaction bed tube form an annular gap. Additionally, several of these tubular reaction beds can be combined to build up a system with the desired output power. Here, the modular inner part (hydrogen side) of the reaction is used as a single tube in a tube bundle heat exchanger [43, 44]. If the hydrogen connections are joined, the modular reaction beds form a reactor containing the desired amount of metal hydride.

An application of this reaction bed with air as heat carrier was also realized - with fins instead of a surrounding tube [45, 46]. Several inner parts of the reaction bed were combined and thermally connected with fins to form a fin and tube heat exchanger.

This basic geometry was intensively used to investigate and optimize the heat transfer process inside metal powders. A fundamental heat transfer improvement was achieved with an Al-foam structure and was mainly used in sorption systems. Other heat transfer matrices, like foams made of Cu or Ni, internal fins, aluminium-bands soldered to the wall or cassettes made of Cu or Al, have also been tested with this reaction bed configuration [44, 47-49]. As the hydrogen distribution is not affecting the kinetics (due to the filter artery) [11], major improvements can only be expected by improving the overall heat transfer from the fluid to the powder. Expanded natural graphite compressed with metal hydride to form compact pellets is a recently investigated option for this type of reaction bed but their long-term stability is up to know unclear [50-53].

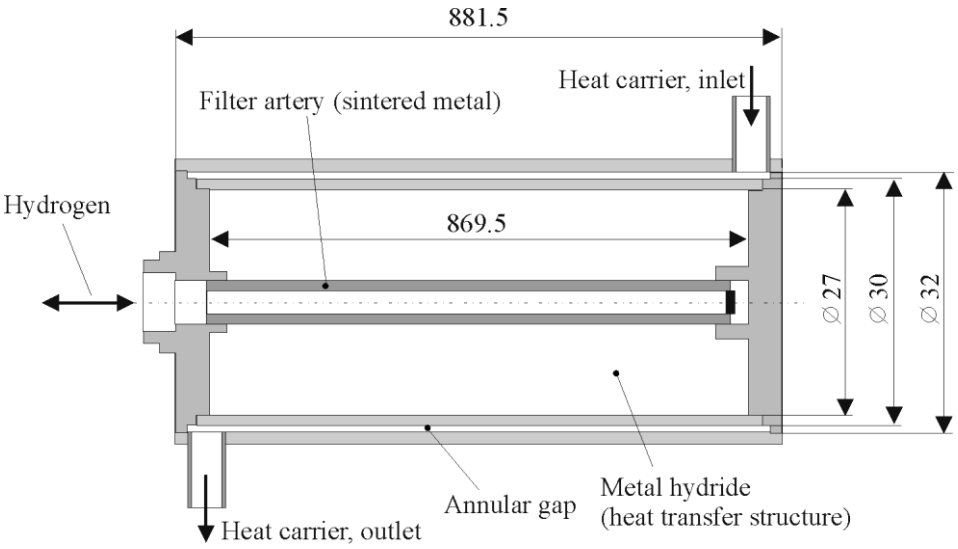

Figure 1-9: Reaction bed with annular coolant gap and filter artery for hydrogen transport (taken from [48])

Based on a comparable reaction bed configuration, Kim *et al.* developed porous powder metal hydride (PMH) compacts [54, 55]. Metal hydride particles were coated with a thin layer of copper and compressed to PMH compacts. As the metal hydride particles are fixed within the compact, a filter is not necessary and a simple hole is sufficient to ensure the distribution of hydrogen within the reaction bed.

Another reaction bed design (Figure 1-10) using a central filter tube for hydrogen distribution was investigated by Ram Gopal *et al.* [56]. The inner part of the reaction bed is comparable to the one described above: The central porous tube and a surrounding tube (here in Cu) form an annular space in which the powder is packed. However, the heat carrier flows through a copper coil brazed on the cladding tube of the reaction bed.

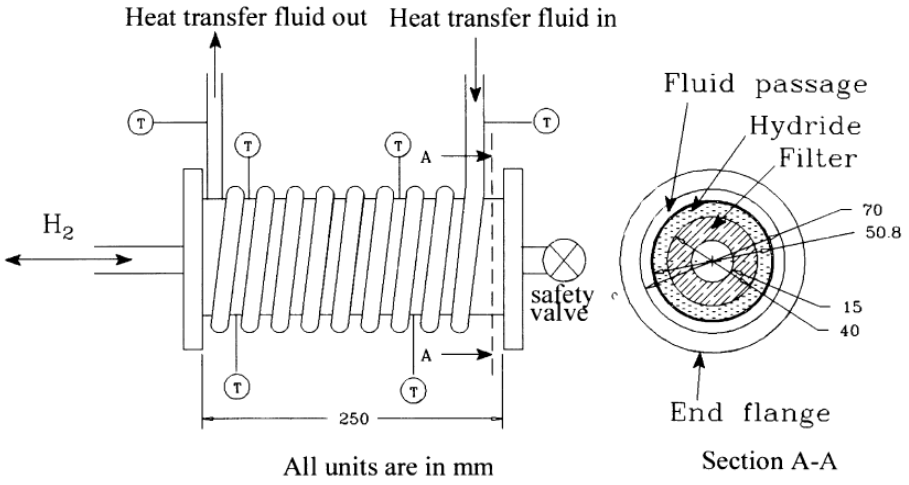

Figure 1-10: Reaction bed with copper coil and filter artery for hydrogen transport (taken from [56])

Reaction beds with different hydrogen distribution systems

Figure 1-11 shows another possibility to improve the distribution of hydrogen, which was investigated and published by Qin *et al.* [57] and Ni *et al.* [58]. Instead of a central filter tube, the filter surrounds the metal powder bulk: Therefore, hydrogen enters the reaction bed from one side, is easily distributed in the annular gap around the filter and enters in radial direction into the powder bulk. A finned copper tube is inserted through the bulk to divide the bed into several sections and to improve the heat transfer characteristics.

Kang *et al.* used a comparable design [59]: The inner reaction bed consisted of two identical Al-finned copper tubes working serially in an U-shaped heat exchanger and the hydrogen distribution was realized by a gap around the inner reaction bed and the pressure vessel. Mellouli *et al.* investigated a reaction bed with inner copper coil as heat exchanger and a hydrogen inlet with filter at the top of a cylindrical reaction bed [60]. It was mainly designed for investigations on absorption and desorption processes and not for an application in sorption systems.

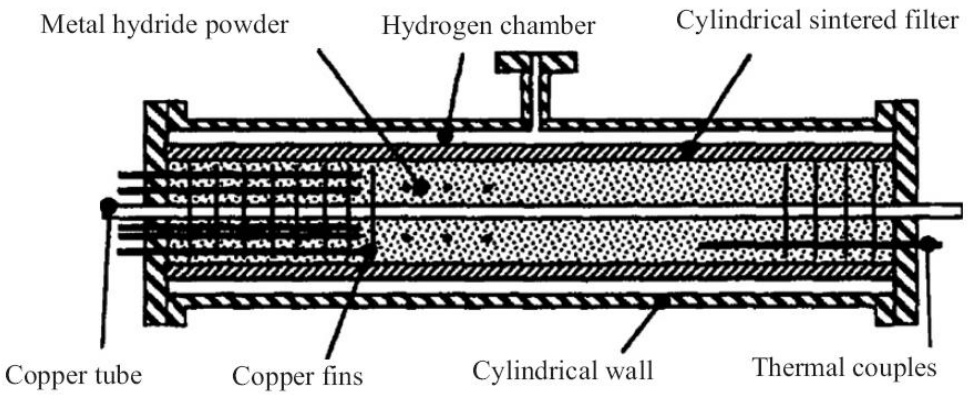

Figure 1-11: Reaction bed with copper fins and surrounding filter tube for hydrogen transport (taken from [57])

Capillary tube bundle reaction bed

The capillary tube bundle reaction bed (Figure 1-12) has been described in literature [61, 62] and additionally, a detailed simulation analysis and comparison with a reaction bed design using Al-foam and internal artery was published for a combined heating and cooling system based on metal hydrides [31]. The main result was a calculated increasing specific cooling power of around 30 % due to the utilisation of the capillary tube bundle reaction bed. It was constructed at the IKE in 1994 and experimentally investigated within a student research project in the same year [1]. Due to the high parasitic mass of the construction, the efficiency of the intended application in a two-stage heat transformer was very low.

In this reaction bed, hydrogen enters the metal hydride bulk through a filter tube that forms an annular gap with the outer cladding tube. The metal hydride powder is located between the capillary tubes in the inner part of the reaction bed.

[1] T. Rühl: Experimentelle Untersuchung einer neuartigen Reaktionsbettkonstruktion für Metallhydrid-Sorptionsmaschinen., Studienarbeit, IKE 5-D-238, 1994

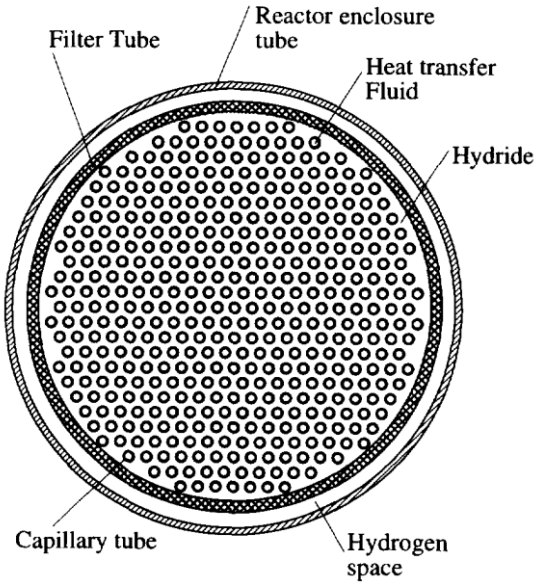

Figure 1-12: Capillary tube bundle reaction bed (taken from [31])

1.2.3 Metal hydride sorption systems

Sorption systems are generally closed systems that utilize the respective associated enthalpy of the process, generally for heat pumping or refrigeration. The driving energy is derived from a high temperature heat source, e.g. process heat, gas burner, waste heat, or solar energy. According to the classification of sorption systems based on the working pair, the metal-hydrogen system belongs to the solid sorption systems [11]. In contrast to solid adsorption systems, like "silica gel-water" or "zeolite-water", the solid and the gaseous phase are chemically bonded. The main difference between both principles is the volume expansion of the solid due to the chemical reaction [11].

The working principle of coupled metal hydrides

The basic configuration of metal hydride sorption systems consists of two reaction beds coupled by a hydrogen connection (see Figure 1-13). Each reaction bed contains a different metal hydride. As long as the hydrogen valve is closed, both metal hydrides are in equilibrium - the hydrogen pressures p_1 and p_2 correspond to the temperatures T_1 and T_2. As soon as the hydrogen valve is opened, the hydrogen pressure equalizes and each individual equilibrium is disturbed: The metal hydride possessing a higher equilibrium pressure as the equalized hydrogen pressure is forced to

release hydrogen, whereas the coupled metal hydride absorbs it. According to equation (1-1), the desorbing metal hydride along with the whole reaction bed will cool down and correspondingly the coupled bed will heat up. Assuming an adiabatic system, the two temperatures will change until the coupled system is stabilized at its equilibrium with $p_1 = p_2$. The amount of exchanged hydrogen is proportional to the heat capacity of the respective reaction bed.

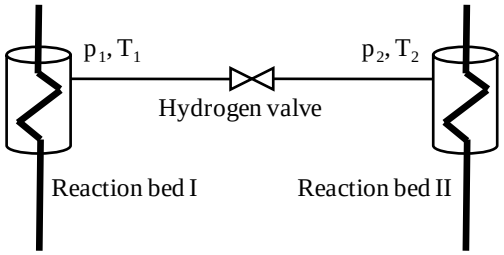

Figure 1-13: Working principle of coupled metal hydrides

If the system is kept artificially away from equilibrium by counterbalancing the reaction heat by means of heat exchangers inside the reaction beds, the resulting hydrogen exchange rate is proportional to the heat flux to/from the respective metal hydride.

Depending on the designed application of this basic couple, the enthalpy of desorption or absorption, respectively, generates the useful effect like cooling, heat pumping or heat transformation. The storage capacity (or hydrogen load situation) of the coupled hydrides defines the amount of hydrogen that can be exchanged within on half-cycle. The following second half-cycle is necessary to regenerate the system in order to reach the initial conditions. Cycle time is therefore defined as the total time necessary for the useable and the regeneration half-cycle.

Metal hydride sorption cooling systems

A metal hydride based sorption cooling system works generally with two metal hydrides (A and B) in separated reaction beds and hydrogen as working fluid. The useful effect, removing heat (Q_{Cool}), is generated by the high-pressure metal hydride (A) desorbing at the designed cooling temperature (T_{Cool}). The corresponding desorption pressure p_{Cool} is determined by the van't Hoff plot of the respective hydride shown schematically in Figure 1-14.

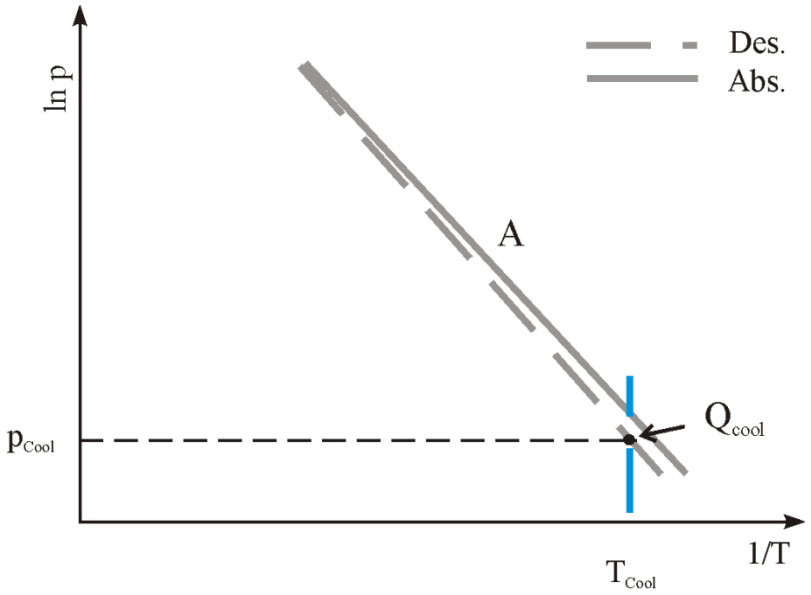

Figure 1-14: Van't Hoff diagram of sorption cooling system (idealized) – I

If the coupled low-pressure metal hydride (B) is able to absorb the released hydrogen (see Figure 1-15), a hydrogen exchange along with the corresponding cooling effect is obtained. The absorption of hydrogen from the coupled low-pressure hydride (B) generates heat (Q_{Amb_cool}) that must be released to a heat sink to prevent a temperature increase of the alloy. The environment is generally used as heat sink and therefore its temperature (T_{Amb}) determines the necessary van't Hoff characteristic of the coupled low-pressure alloy (B). The process of desorption of the high-pressure hydride (A) and absorption of the low-pressure hydride (B) is called the cooling half-cycle of the metal hydride sorption cooling system.

During the cooling half-cycle shown in Figure 1-15, an exchange of hydrogen from the high-pressure alloy (A) to the low-pressure alloy (B) is obtained. The transferred mass of hydrogen during the half-cycle time depends on the storage capacity and the total mass of the respective metal hydrides. As soon as a maximum amount of hydrogen is exchanged, the flow direction must be reversed.

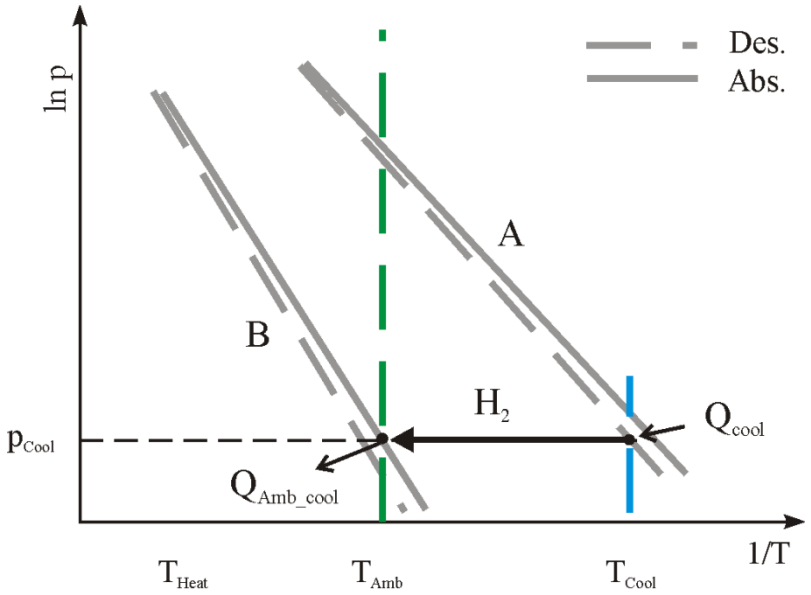

Figure 1-15: Van't Hoff diagram of sorption cooling system (idealized) – II

During the regeneration half-cycle, the metal hydride (B) works as a thermal compressor. As the absorption heat during regeneration (Q_{Amb_reg}) is released to the environment, the absorption pressure of metal hydride (A) at ambient temperature determines the necessary regeneration pressure level (p_{Reg}).

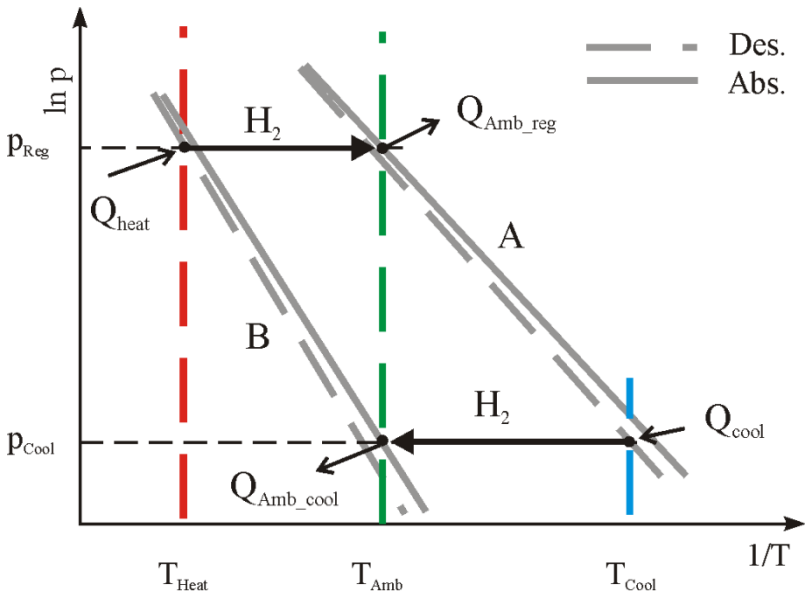

Figure 1-16: Van't Hoff diagram of sorption cooling system (idealized) – III

Therefore, based on the van't Hoff plot of metal hydride (B), the necessary heating temperature (T_{Heat}) is defined. For a given ambient temperature, the distance between the van't Hoff plots (A) and (B) determines the necessary heating temperature (T_{Heat}). Concurrently, the achievable cooling temperature (T_{Cool}) and/or the pressure difference during the cooling half-cycle are defined.

The described system is not able to supply a continuous cooling effect. As the reaction bed pair is either in regeneration or cooling mode, two identical reaction bed couples working in opposite direction are necessary to realize a quasi-continuous cold output. Therefore, the necessary time for regeneration must be shorter or at least the same as the cooling half-cycle time.

Specific power and half-cycle time

With regard to mobile applications, a high specific power (P_{spec}) is necessary in order to minimize the weight of the system. Comparable to the characteristic power P_{char} in equation (1-8) for a individual reaction bed, the specific power of coupled reaction beds P_{spec} is determined by the time necessary to exchange the maximum amount of hydrogen ($t_{half\text{-}cycle}$) and the specific reaction enthalpy of the metal hydride inventory (Δh):

$$P_{spec} = \frac{\dot{Q}}{m_{MeH\_des}} = \frac{\frac{Q_{cool}}{m_{MeH,des}}}{t_{half-cycle}} = \frac{\Delta h}{t_{half-cycle}} \qquad \left[\frac{W}{kg}\right] \qquad (1\text{-}11)$$

However, due to the dynamic coupling of two metal hydride reaction beds, the half-cycle time $t_{half\text{-}cycle}$ of the sorption system is influenced by both, the absorption reaction as well as the desorption reaction. Consequently, as the slower reaction dynamics determines the achievable specific power of the sorption system, the applied reaction beds are generally identical for both alloys.

Realized metal hydride sorption systems

According to above described problems in comparing different reaction beds (mainly step function of hydrogen pressure increase), in this anthology only thermally driven systems are taken into account that have been experimentally investigated and both, regeneration and cooling half-cycle data have been published. From these data, two characteristic values are derived, specific power and half-cycle time, in order to compare different designs regarding their weight specific performance.

Although the different systems were designed for different applications, like combined heat/cold generation or heat transforming, each system applies the same principle: the thermally driven hydrogen exchange between two reaction beds. The limiting factors (quantified by P_{spec} and $t_{half-cycle}$) are therefore independent of the designed application, the total amount of reaction beds or the amount of different metal hydrides.

In order to reduce the amount of systems, the summary was restricted to literature published since 1994. Werner and Nagel give detailed compilations of metal hydride sorption systems realized earlier [40, 45]. However, both do not contain additional, for this study relevant sorption systems or reaction beds with proved experimental results.

Although, heat recovery measures of the systems and different working temperatures complicate a direct comparison of the compilation in Table 1-2, the proportional behavior of P_{spec} and $t_{half-cycle}$ is obvious. Therefore, relevant characteristics for sorption systems realized within the last 15 years can be summarized as follows:

- The half-cycle times of the state of the art sorption systems range between 10 and 20 min, depending on the applied reaction bed design.
- A maximum specific power of 140-170 W/kg related to the desorbing alloy has been achieved.

As most of the intended applications were stationary, the necessity to increase the reaction bed dynamics was mainly based on the reduction of metal powder and not implicitly on weight and volume optimisations.

Table 1-2: Experimentally investigated metal hydride sorption systems

Heat transfer enhancement/ Hydrogen supply/ Application	Heat carrier	m_{MeH} [kg]	P_{spec} [W/kg] *)	$T_{half\text{-}cycle}$ [s]	Year/Ref.
Not described in detail/ Not described in detail/ Cooling system	Pressurized Water	90	80	~ 1200	1995/ [63]
Al-finned Cu-tube/ Surrounding external measure/ Cooling system – batch mode only	Water/ Oil	~ 10	170	600	1996/ [59]
Helical Cu-band/ Internal artery (sintered metal)/ 2-stage heat transformer	Pressurized Water	210	180 **)	600	1999/ [64]
Al-foam matrix/ Internal artery (sintered metal)/ Combined heating/cooling system (Thermal wave)	Water/ Oil	31	~ 65	~ 1200	1999/ [41, 65]
Cu-coil / no internal matrix/ Internal artery (ceramic)/ Cooling system – batch mode	Water/ Oil	1.5	60-90	< 720 (not fixed)	1999/ [56]
Longitudinal finning with Al-foil/ Internal artery/ Water cooling/heating system	Electr. Heater/ Water	3	100	1200	2002/ [66]
Al-foam matrix/ Internal artery (sintered metal)/ Combined heating/cooling system	Water/ Oil	45	80-140	~ 900	2002/ [11, 67]
Finned tube/ Surrounding sintered metal tube/ Automotive cooling system	Water/ Oil	11	~ 80	~ 1300	2007/ [57, 58]

*) per desorbing metal hydride

**) expected value (leakage problems)

1.2.4 Metal hydride sorption systems for automotive cooling

A complete sorption system for automotive cooling including all main secondary components is schematically shown in Figure 1-17. It consists of four reaction beds (RB I-IV), arranged as two independent couples (grey) with a hydrogen connection (thin lines) and a hydrogen valve (V_{H2}). The valve is necessary to prevent a hydrogen exchange between the reaction beds if cooling is not required. The interfaces of the sorption system are four heat exchangers working at three different temperatures levels (red, green, blue). The heat distribution to the respective reaction beds is realized by four water cycles (thick lines) consisting of water pumps and necessary water valves. In principle, the two water cycles working at ambient temperature (green) can be combined to reduce the amount of secondary components. The cooling effect of the sorption system (Q_{Cool}) is generated if the blue water cycle is connected to the desorbing blue reaction bed (RB III or I, depending on the cycle). The corresponding red reaction bed (RB II or IV) is absorbing and the reaction heat is released to the ambient by the connected green water cycle (Q_{Amb_cool}).

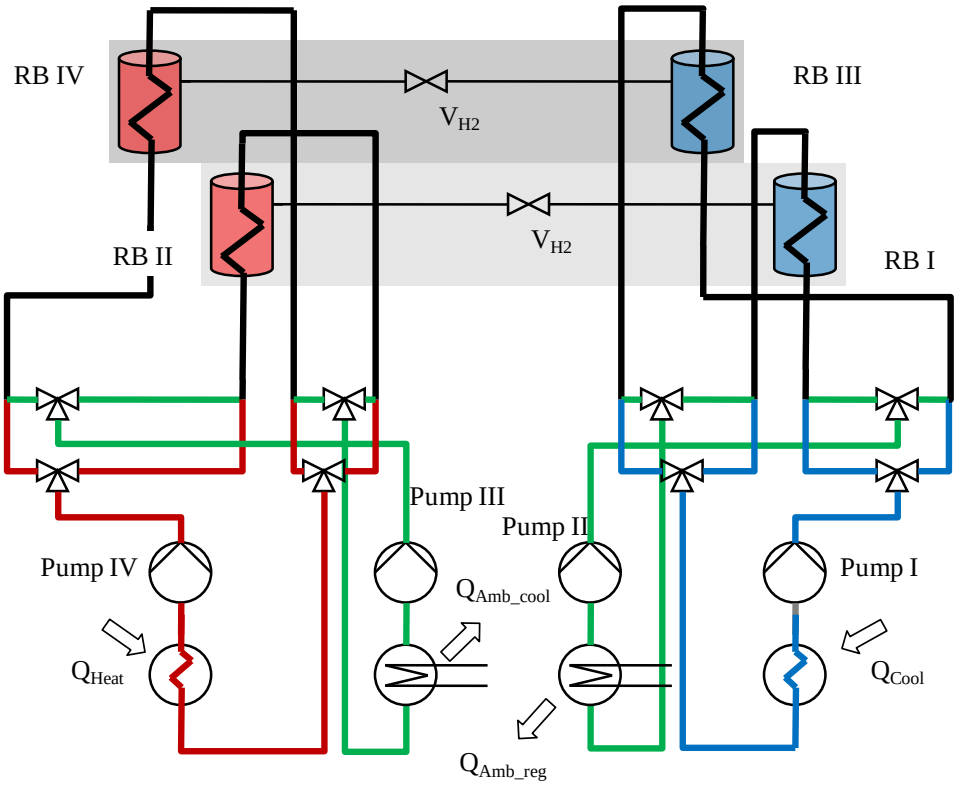

Figure 1-17: Schematic principle of the thermally driven sorption system including all major secondary components (three temperature levels: red, green, blue)

At the same time, the second reaction bed couple is regenerated. Therefore, the heating energy (Q_{Heat}) is transferred to the red reaction bed by the red water cycle. The absorption heat in the coupled reaction bed (Q_{Amb_reg}) is again released to the ambient by the second green water cycle.

Although, the water part of the system (thick lines) is rather complex, the respective components are available as standard products for automotive applications. Therefore, the overall weight constraints are mainly determined by the hydrogen part, especially by the necessary amount of metal hydride and the reaction beds.

Weight constraints

Concerning automotive applications, volume and weight constraints finally determine the applicability of the respective technology. For metal hydride sorption systems, the specific power is an important characteristic that gives the achievable cooling power per kg metal hydride in each reaction bed. It does not include the mass of the reaction bed itself or any secondary components like valves, heat exchangers or piping.

During the driving cycle, the peak cooling load is required at the beginning, as the car cabin is at ambient temperature (in summer) or even higher due to sun radiation. The time necessary to cool down the cabin depends on the thermal comfort demand of the costumer and determines therefore directly the capability of the system. As soon as the cabin reaches its nominal temperature, the necessary cooling power is reduced and the system is now counterbalancing the thermal load of the cabin, e. g. passenger heat and radiation.

Assuming an average cooling power of 2 kW [2], the low power density of realized metal hydride sorption systems mainly designed for stationary applications (maximum value: ~170 W/kg), leads to a necessary metal hydride mass of around 11.8 kg per reaction bed or around 47 kg total metal hydride mass (two pairs of coupled hydrides). This value does not include any additional mass for the metal hydride tank, heat exchangers and piping. Therefore, an automotive application of the state of the art metal hydride sorption system is not reasonable and the necessity of improving the power density of the system is obvious.

[2] According to the decision drawn within the ‘TOPMACS’ project [4]

Temperature constraints and available waste heat

For waste heat recovery, two different thermal heat flows from the automotive engine are in principal available: the exhaust gases and the coolant loop. The exhaust gas energy is so far partly used for turbo-charging and the cooling loop generally supplies cabin heat. Whereas the exhaust gas temperature mainly depends on the type of engine and its load situation, the coolant temperature is restricted to 90 °C.

Based on investigations of available metal hydrides and their characteristics, a reasonable cooling temperature is practically not achievable with basic metal hydride sorption systems and a heating temperature of 90 °C [68]. Especially, the plateau slope and hysteresis effects increase the necessary heating temperature:

- As the desorption pressure is always lower than the absorption pressure at the same temperature, the pressure difference between the desorbing and the absorbing alloy is reduced (hysteresis effect). This has to be compensated, e.g. for the regeneration half-cycle with a higher heating temperature.

- The plateau pressure of both alloys at the end of the half-cycle must be taken into account, as the equilibrium pressure during the reaction is not constant (plateau slope). During one cycle, the necessary pressure for absorption is increasing whereas the available desorption pressure is decreasing. This has to be also compensated with a higher heating temperature for the regeneration half-cycle.

Applying an additional reaction bed in the basic sorption system, double effect systems or two-stage thermal compressors, respectively, can be realized [11, 40, 69, 70]. With this operation principle a reduction of the necessary driving energy temperature is possible but has not been taken into account as it drastically increases the complexity of the system and consequently its weight and volume constraints [68].

Talom *et al.* demonstrated the general possibility of using exhaust gases from an internal combustion engine for a thermally driven cooling system [71]. Due to the working principle of the catalytic converter, at least 300 °C hot exhaust gases from gasoline engines are in principle available for waste heat utilisation. Therefore, waste heat from the exhaust gases seems to be suitable to power the thermally driven cooling system.

1.3 Aim of work

Due to the low specific power of the state of the art metal hydride sorption systems, an application of this technology for automotive cooling is so far not practicable. The main reason is the slow hydrogen exchange between the two coupled reaction beds. However, only three parameters can principally limit the kinetics of the metal-hydrogen reaction and therefore the dynamics of the reaction bed:

1. The intrinsic reaction kinetics of the metal hydride
2. The hydrogen distribution within the reaction bed
3. The heat transfer from/to the reacting metal hydride

Comparing the half-cycle time of realized sorption systems (≥ 600 s) with the intrinsic reaction kinetics of relevant metal hydrides (≤ 200 s), it is obvious that the main reason for the low specific power density is due to the slow dynamics of the so far applied metal hydride reaction beds (insufficient heat or mass transfer). However, the fast intrinsic reaction kinetics of metal hydrides provides the possibility to increase the specific power of metal hydride sorption systems with optimized reaction bed designs.

The aim of this work is therefore to investigate and demonstrate experimentally the realisation of a metal hydride based sorption system with high specific power. As the achievable specific power of the sorption system depends mainly on the reaction beds, the analysis and understanding of the dynamics of fast metal hydride reaction beds is one keynote of this work as it is the underlying issue for the automotive applicability and the optimisation potential of this technology.

Based on the literature review of so far realized sorption systems and reaction beds, the capillary tube bundle principle was chosen as underlying reaction bed design idea for the sorption system. Especially the large heat transfer surface and the short distances between the tubes promised fast reaction bed dynamics. However, a considerable specific power increase of the sorption system is only possible if the intrinsic reaction kinetics of the applied metal hydrides are fast enough. Therefore, the experimental part of this work starts with the determination of intrinsic metal hydride characteristics and the analysis of individual reaction beds dynamics in order to identify an optimized combination of fast reaction beds and adapted metal hydrides. Based on these investigations, the coupled reaction bed system (cooling system) is analyzed in detail with varied boundary conditions and the applicability of this technology for automotive cooling is estimated.

1. Introduction

2 Test benches and experimental details

2.1 Measurement procedure, test benches and measurement equipment

The only difference between absorption and desorption experiments are the directions of heat flux and hydrogen flow. The absorption of hydrogen is therefore used as reference for the following description of the measurement set-ups and procedures.

Characterisation of metal hydrides

The PCI and intrinsic kinetics measurements of the chosen metal hydrides were performed on the characterisation test-bench described in chapter 1.2.1. The main difference between the PCI and the kinetics measurement is the time dependency of the measurement. Whereas during the PCI measurement a small hydrogen flow rate is applied to the metal hydride sample in order to follow the chemical equilibrium during the hydrogen uptake, the underlying principle of the kinetics measurement is the disturbance of the chemical equilibrium by an abrupt increase of the hydrogen pressure.

The respective reaction bed temperature of the measurement is adjusted with a thermostat. Two thermocouples (T1 and T2, Figure 1-3) measure the temperature progression inside the bulk and of the sample reactor. Whereas during the PCI experiment the mass flow controller defines the generated thermal power inside the reaction bed, the thermal power generation during the kinetics measurement depends on the intrinsic reaction kinetics of the respective sample. Due to the generally very fast reaction kinetics, special measures are necessary to keep the system as close as possible to the desired temperature. In general, very small samples are used for kinetics measurements (e. g. 1 g) as the generated heat is proportional to the sample mass. Additionally, the heat and mass transfer inside the reaction bed must be sufficient.

2.1.1 Test bench for reaction bed characterisation

The underlying principle of this test bench is the investigation of the hydrogen absorption as a function of time (reaction bed dynamics) after a sudden hydrogen pressure increase (step function, see chapter 1.2.1).

The hydrogen part of the test bench shown in Figure 2-1 is similar to the set-up for PCI and intrinsic reaction kinetics measurements (see chapter 1.2.1). The technique used to investigate the hydrogen uptake of the reaction bed is based on the volumetric measurement principle. The hydrogen part of the set-up (Area 1 and 2 in Figure 2-1) consists of absolute pressure sensors (p1 and p2), a differential pressure sensor (Δp), hydrogen volumes and several thermocouples (T3-T6). The metal hydride temperature is measured by the thermocouple (T7). Its main difference in comparison to the set-up for PCI measurements is the bigger metal hydride mass (~ 900 g) and its quantity of hydrogen uptake. In order to keep the pressure changes reasonably small, hydrogen bottles of a total volume of 51.6 l are used.

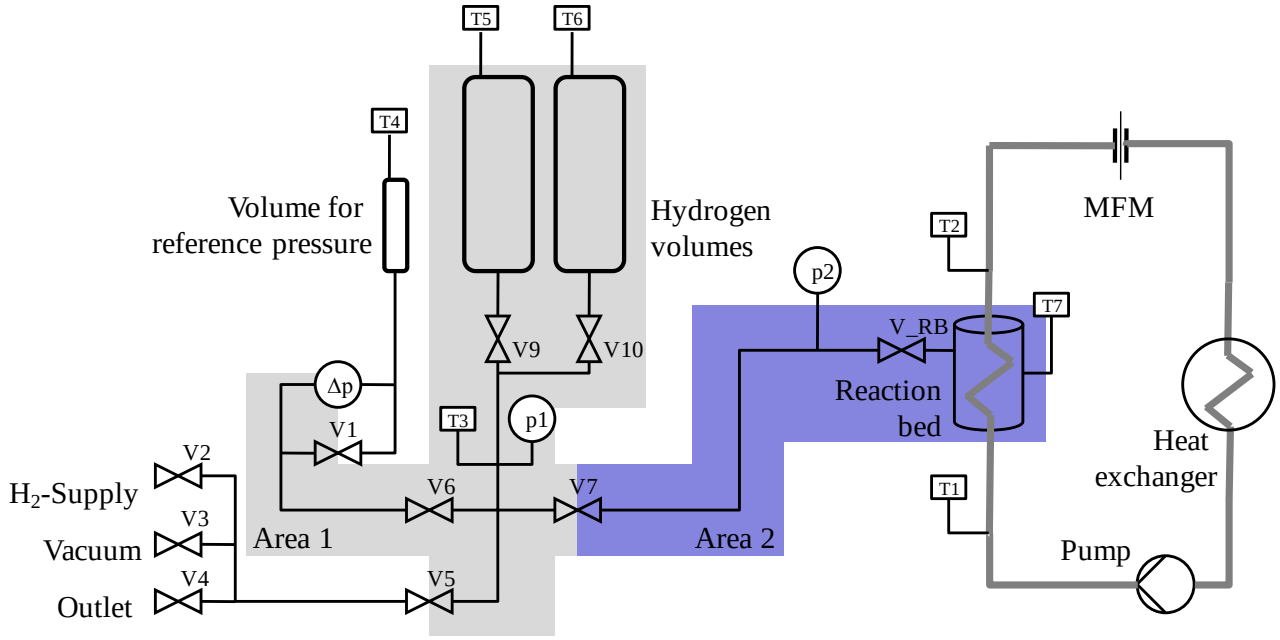

Figure 2-1: Schematic flow diagram of test bench for reaction bed dynamics measurement (Area 1 in grey; Area 2 in blue)

The hydrogen side (thin lines, Figure 2-1) of the set-up is divided into two areas (Area 1 and 2) by a manually operated hydrogen valve (V7). At the beginning of the measurement, the reaction bed valve (V_RB) and valve V7 are open and area 2 of the system including the reaction bed is evacuated. As soon as a sufficient vacuum is reached, valve V7 is closed and area 1 including the hydrogen volumes is filled with hydrogen up to the necessary pressure for the respective experiment. After a short time interval (~ 5 min), the hydrogen gas is in equilibrium state and valve V1 is closed. The initial mass of hydrogen ($m_{H2,\ initial}$) available in the set-up can then be calculated with equation (2-1) based on the ideal gas law and a real gas factor Z(p,T) that accounts for the non-

ideal behavior of hydrogen at higher pressures:

$$m_{H_2,initial} = \frac{p1_{initial} \cdot V_{Area1} \cdot M_{H_2}}{Z(p,T) \cdot R \cdot T3} \qquad (2\text{-}1)$$

with the volume of area 1 V_{Area1}, the universal gas constant R, the molar mass of hydrogen M_{H2} and measured absolute pressure and temperature $p1_{initial}$ and T3, respectively. The calculation procedure of the real gas factor for hydrogen Z(p,T) is given by Friedlmeier [9] and Fu [72].

The experiment starts with the manual opening of valve V7 as it leads to a sudden pressure increase in area 2 that is used as step function for the reaction bed dynamics measurement. As hydrogen is now distributed within the complete set-up (area 1 and 2) and the metal hydride starts to absorb, the mass balance for hydrogen is given by equation (2-2):

$$m_{H_2,initial} = m_{H_2,Area1}(t) + m_{H_2,Area2}(t) + m_{H_2,MeH}(t) \qquad (2\text{-}2)$$

with the mass of hydrogen $m_{H2}(t)$ in the respective areas and the absorbed mass of hydrogen in the metal hydride $m_{H2,\,MeH}(t)$ as functions of time. The differential pressure sensor (Δp) measures the pressure difference between the pressure at beginning of the measurement ($p1_{initial}$) and the pressure p1 as a function of time. Therefore, the amount of hydrogen stored in the metal hydride can be calculated by equation (2-3):

$$m_{H_2,MeH} = m_{H_2,Area1}(\Delta p, T3) - m_{H_2,Area2}(p_2, T7) \qquad (2\text{-}3)$$

where the first term gives the change of hydrogen mass within area 1 as a function of the pressure difference Δp and the gas temperature T3. The second term accounts for the gaseous hydrogen in area 2 as a function of the absolute pressure sensor p2 and the hydrogen gas temperature T7.

The amount of heat generated during the absorption of hydrogen is removed and measured with the water cycle of the test bench (thick lines). It consists of a heat exchanger, a water pump, a mass flow meter (MFM) and two resistance thermometers (T1, T2). The resistance thermometers (T1) and (T2) measure the temperature difference of the water between in- and outlet of the reaction bed. Together with the known heat capacity of water c_p, the measured flow rate $\dot{V}$ and the density of water ρ, the generated thermal power P can be calculated based on equation (2-4):

$$P = \dot{V} \cdot \rho \cdot c_p \cdot (T_2 - T_1) \qquad (2\text{-}4)$$

In Table 2-1, the description of the implemented measurement equipment is summarized. The hydrogen part of the system was verified by means of reference measurements and by comparison with experimental results of the PCI measurement set-up designed for precise determination of hydrogen uptake of small sample masses (see appendix). Figure 2-2 shows the picture of the test bench for reaction bed characterisation.

Table 2-1: Equipment of experimental set-up for reaction bed dynamics measurements

Component	Measurement range	Accuracy	Max. deviation
Resistance thermometers Pt 100	-100 to + 450 °C	± (0.15 + 0.002*T)	± 0.35 K (< 100 °C)
Thermocouples, Type K (reaction bed and ambient temp.)	-200 to + 900 °C	± 1.5 K / 0.4 %*T	± 1.5 K (0 to 50 °C)
Absolute pressure transducer Keller Druck, PA 23	0 to 50 bar	0.5 % F. S.	0.25 bar
Differential pressure transducer Keller Druck PD-23	± 10 bar	0.5 % F. S.	0.025 bar
Flow meter Kobold DFWM A	0 to 12.5 l/min	2.5 % F. S.	0.31 l/min
AGILENT Data Acquisition/Switch Unit (34970 A)			

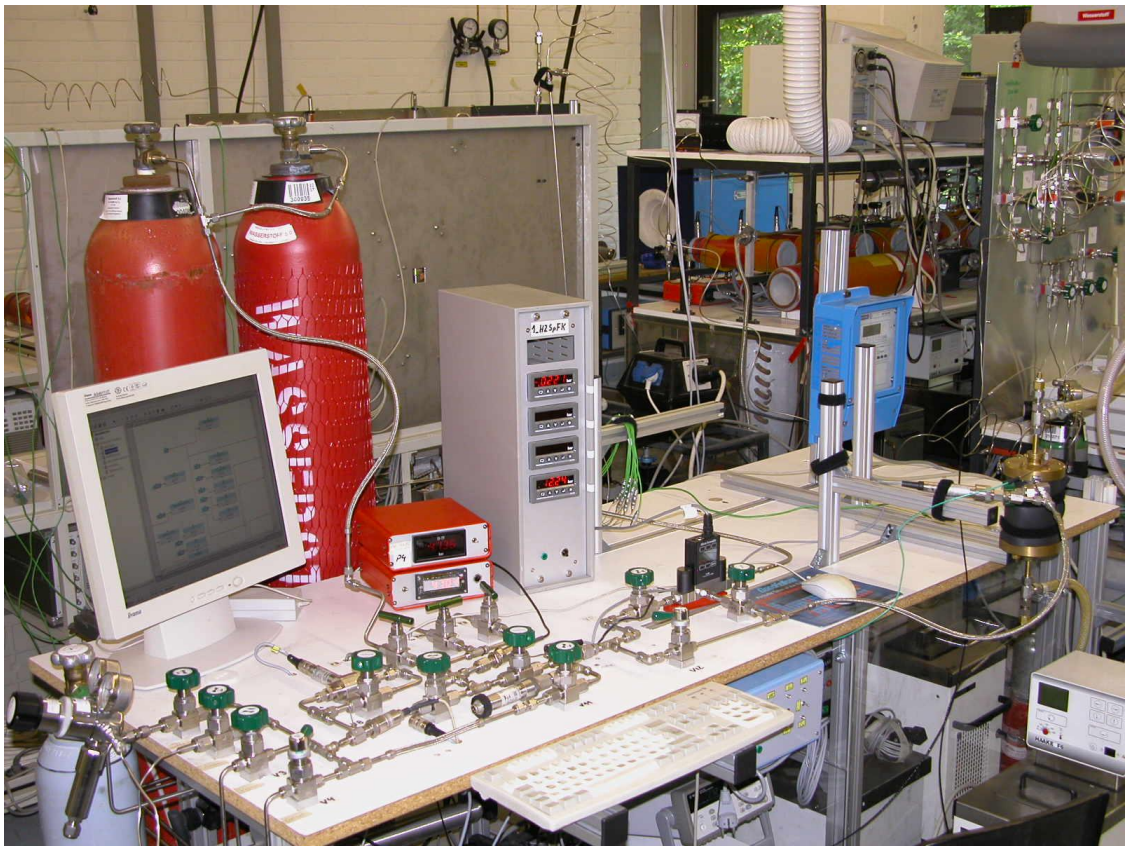

Figure 2-2: Test bench for reaction bed dynamics measurements

2.1.2 Test bench for coupled reaction bed measurements

The test bench for coupled reaction beds (Figure 2-3) consists of a hydrogen part (blue), the two reaction beds (A and B) and two separated water cycles (fully drawn and dashed line, respectively). The main component of the hydrogen part is the mass flow meter for hydrogen (MFM H_2) installed in the hydrogen connection pipe. Additionally, a pneumatically actuated hydrogen valve (V3) allows the separation of the reaction beds.

Each water cycle consists of a pump, a mass flow meter for water, two resistance thermometers, two electromagnetic 3-way valves (EMV 1-4) and two heat exchangers. The connected thermostats and electrical heaters, respectively (not shown in Figure 2-3) control the set-point temperatures of the heat exchangers. During regeneration mode, the necessary driving heat is supplied by the left heat exchanger (Q_{Heat}) in the water loop (dashed lines), whereas the left heat exchanger in the full-drawn loop rejects heat (Q_{Amb}) at simulated ambient temperature. Switching of the electro-magnetic valves leads to a temperature (and corresponding equilibrium pressure) change of the reaction beds.

During the following cooling half-cycle, the heat input (Q_{Cool}) at cooling temperature and heat rejection (Q_{Amb}) at ambient temperature are realized by the second heat exchanger in the respective water cycles. As pure water is used as heat carrier, the hot water cycle is pressurized to around 4 bar to prevent boiling at temperatures of around 130 °C.

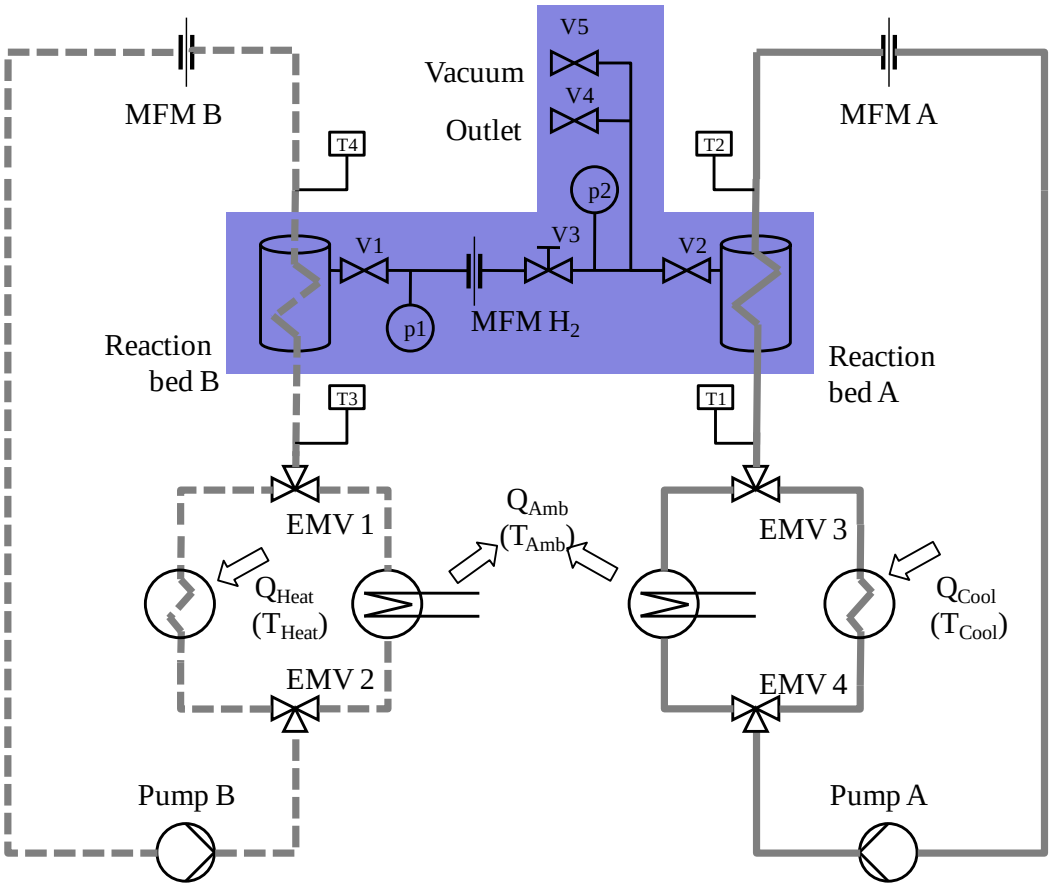

Figure 2-3: Schematic flow diagram of test bench for coupled reaction beds (hydrogen part in blue)

For a given half-cycle time (time between the switching of the electromagnetic valves) and adjusted heat exchanger temperature levels, the system is working automatically. A software program based on HP VEE Pro 6.2 (Agilent) realizes the controlling of the test bench. The description of the implemented measurement equipment is summarized in Table 2-2 and an uncertainty analysis of the relevant measurement parameters is given in the appendix.

Table 2-2: Equipment of experimental set-up for coupled reaction beds

Transducer	Measurement range	Accuracy	Max. Deviation
Resistance thermometers Pt 100	-100 to + 450 °C	± (0.15 + 0.002*T)	± 0.55 K (< 200 °C)
Absolute pressure transducer Keller Druck, PA 23	0 to 50 bar	0.5 % F. S.	0.25 bar
Mass flow meter (hydrogen) Hastings HFM-201	0 to 100 sl/min*)	± 1.3 % F. S.	1.3 sl/min
Flow meter (water) Krohne, IFS 6000F	0 to 14.97 l/min	± 0.3 % F. S.	0.045 l/min
AGILENT Data Acquisition/Switch Unit (34970 A)			

*) standard liter, for T = 0 °C and p = 1.013 bar

Figure 2-4 shows the picture of the test bench for coupled reaction bed measurements. The reaction beds are located in the middle of the system between the in- and outlet components made of brass. The required water management (pumps, heat exchanger and valves) is located below the test bench table and not visible on the picture.

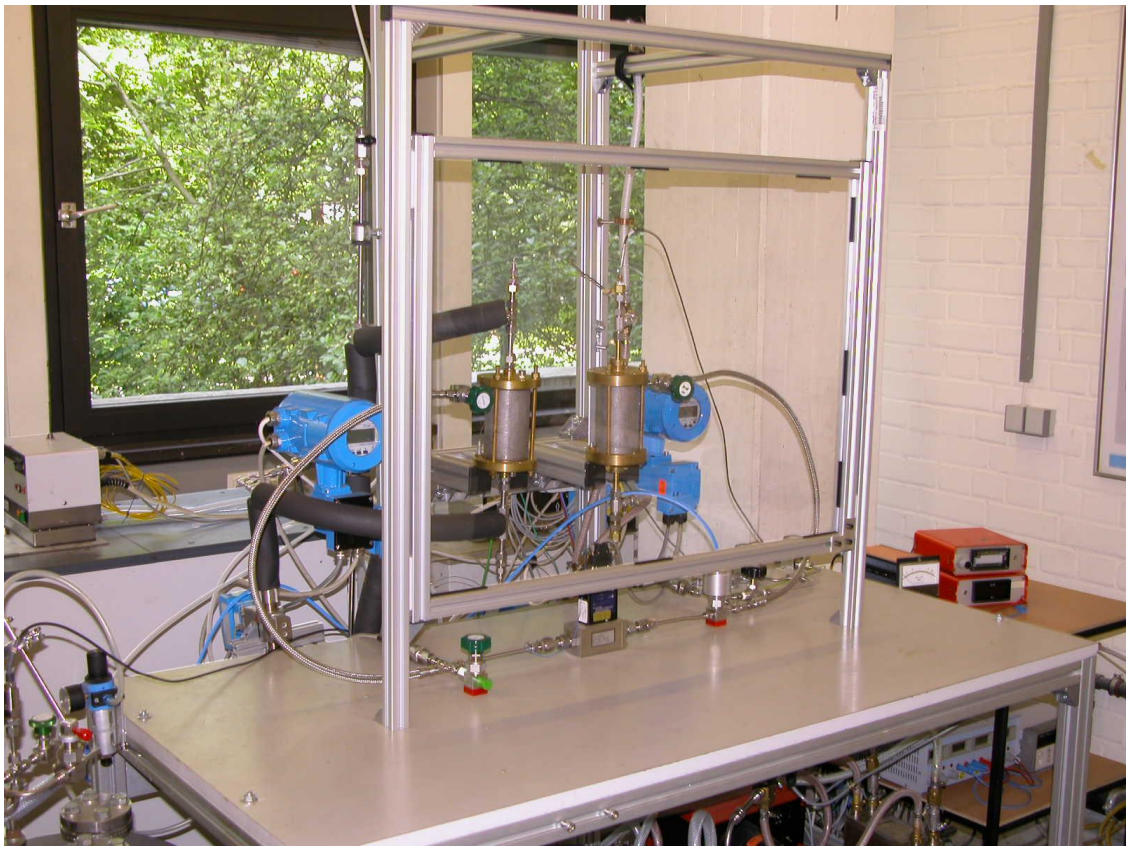

Figure 2-4: Test bench for coupled reaction bed measurements

2.2 Metal hydride reaction beds

2.2.1 Sample reactor for intrinsic metal hydride kinetics measurements

For intrinsic reaction kinetics measurements, the sample reactor (Figure 2-5) is kept in a water bath with constant temperature (thermostat). The main part of the sample reactor is a massive copper cylinder of 45 mm in diameter and 37 mm in length. The metal hydride powder is located in a 3 mm drill in the central axis. On the hydrogen supply side (right), a stainless steel tube is brazed into the cylinder and connected to the test bench with a VCR sealing. The VCR sealing contains a filter plate (0.5 µm) that prevents the discharge of metal powder and protects the measurement set-up. The opposite side of the cylinder is sealed with an O-ring and a screw. A thermocouple (diameter = 1 mm) is brazed through the screw and is located in the central axis of the drill. Therefore, it measures directly the metal hydride bulk temperature.

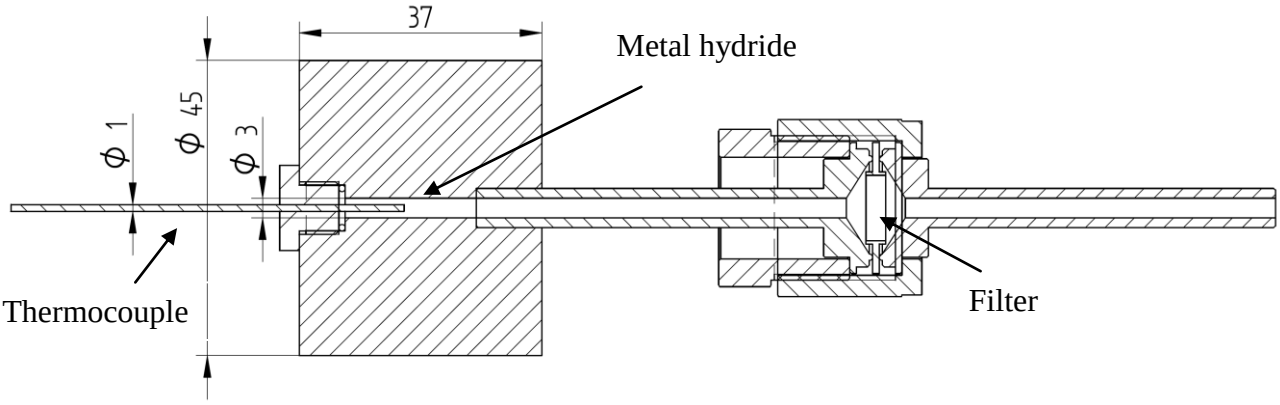

Figure 2-5: Reaction bed for intrinsic kinetics measurement

Between 0.5 g and 1 g of metal hydride is filled into the reaction bed, depending on the density of the powder bulk. The massive copper block is used to absorb the necessary reaction enthalpy in order to prevent an influence of the external heat transfer (reaction bed to the water) on the temperature of the reaction.

Based on the known maximum storage capacity x_{max}, the sample mass m_{MeH} and the reaction enthalpy of the investigated metal hydride ΔH, the amount of released heat during absorption Q can be calculated according to equation (2-5):

$$\Delta H \cdot \frac{x_{\max}}{100} \cdot \frac{m_{MeH}}{M_{H_2}} = Q = m_{Cu} \cdot c_{p_{Cu}} \cdot \Delta T \qquad (2\text{-}5)$$

With the known specific heat capacity of copper c_{pCu} and the accepted temperature difference of the copper bulk ΔT during the absorption, the necessary copper m_{Cu} mass can be calculated. Therefore, the external heat transfer (from the reaction bed to the water) can be neglected as it is not influencing the requested isothermal measurement conditions inside the sample reactor.

However, the internal heat transfers from the powder to the copper wall as well as the conductivity of the powder bed still determine the maximum heat transfer. As fast intrinsic reaction kinetics lead to a high thermal power generation and consequently to a temperature increase of the alloy, the applicability of ensuring quasi-isothermal measurement conditions depends directly on the intrinsic reaction kinetics of the alloy and on the accepted temperature increase during the measurement. The reaction bed is able to keep the metal powder at nearly isothermal conditions ($\Delta T \leq 2$ K) for metal-

hydrogen-reactions absorbing hydrogen within around 150 s. If the reaction is faster, the heat generation exceeds the heat transfer capability of the bed, which leads to an increase of the metal powder temperature ($\Delta T > 2$ K).

Figure 2-6 shows the picture of the sample reactor for intrinsic reaction kinetics measurements with the reaction bed valve, the copper block and the VCR-connection containing the filter.

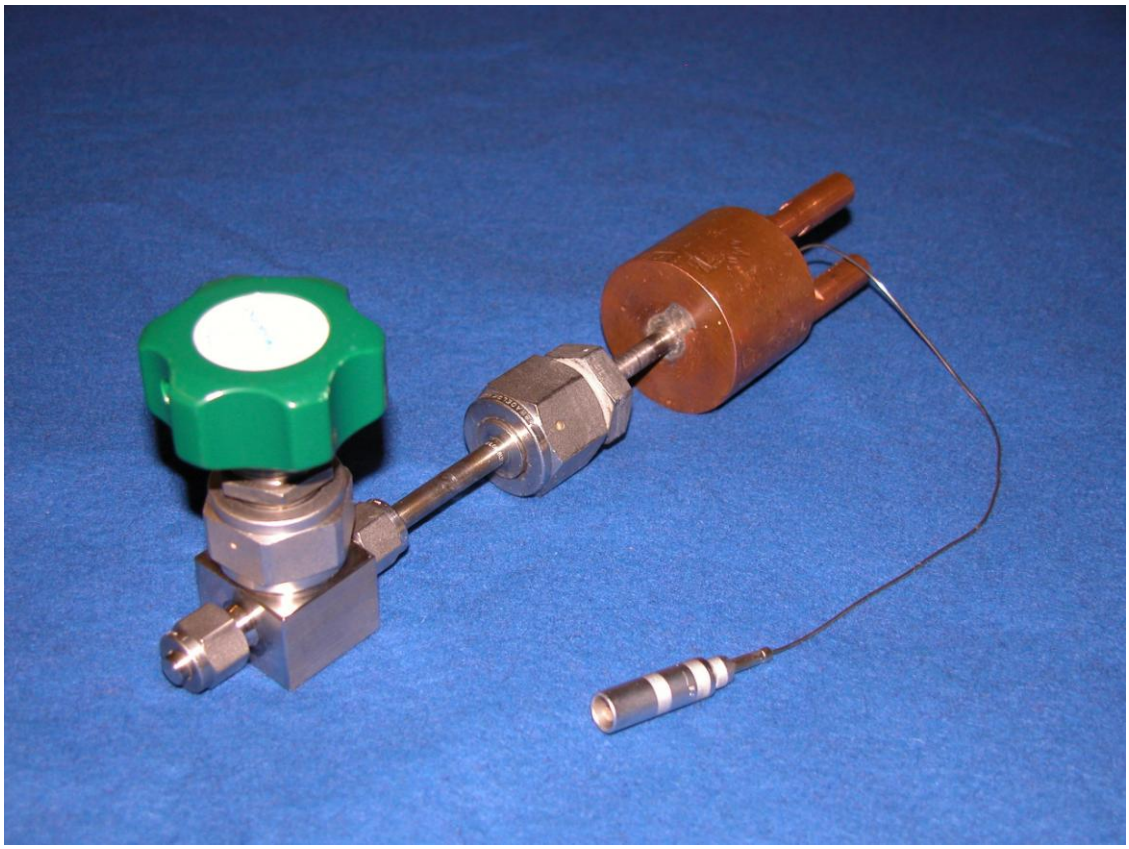

Figure 2-6: Sample reactor for intrinsic reaction kinetics measurements

2.2.2 Capillary tube bundle reaction bed

In order to reutilize main components, the original reaction bed (constructed at IKE in 1994) was dismantled and the inner part containing the capillary tube bundle surrounded by the filter tube was opened to discharge the old metal powder. After reassembling the bed with a new containment construction and hydrogen supply connection, it was charged with the respective alloys. Due to the

new design of the capillary tube bundle reaction bed, the metal hydride powder can be removed without dismantling.

The main part of the reaction bed is the capillary tube bundle heat exchanger shown in Figure 2-7 that consists of 372 stainless steel tubes with a length of 123 mm and an inner diameter of 1.4 mm (d_o = 1.8 mm).

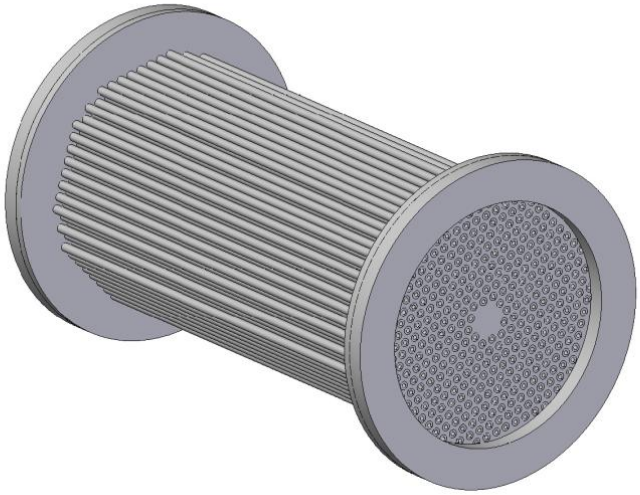

Figure 2-7: Capillary tube bundle of the reaction bed

The heat carrier flows through the capillary tubes that are surrounded by the loosely distributed metal powder. The total heat transfer surface (total inner surface of the capillary tubes) is around 0.2 m^2.

In order to prevent discharge of the metal powder, a sintered metal filter tube surrounds the capillary tube bundle (see Figure 2-8). Its filter mesh is 1 µm.

Figure 2-8: Tube bundle surrounded by the sintered metal filter tube

The capillary tube bundle with filter tube is surrounded by the reaction bed containment (see Figure 2-9). The formed annular gap (width ≈ 3 mm) between the cladding tube and the inner filter tube facilitates the axial hydrogen distribution Therefore, one hydrogen supply connection is sufficient.

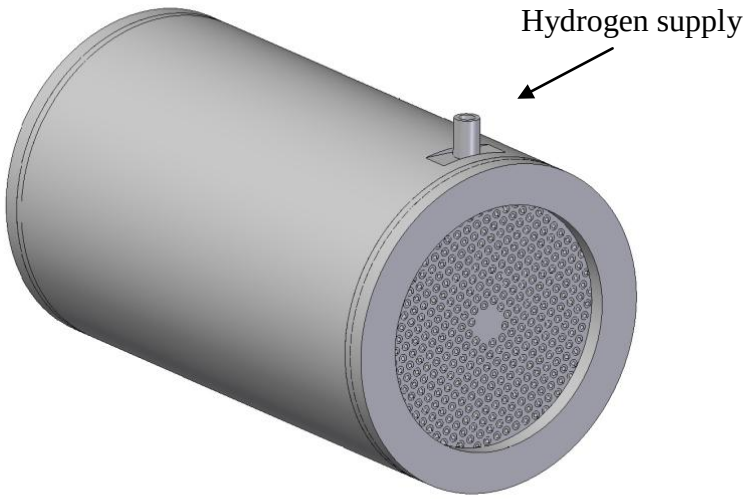

Figure 2-9: Capillary tube bundle reaction bed

The total length of the assembled reaction bed is 135 mm. With an outer diameter of 76 mm the total volume of the reaction beds is around 0.6 l. Its weight without metal powder is around 1.7 kg. The volume within the sintered metal tube ($V_i \approx 0.23$ l) is sufficient to charge 800-1000 g of powder, depending on the density of the alloy. In Figure 2-10, a picture of the capillary tube bundle reaction bed with reaction bed valve is shown.

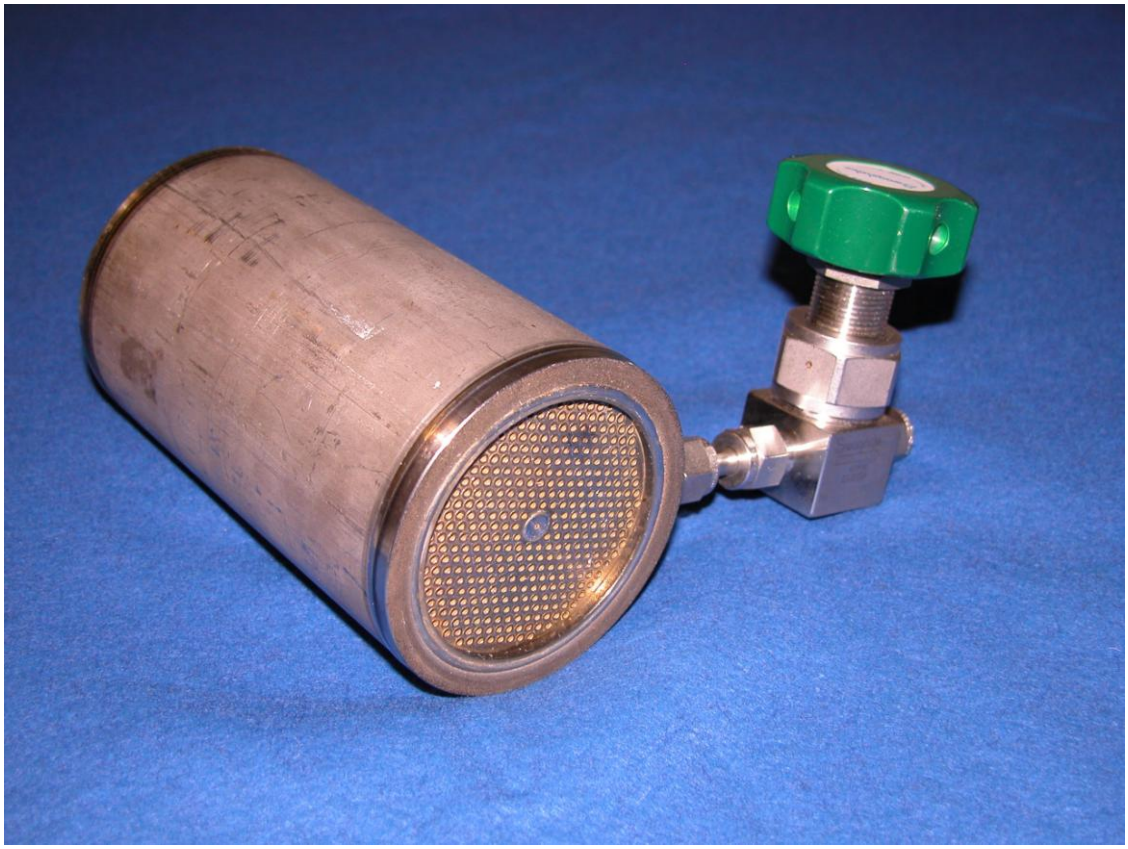

Figure 2-10: Capillary tube bundle reaction bed

3 Experimental results

3.1 Characterisation of metal hydrides

3.1.1 PCI measurements

PCI measurements of available alloys are necessarily the first steps of a sorption system design as they reveal the metal hydride properties that consequently define the working conditions of the system. Even though experimental data are available for a variety of metal hydride alloys, a detailed examination of the respective metal hydride characteristics is important. Especially hysteresis, plateau pressure and slope depend on the compositions of the used misch metal (= Mm, mainly Cr and La) or the respective production processes and are only to a certain extent predictable. Therefore, PCI measurements of around 20 different alloys partly done in a previous study [68] and completed within this work form the basis for the realization of the sorption cooling system. Figure 3-1 shows deduced van't Hoff plots of selected metal hydrides. Due to a clear arrangement, only alloys with acceptable PCI characteristic are considered of which only one van't Hoff plot is drawn for each material.

Although neglecting other important characteristics, like storage capacity, hysteresis and plateau slope, this figure provides an overview of the adaptability of metal hydrides. Equilibrium pressures of $LaNi_5$ and $MmNi_5$, respectively can be almost precisely varied by alloyed substituting elements, e.g. Fe or Al [7, 14]. The 'C-alloys' are based on the alloy $TiMn_2$ with various substituting elements. The respective number represents the Zr amount in the A-metal lattice. The equilibrium pressure of the alloy decreases with increasing amount of Zr as the occupation of interstitial sites is facilitated due to the larger atomic diameter of Zr [73].

Taking all measureable PCI characteristics, like equilibrium pressure, plateau slope and hysteresis of the investigated alloys into account, the most favourable metal hydride is $LmNi_{4.91}Sn_{0.15}$. Additionally, due to its moderate equilibrium pressure, the alloy can be used as "A" or as "B" metal hydride for the sorption cooling system (see Figure 1-16).

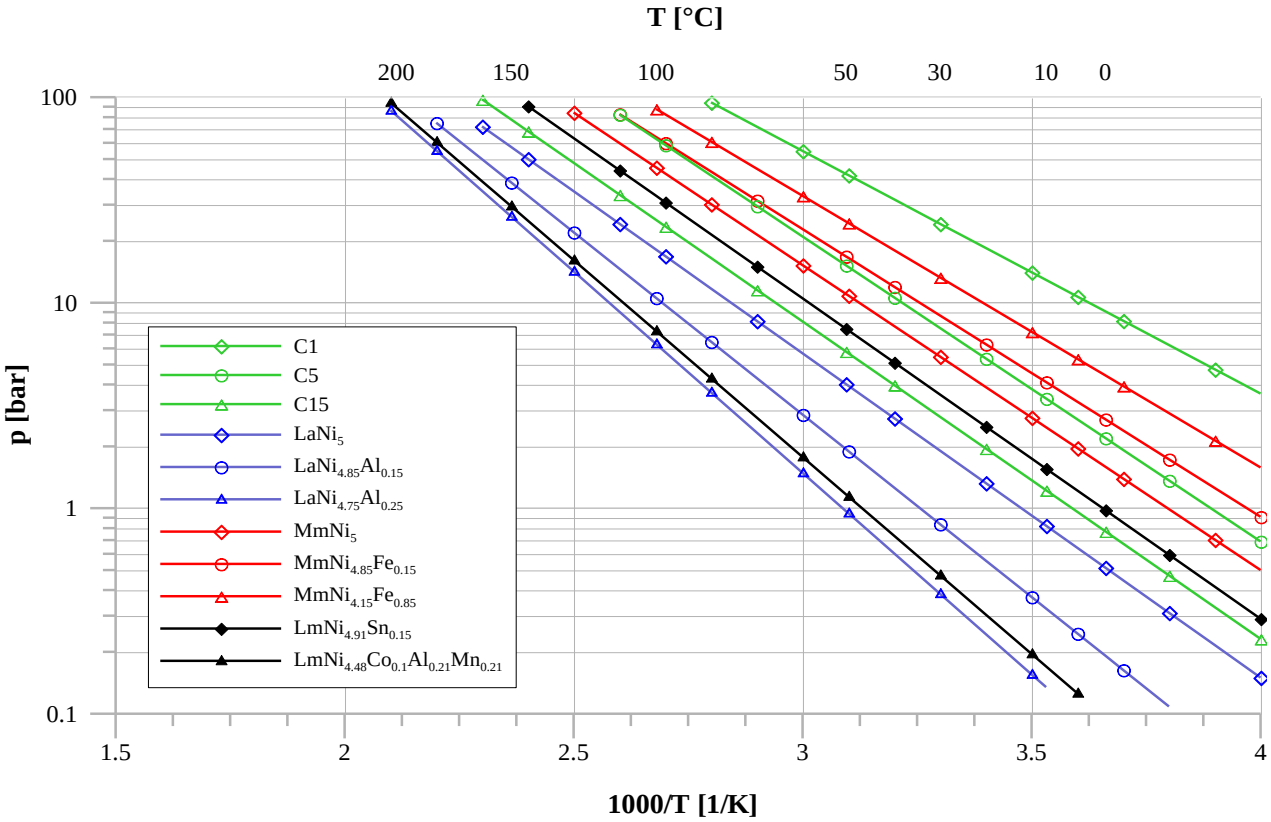

Figure 3-1: Van`t Hoff plots of chosen experimentally examined metal hydrides

However, the most important parameter for an automotive cooling system, the specific cooling power, depends on the design of the reaction bed as well as on the intrinsic reaction kinetics of the applied metal hydrides. Here, the C-alloys are clearly favorable as their intrinsic reaction kinetics were reported to be faster than the one of AB_5 materials [12]. Based on its PCI characteristics, the most suitable "A" metal hydride of this group is $Ti_{0.99}Zr_{0.01}V_{0.43}Fe_{0.09}Cr_{0.05}Mn_{1.5}$ (C1).

PCI measurement and experimental details of $LmNi_{4.91}Sn_{0.15}$

The metal hydride was delivered and stored as powder (particle size < 1 mm) under Argon-atmosphere in a glove box device. Activation of the alloy was carried out over night at room temperature and at medium hydrogen pressure (~ 20 bar). Figure 3-2 shows the experimental PCI measurement on the volumetrically measuring set-up (see chapter 1.2.1). The examined storage capacity at 27 °C is 1.30 % and decreases with increasing temperature (1.25 % at 42 °C resp. 1.15 % at 100 °C). The hysteresis effect is comparably small but the plateau slope increases towards the end of the plateau region.

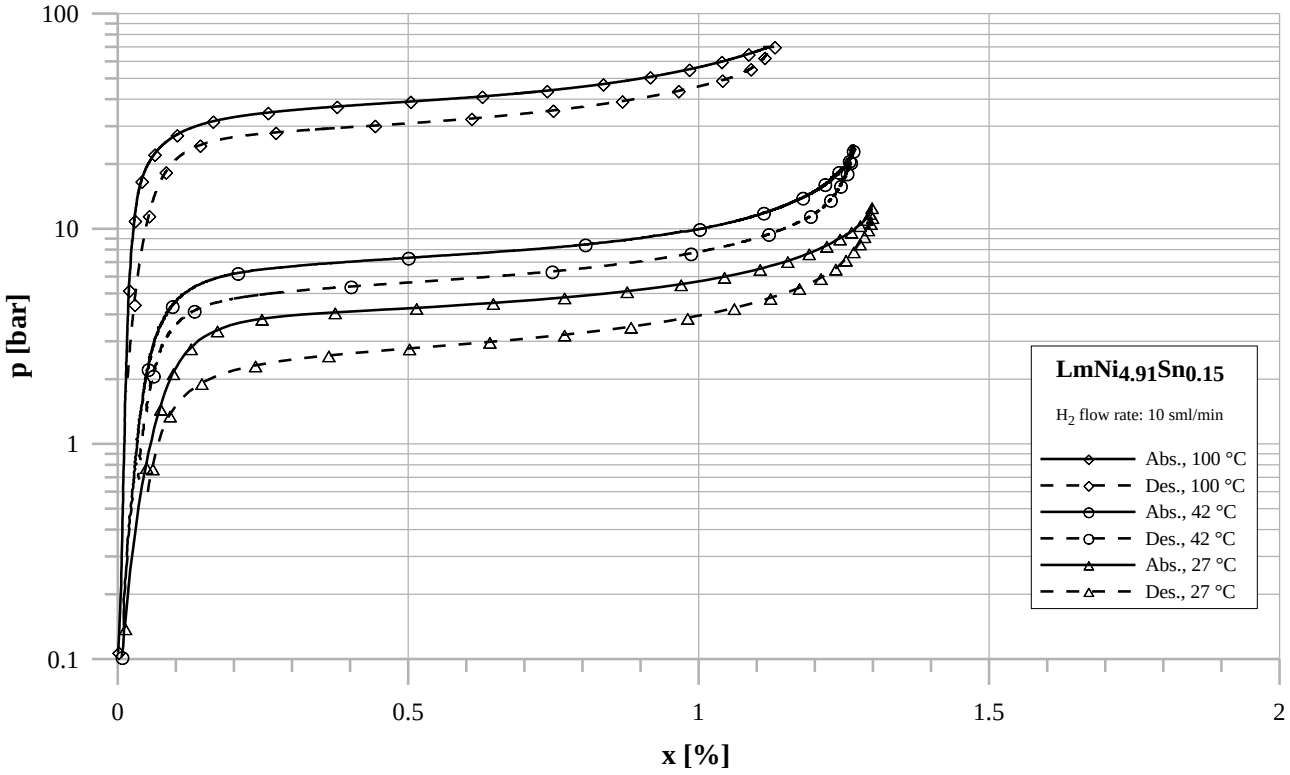

Figure 3-2: PCI measurements of $LmNi_{4.91}Sn_{0.15}$

Based on the PCI data, the characteristic properties of the alloy were calculated. The data given in Table 3-1 are average values as they depend on the calculation model as well as on the load situation of the respective hydride [74, 75].

Table 3-1: Metal hydride properties of $LmNi_{4.91}Sn_{0.15}$

	Absorption	Desorption
Reaction enthalpy [J/mol]	- 27411	- 29849
Reaction entropy [J/(mol K)]	- 103.9	- 109.1
Plateau slope factor [-]	0.43	0.48
Density [kg/m^3]	8.1	

PCI measurement and experimental details of $Ti_{0.99}Zr_{0.01}V_{0.43}Fe_{0.09}Cr_{0.05}Mn_{1.5}$

This material was also delivered and stored as powder (particle size < 1 mm) under Argon-atmosphere in a glove box device. Activation of this metal hydride was more complicated in comparison to the AB_5 alloy $LmNi_{4.91}Sn_{0.15}$: After evacuation over night at about 150 °C, a hydrogen pressure of 50 bar was applied on the metal powder and its temperature was decreased to 5 °C (by means of a thermostat). The first absorption process started slowly and took several days until the material reached its maximum storage capacity of 1.75 % at 5 °C (Figure 3-3). The experimental PCI results show a slightly decreasing storage capacity with increasing temperature (1.68 % at 35 °C) and, in comparison to the AB_5 alloy $LmNi_{4.91}Sn_{0.15}$, the storage capacity is around 25 % higher. However, the enlarged α-phase region reduces the useful storage capacity to around 1.2 % [73]. In comparison to the AB_5 alloy, the hysteresis is higher but the plateau slope is constant over the whole plateau region. An interesting characteristic of this alloy is the difference in the plateau slope between absorption and desorption - the pressure difference in the plateau region between absorption and desorption is smaller at the beginning than towards the end of the plateau (plateau slope factor m_{Pl} = 0.42 for absorption and 0.22 for desorption).

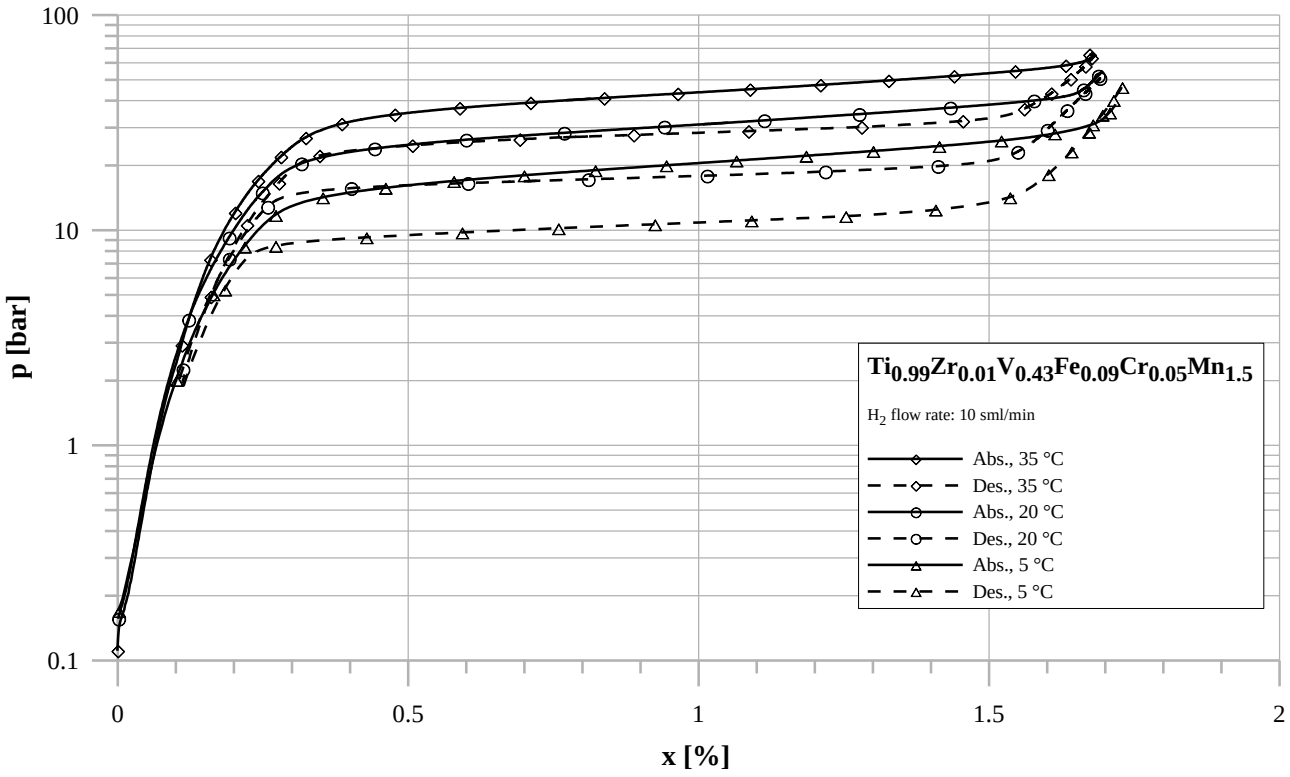

Figure 3-3: PCI measurements of $Ti_{0.99}Zr_{0.01}V_{0.43}Fe_{0.09}Cr_{0.05}Mn_{1.5}$

Based on the PCI data, the characteristic properties of the alloy were calculated and are summarized in Table 3-2. The given data for this material depends also on the calculation model as well as on the load situation of the respective hydride [74, 75].

Table 3-2: Material properties of $Ti_{0.99}Zr_{0.01}V_{0.43}Fe_{0.09}Cr_{0.05}Mn_{1.5}$

	Absorption	Desorption
Reaction enthalpy [J/mol]	- 17922	- 22606
Reaction entropy [J/(mol K)]	- 89.2	- 101.1
Plateau slope factor [-]	0.42	0.22
Density [kg/m^3]	6.3	

3.1.2 Intrinsic kinetics measurements

The second part of the metal hydride characterisation for the automotive cooling system is the intrinsic reaction kinetics measurement of the alloys. As the dynamics of the reaction bed can also be affected by the intrinsic reaction kinetics, this part of the metal hydride characterisation is very important for the understanding of the reaction coherences within fast metal hydride reaction beds. However, external factors like impurities on the surface of the powder (storing method) or different production and annealing conditions affect the reaction rate. Therefore, measurement data from literature can be used as indication for the intrinsic reaction kinetics but in order to be able to compare properly different reaction rates, intrinsic reaction kinetics measurements of the original samples are necessary.

Based on the assumption that the intrinsic reaction kinetics depends on the reaction temperature and obeys Arrhenius law (see chapter 1.2.1), it can be reasonably assumed that the reaction kinetics of the "B" metal hydride is sufficiently fast at high temperatures (T_{Heat}) and does not limit the regeneration phase of the sorption system. Therefore, the important parameter for an application in the cooling system is the intrinsic reaction kinetics of the alloys at ambient temperature and below.

A general problem of the volumetric measurement method derives from the abrupt disturbance of

the equilibrium in the system (intrinsic reaction kinetics measurement, see chapter 1.2.1). The high pressure difference (between Area 1 and Area 2, Figure 1-3) leads to high hydrogen flow rates and coherently to accuracy problems of the experimental set-up. The measurement of the metal hydride temperature (T_{MeH}) is not affected. The time necessary to stabilize the system (delay time) depends mainly on the original pressure difference. Until the measurement set-up works properly, the progression of the time dependent hydrogen uptake possesses a peak that is negligible as it is an inherent characteristic of the measurement process. Therefore, the plotted data is reduced to values derived from the stabilized measurement system. Additionally, the measured intrinsic kinetics data are plotted as reacted fraction according to equation (1-6). The important value deriving from the different kinetics measurements, the necessary time to reach equilibrium (no further hydrogen uptake), is not affected by the normalisation.

As the intrinsic reaction kinetics depends on the applied pressure difference between equilibrium and gas pressure and, according to the Arrhenius relation, on the reaction temperature, both parameters have been varied for ab- and desorption reactions of both alloys.

$\boldsymbol{LmNi_{4.91}Sn_{0.15}}$

The intrinsic kinetics measurements were performed using 1.0 g of $LmNi_{4.91}Sn_{0.15}$ in the sample reactor described in chapter 2.2.1 and measured on the volumetric measurement set-up for PCI measurements (chapter 1.2.1). The characteristic time of the respective measurement is derived with an adapted exponential function based on equation (1-7) that is shown in grey.

Pressure dependency for the absorption reaction

The pressure dependency of the reacted fraction and the metal hydride temperature development is shown in Figure 3-4. For all experiments, the initial metal hydride temperature (T_{MeH}) is 28 °C at the beginning of the reaction. Fully drawn lines represent the reacted fraction (left y-axis) and dashed lines correspond to the temperature (right y-axis). The time is given by the x-axis. Comparing the respective metal hydride temperatures (T_{MeH}), a quasi-isothermal condition (< 2 K) is only achieved for the measurement with the lowest hydrogen gas pressure. During the fastest measurement with 17 bar hydrogen pressure, the metal hydride temperature reaches 33 °C ($\Delta T \sim 5$ K). However, as the metal hydride temperature is constantly increasing until the absorption reaction is over, the reaction kinetics is still limited by intrinsic and not by heat transfer processes [76].

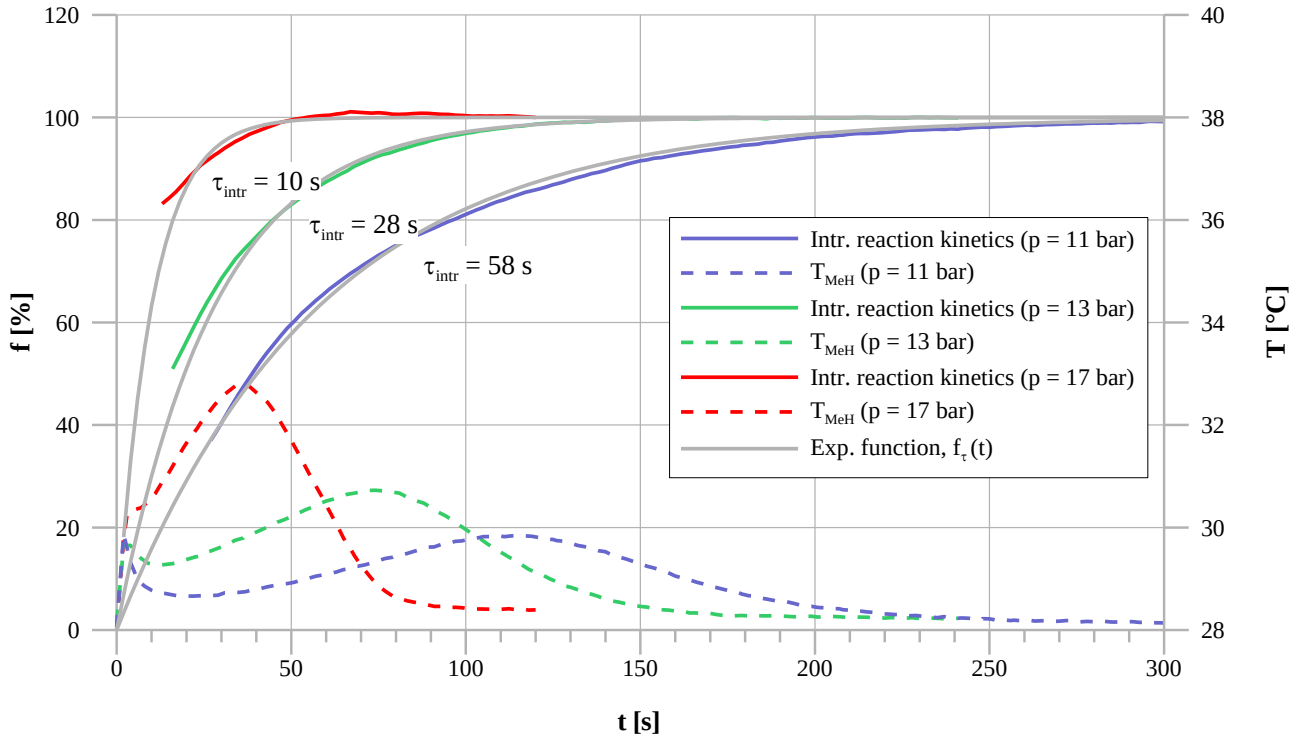

Figure 3-4: Absorption kinetics of $LmNi_{4.91}Sn_{0.15}$ at 28 °C initial metal hydride temperature

Whereas the characteristic time for absorption with a hydrogen pressure of 11 bar is 58 s, the same reacted fraction is reached after 10 s for a hydrogen pressure of 17 bar. A comparison of intrinsic reaction kinetics or reaction bed dynamics is therefore only reasonable if the applied hydrogen pressures are comparable or taken into account (see chapter 1.2.2).

The measured time spans for the reaction kinetics of $LmNi_{4.91}Sn_{0.15}$ agree to the measured kinetics of similar AB_5 metal hydrides that are in the order of 90-200 s for complete absorption [47, 57, 77, 78]. If Al is used as substituting element in AB_5 alloys the reaction kinetics of the metal hydride can be even faster because the reaction rate increases with increasing Al content [78, 79]. However, an increasing amount of Al reduces the equilibrium pressure of the metal hydride and changes its applicability (see Figure 3-1).

Temperature dependency for the absorption reaction

Figure 3-5 shows the temperature dependency of the intrinsic reaction kinetics of $LmNi_{4.91}Sn_{0.15}$. The left y-axis gives the reacted fraction and corresponds to the fully drawn lines. Comparing the PCI at a metal hydride temperature of 28 °C with the PCI at 40 °C (see Figure 3-2), the necessary

pressure to reach the end of the plateau region is 11 bar and 19 bar, respectively. Therefore, in order to reach comparable absorption conditions and load situations, a change of the reaction temperature (Arrhenius term in equation (1-5)) has necessarily be complemented by an adapted hydrogen pressure change. In order to reduce this influence of the pressure difference, the ratio of hydrogen pressure to equilibrium pressure (logarithmic term in equation (1-5)) was kept constant for both measurements:

$$\ln\left(\frac{p}{p_{eq}}\right) = const. \approx 0.875 \qquad (3\text{-}1)$$

The blue curve in Figure 3-5 corresponds to the already described intrinsic reaction kinetics measurement at 28 °C with a hydrogen pressure of 11 bar.

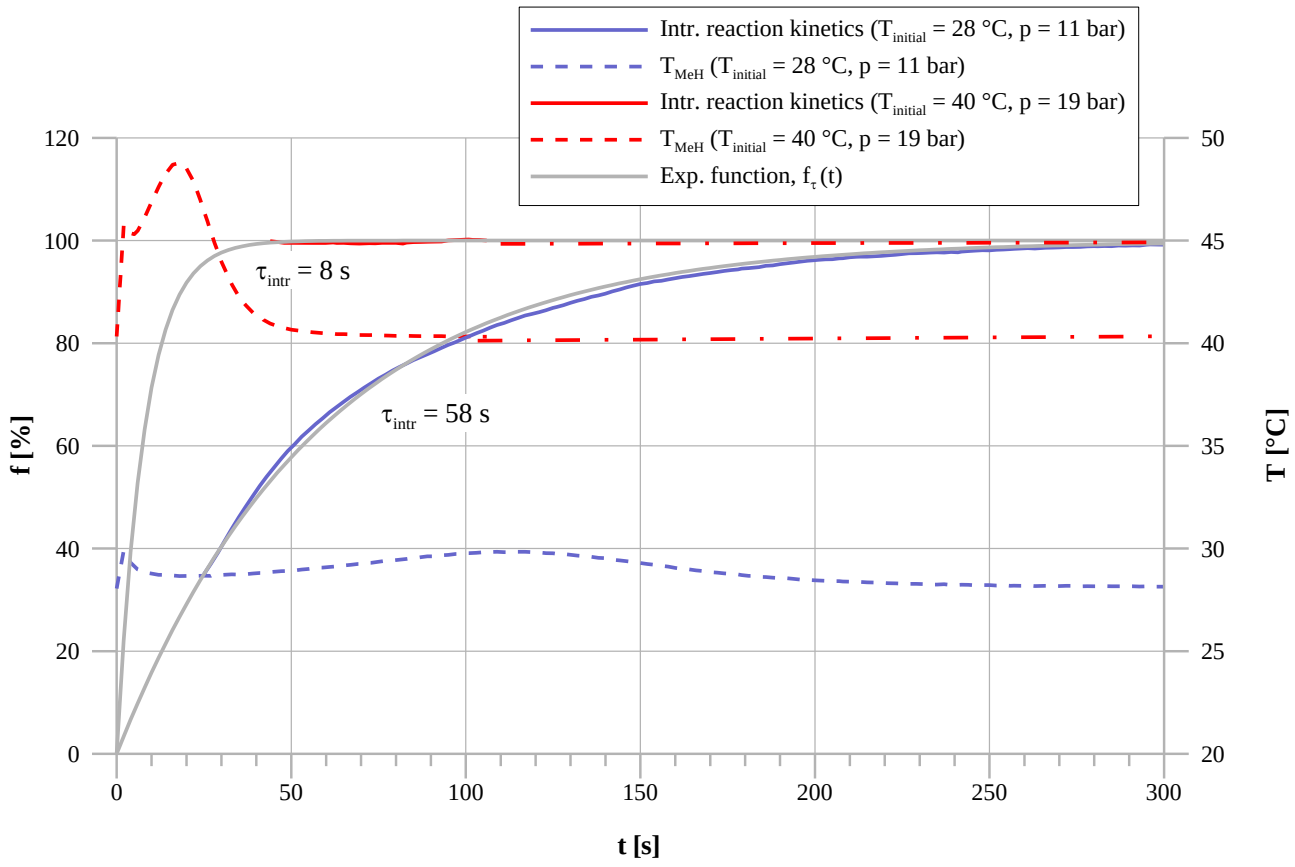

Figure 3-5: Temperature dependency of absorption kinetics of $LmNi_{4.91}Sn_{0.15}$

Due to the above described general problem of volumetric kinetics measurements, the hydrogen uptake cannot be measured at the beginning of the reaction. And as the reaction kinetics of the alloy at 40 °C (red curve) is already faster than the time necessary for a measurement, only a restricted result for this temperature condition is obtained: The time for full absorption is less than 30-40 s and the temperature increase during the reaction is around 8 K (dashed lines, right y-axis). Based on the metal hydride temperature development, the characteristic time of the reaction can be estimated to around 8 s.

Kinetics measurements at higher metal hydride temperatures are not reasonable, as the reaction is faster and the necessary increased pressure difference even extends the delay time of the measurement.

Desorption reaction

All desorption experiments of $LmNi_{4.91}Sn_{0.15}$ were preformed against nearly vacuum. Although, this method possesses the drawback that different equilibrium pressures (at different temperatures) cannot be avoided, desorption against vacuum generally represents the fastest possible desorption reaction. Therefore, the intrinsic desorption kinetics shown in Figure 3-6 correspond to the fastest desorption reaction that can be reached by $LmNi_{4.91}Sn_{0.15}$. Based on the measured reacted fraction progressions shown as fully drawn lines (left y-axis), the intrinsic desorption kinetics is accelerated with temperature. Due to the endothermic desorption reaction, the metal hydride temperature decreases during the reaction (dashed lines, right y-axis).

The characteristic time of the desorption reaction at 28 °C is 48 s and is reduced to 28 s and 12 s at a reaction temperature of 40 °C and 60 °C, respectively. Therefore, a complete desorption (> 99.5 %) of $LmNi_{4.91}Sn_{0.15}$ at 28 °C takes more than 250 s.

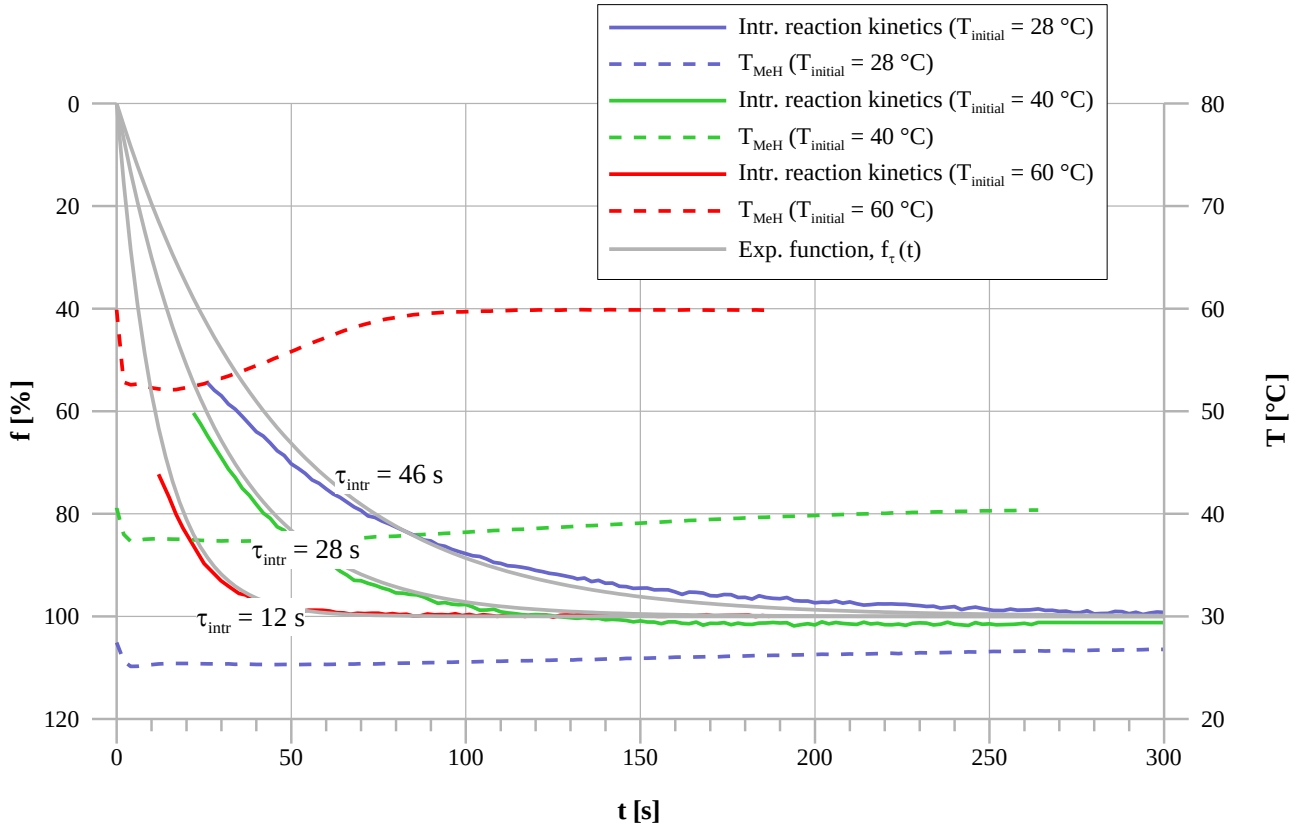

Figure 3-6: Desorption kinetics measurements of $LmNi_{4.91}Sn_{0.15}$ (into vacuum)

Forde *et al.* [80] measured a comparable behavior of an AB_5 alloy but with clearly faster desorption kinetics. Full desorption at 3 °C took around 150 s and was reduced to less than 10 s for a metal hydride temperature of 45 °C. One reason for the faster intrinsic reaction kinetics might be the high Al-content of the used alloy ($La_{0.83}Ce_{0.10}Pr_{0.04}Nd_{0.03}Ni_{4.40}Al_{0.60}$).

$Ti_{0.99}Zr_{0.01}V_{0.43}Fe_{0.09}Cr_{0.05}Mn_{1.5}$

Due to the lower density in comparison to $LmNi_{4.91}Sn_{0.15}$, the sample reactor for intrinsic reaction kinetics measurements was filled with 0.7 g of $Ti_{0.99}Zr_{0.01}V_{0.43}Fe_{0.09}Cr_{0.05}Mn_{1.5}$. However, due to the higher equilibrium pressure of the reaction, the time span until a proper measurement of the reacted fraction is possible is extended for this material.

Absorption reaction

Figure 3-7 shows the absorption kinetics of $Ti_{0.99}Zr_{0.01}V_{0.43}Fe_{0.09}Cr_{0.05}Mn_{1.5}$ at different temperatures. The applied hydrogen pressures have been adapted to the pressure at the end of the respective plateau (depending on the temperature, see PCI in Figure 3-3). The reacted fraction is shown on the left y-axis and corresponds to the fully drawn lines. Due to the high hydrogen pressures (e. g. 50 bar at 35 °C) in comparison to the low-pressure alloy $LmNi_{4.91}Sn_{0.15}$ and the additional small sample mass (0.7 g), the measured data of the storage capacity is strongly fluctuating.

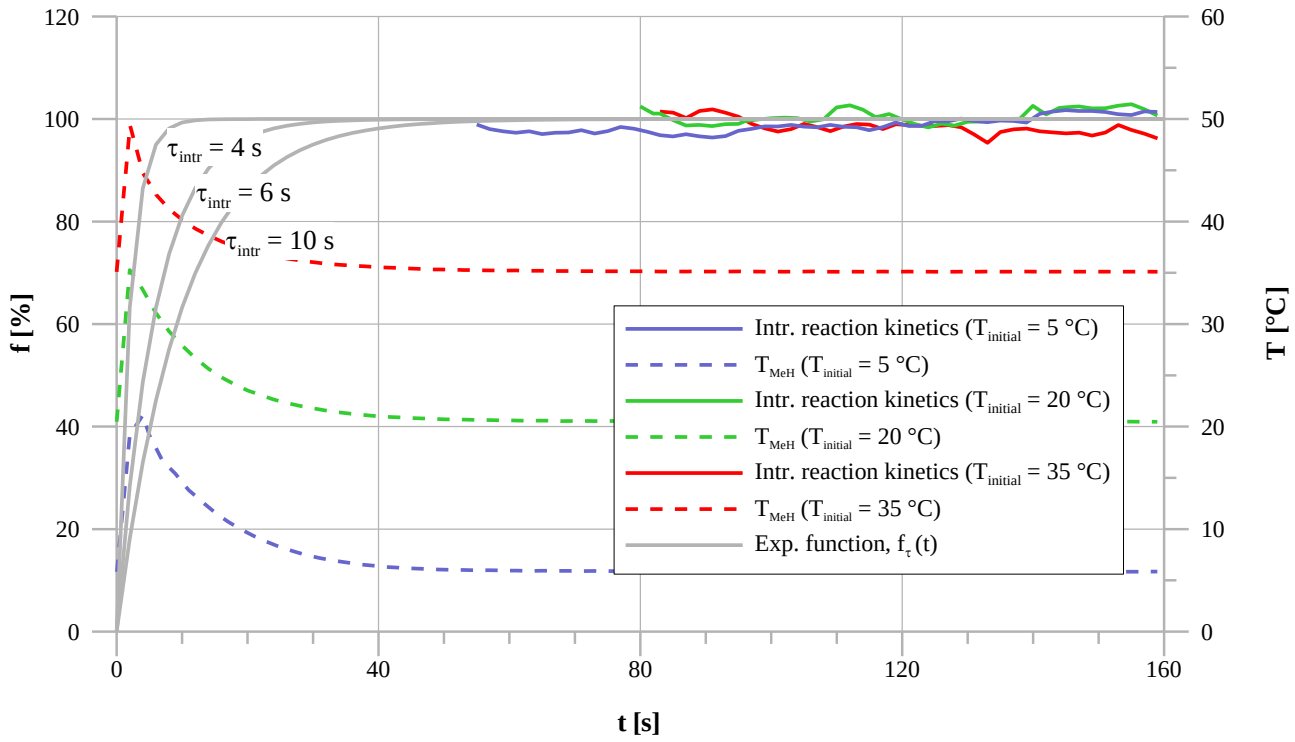

Figure 3-7: Absorption kinetics of $Ti_{0.99}Zr_{0.01}V_{0.43}Fe_{0.09}Cr_{0.05}Mn_{1.5}$ (resp. pressure is based on PCI measurement)

Although the absorption at 5 °C is already completed when the test bench starts to measure properly, two main results can be derived from the measurement:

- The characteristic time of the respective reactions can only be estimated according to the metal hydride temperature development (T_{MeH}) during the reaction and is in the range of 4 to 10 s depending on the initial metal hydride temperature. However, the AB_2 alloy

$Ti_{0.99}Zr_{0.01}V_{0.43}Fe_{0.09}Cr_{0.05}Mn_{1.5}$ is fully loaded within less than 30 s, even at 5 °C. Cuevas *et al.* [81] published similar results for a $TiMn_2$-based alloy that reached 80 % of the maximum storage capacity within 4 s.

- In comparison to the investigated AB_5 alloy $LmNi_{4.91}Sn_{0.15}$ (τ_{intr} = 58 s at 28 °C), the absorption kinetics of $Ti_{0.99}Zr_{0.01}V_{0.43}Fe_{0.09}Cr_{0.05}Mn_{1.5}$ is clearly faster ($\tau_{intr} \approx$ 10 s at 10 °C).

Desorption reaction

Due to the high equilibrium pressure of the metal hydride and a better comparability with the application in sorption systems, the experimental data shown in Figure 3-8 are desorption experiments against a defined hydrogen pressure. The pressure corresponds to the left end of the plateau region (for desorption) at the respective temperature. Fully drawn lines represent the reacted fraction on the left y-axis. The temperature progressions are drawn as dashed lines and correspond to the right y-axis.

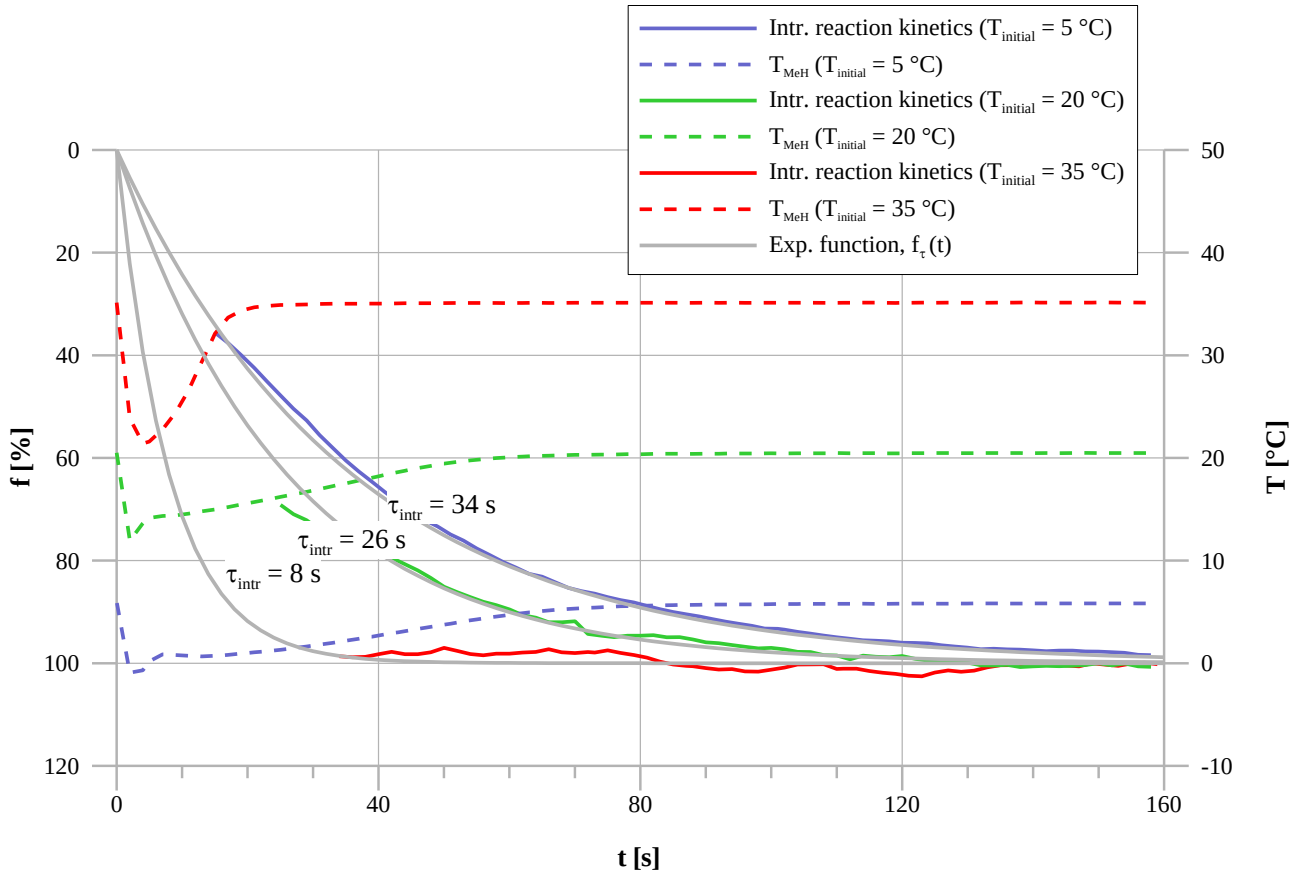

Figure 3-8: Desorption kinetics measurements of $Ti_{0.99}Zr_{0.01}V_{0.43}Fe_{0.09}Cr_{0.05}Mn_{1.5}$ (resp. pressure is based on PCI measurement)

The characteristic time of the desorption experiment at 5 °C is 34 s and is reduced to around 26 s at 20 °C. The desorption at 35 °C is again too fast to be measured properly but its characteristic time can be estimated in the order of 8 s. Comparable to the measurements with $LmNi_{4.91}Sn_{0.15,}$ the desorption kinetics of $Ti_{0.99}Zr_{0.01}V_{0.43}Fe_{0.09}Cr_{0.05}Mn_{1.5}$ also depends clearly on the desorption temperature.

However, a comparison with the intrinsic reaction kinetics of an AB_2 alloy (also $TiMn_2$-based) published by Ron [12] reveals a difference: The AB_2-type ($TiMn_2$-based) alloy needs less than 2 s to desorb 50 % of its hydrogen content at 20 °C, in comparison to approximately 18 s for the experiment at 20 °C described above. One reason for the clear different reaction kinetics of comparable $TiMn_2$ materials is the desorption procedure. As the desorption experiment from Ron was measured against vacuum, the pressure difference is clearly higher and accelerates the reaction.

With the available set-up, the results of the intrinsic kinetics reaction bed measurements of the very fast AB_2 alloy $Ti_{0.99}Zr_{0.01}V_{0.43}Fe_{0.09}Cr_{0.05}Mn_{1.5}$ are limited. However, it is shown that the alloy is clearly faster than the AB_5 alloy $LmNi_{4.91}Sn_{0.15}$: Its characteristic time for a desorption at 20 °C is 25 s in comparison to 46 s of $LmNi_{4.91}Sn_{0.15}$ at an even higher temperature of 28 °C.

3.2 Experimental analysis of individual reaction beds

The experimental results presented in this chapter were measured applying the test bench for individual reaction bed experiments described in chapter 2.1.1 with the capillary tube bundle reaction bed (see chapter 2.2.2) and the respective metal hydride. The thermocouple measuring the ‘metal hydride’ temperature was inserted into one capillary tube of the tube bundle. The experimental analysis of the capillary tube bundle reaction bed with different metal hydrides was done in order to evaluate the limiting factors for the dynamics of the reaction bed separately. Besides the heat and hydrogen transfer within the reaction bed, the intrinsic reaction kinetics of the applied metal hydrides (see chapter 3.1.2) can additionally influence the reaction bed dynamics.

3.2.1 Hydrogen distribution

The new design of the capillary tube bundle offers the possibility to measure metal hydride temperatures at different locations. As hydrogen enters the metal hydride bulk from a surrounding

gap through the filter tube, the interesting parameter is the hydrogen distribution in radial direction.

Based on the modified van't Hoff equation (equation (1-4)) the metal hydride temperature is directly correlated to the hydrogen pressure:

$$T = \frac{\Delta H}{R \cdot \ln(\frac{p_{H_2}}{p^0}) + \Delta S + R \cdot m_{Pl} \cdot (x_{mid} - x)} \qquad (3\text{-}2)$$

With the calculated values of the plateau slope m_{Pl}, the storage capacity in the middle of the plateau x_{mid}, the reaction enthalpy ΔH and entropy ΔS (for the absorption, see chapter 3.1.1), the pressure-temperature correlation of $LmNi_{4.91}Sn_{0.15}$ as a function of the load situation x is derived:

$$T = \frac{-27{,}411}{8.314 \cdot \ln(\frac{p_{H_2}}{p^0}) - 103.9 + 3.58 \cdot (0.65 - x)} \qquad (3\text{-}3)$$

As equation (3-3) is derived from characteristic values for the absorption case, it is valid for the hydrogen absorption, only. A modification of the pressure-temperature correlation for the desorption case can be derived from equation (3-2) with the respective values for hydrogen desorption (see chapter 3.1.1).

Based on this correlation, temperature measurements in the reaction bed can be used to monitor the hydrogen pressure development during the charging of the metal hydride at various radial positions. As soon as the hydrogen pressure is sufficiently high, the exothermal absorption leads to a temperature increase of the metal hydride bulk. Therefore, the five K-type thermocouples inserted into five capillary tubes in radial direction (see Figure 3-10) measure the metal hydride bulk temperature around the respective capillary tube. The reaction bed is not cooled (no water flow) during this experiment.

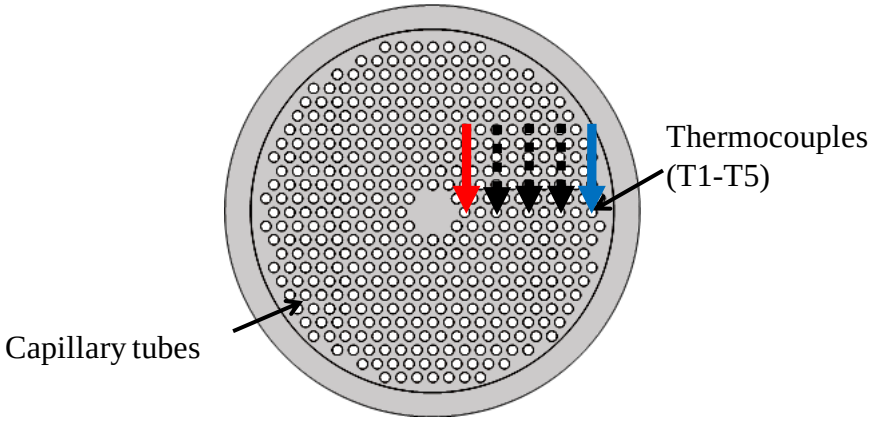

Figure 3-9: Radial thermocouple positions inside the capillary tube bundle reaction bed

At the beginning of the experiment (Figure 3-10) the metal-hydrogen system is in equilibrium (t < 22 s). At ambient temperature (~ 27 °C), the equilibrium pressure of the metal hydride in the reaction bed is around 2.9 bar (green dashed line). The load situation of the metal hydride is therefore determined to x = 0.1 %. The measured temperatures are fully drawn lines and correspond to the left y-axis, whereas the pressures of the system and the reaction bed are drawn with dashed lines and correspond to the right y-axis. As soon as the hydrogen valve is opened, the reaction bed pressure and the system pressure equalize. The higher hydrogen pressure (9.8 bar) disturbs the equilibrium of the metal-hydrogen system and the alloy starts to absorb.

Due to the released reaction enthalpy during absorption, the temperature of the powder increases and the radial distribution of the thermocouples visualizes the hydrogen distribution from the filter into the powder in radial direction. The calculated temperatures (based on equation (3-2)) for the respective hydrogen pressures (load situation x = 0.1 %) are added to the diagram as grey lines and demonstrate the applicability of these experiments. During the first equilibrium (< 22 s), the metal hydride temperature is between the calculated temperature for desorption and absorption. However, as soon as the hydrogen pressure is increased, additional hydrogen is absorbed and the final temperature corresponds to the calculated temperature for the absorption case.

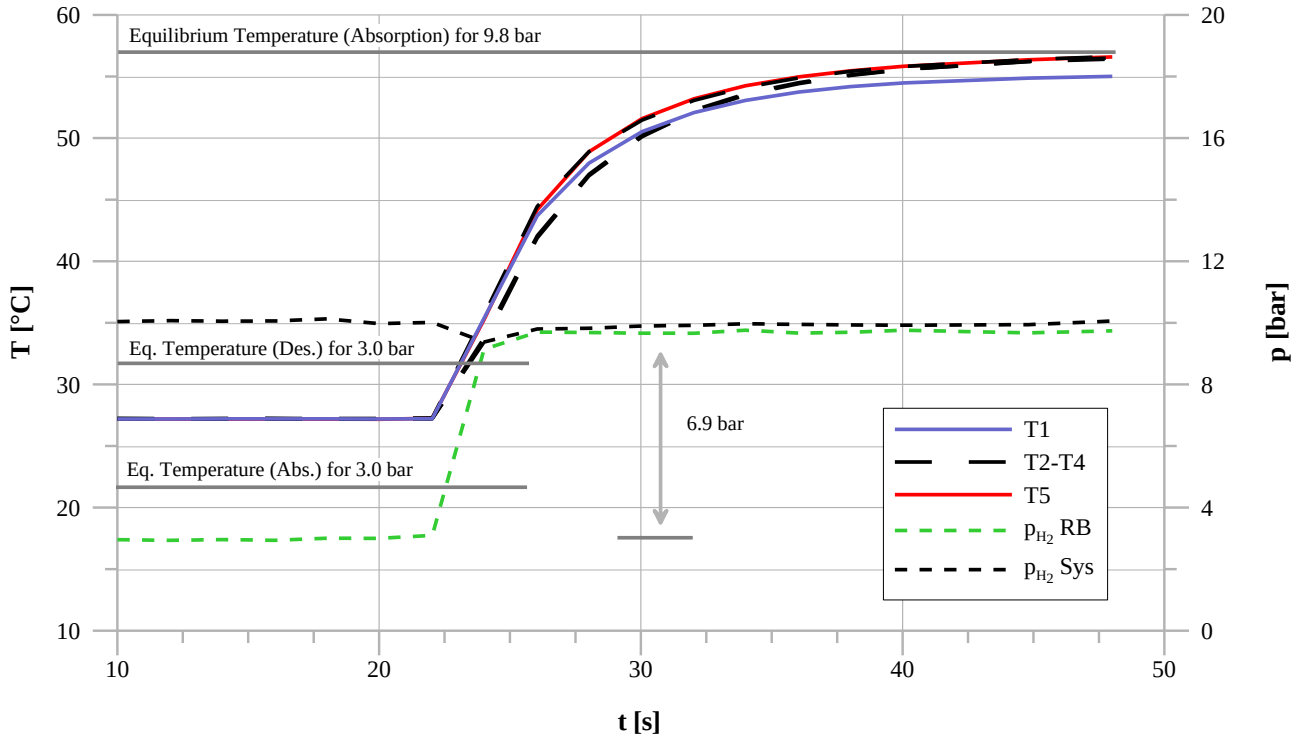

Figure 3-10: Metal hydride temperature development applying a hydrogen pressure increase of 6.9 bar (RB = reaction bed)

Although, the distances to the surrounding filter are different, the measured temperatures increase at the same time until the new equilibrium is reached (t ~ 40 s). As this behavior is independent of the applied pressure difference (see Figure 3-10 and Figure 3-11), a homogeneous hydrogen distribution within the capillary tube bundle reaction bed is demonstrated. Additionally, if the reaction time of the metal hydride (temperature increase) is taken into account, the hydrogen distribution is clearly faster and a quasi-instantaneous homogenous hydrogen distribution can be reasonably assumed. The temperature difference between the outer thermocouple (blue) and the others is due to the heat capacity of the filter and heat losses. This effect vanishes for lower temperature differences (see Figure 3-11).

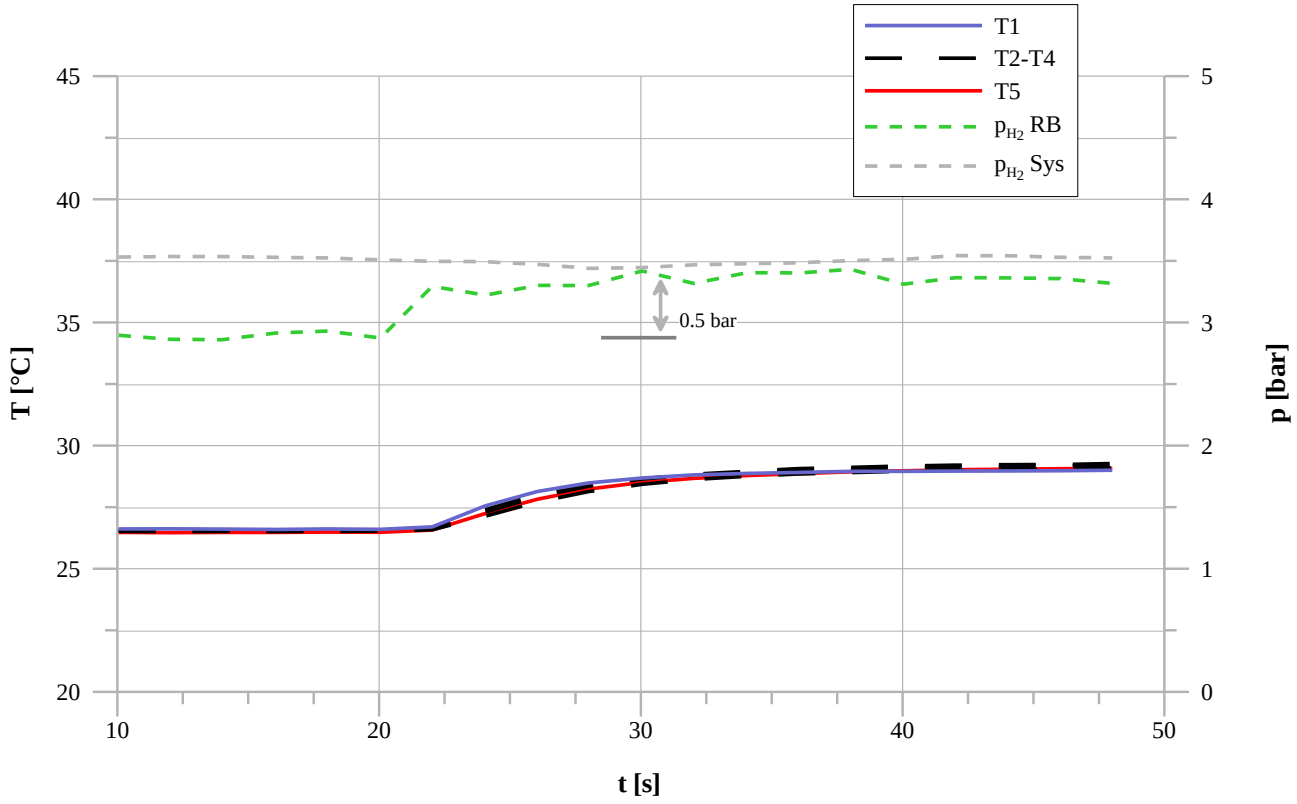

Figure 3-11: Metal hydride temperature development applying a pressure increase of 0.5 bar (RB = reaction bed)

An approximate description of the mass transfer of a heterogenic gas-solid reaction in porous media can be based on a modified diffusion law. In this case, the gas-solid system is assumed to be quasi-homogeneous and the effective diffusion coefficient D_{eff} depends also on the respective flow conditions within the reaction bed [82]. Applying this simplification, the modified mass balance equation in radial direction is given by equation (3-4):

$$\varepsilon \frac{\partial \rho_g}{\partial t} = -D_{eff} \frac{1}{r} \frac{\partial}{\partial r} (r \cdot \frac{\partial \rho_g}{\partial r}) - (1-\varepsilon) \cdot \phi \qquad (3\text{-}4)$$

with the effective diffusion coefficient D_{eff}, the gas density ρ_g, the porosity of the metal powder bulk ε, the reaction rate ϕ and the reaction bed radius r. The effective diffusion coefficient D_{eff} for hydrogen in metal hydride bulks is in the order of $9 \cdot 10^{-3}$ m^2/s [83].

In order to estimate the influence of hydrogen distribution on the reaction bed dynamics, the hydrogen sink term is neglected in the following. Additionally, ideal gas behavior of hydrogen is assumed and the gas density ρ_g is therefore given by equation (3-5):

$$\rho_g = \frac{p_g \cdot M_g}{R \cdot T_g} \qquad (3\text{-}5)$$

with the hydrogen gas pressure P_g, the mol mass of hydrogen M_g, the universal gas constant R and the gas temperature T_g.

The calculated hydrogen pressure Pg as a function of time and reaction bed radius (r) is shown in Figure 3-12. The hydrogen inlet is through the surrounding sinter metal filter tube with an inner diameter of around 0.06 m (see Figure 2-8). As the hydrogen pressure within the reaction bed is already equalized after around 0.1 s and the characteristic time of metal hydride reactions is in the order of 10 to 60 s, the simplified model is able to verify the above described experiments.

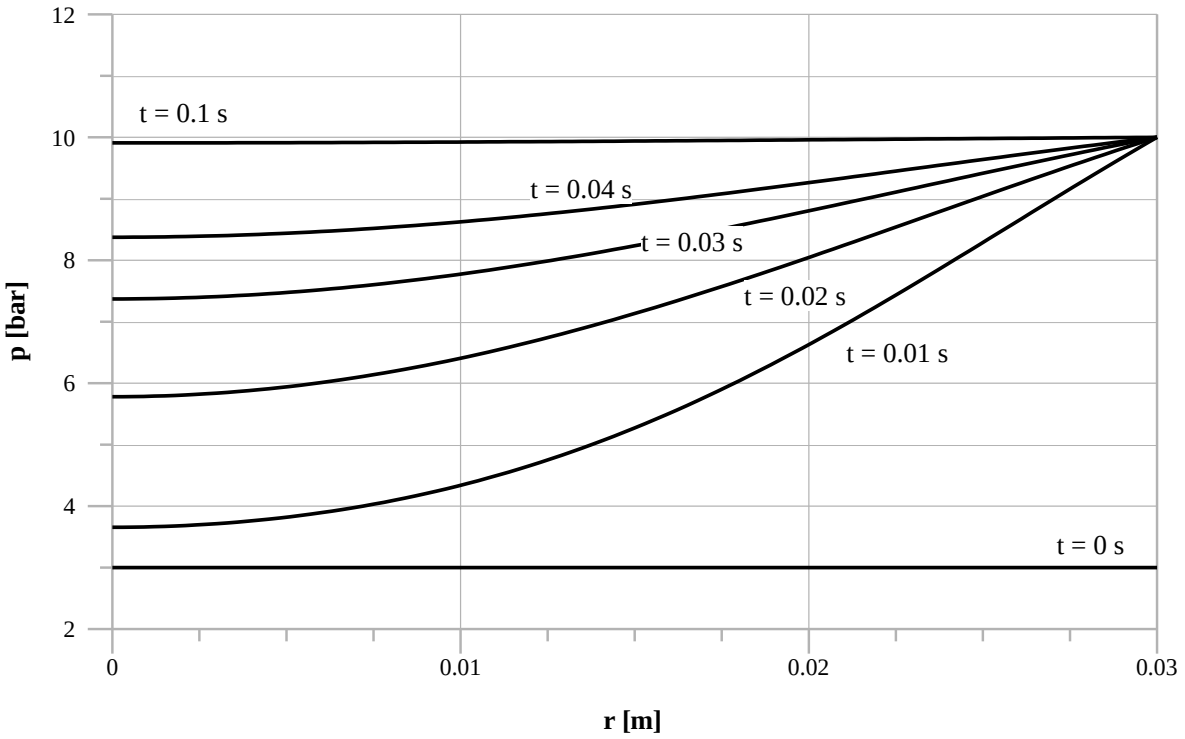

Figure 3-12: Hydrogen pressure as a function of time and radius (effective diffusion model)

A comparable result was published by Brown *et al.* in 2008 [84]. In order to reduce the necessary calculation time of the dynamic model of a metal hydride tank, several simplifying assumptions have been investigated in detail. The time necessary for hydrogen to travel the length of the reaction bed was calculated using Darcy's law and the respective permeability and dynamic viscosity. The length of the reaction bed was 114 mm and hydrogen needed 0.01 s to travel through it. So, the simulation results were independent of the time-dependent hydrogen distribution and as the rate of which hydrogen is absorbed (equation (1-5)) is not a function of time, Brown and colleagues concluded that the energy equation (equation (1-10)) is sufficient for a reasonable accurate simulation of their metal hydride tank.

As these theoretical conclusions are experimentally demonstrated for the capillary tube bundle reaction bed with the hydrogen distribution experiment (indirect measurement based on temperature distribution) and the simplified model described above, an instantaneous hydrogen distribution can be reasonably assumed and the reaction bed dynamics should depend on the heat transfer only.

3.2.2 Heat transfer characteristics

As the hydrogen transport does not limit the chemical reaction in the capillary tube bundle reaction bed, the heat transfer process of the reaction bed is investigated within this chapter. In order to investigate the isolated heat transfer process, the chemical reaction during the measurement has to be excluded. Therefore, the metal hydride was uncharged (complete desorption) and the reaction bed evacuated. The underlying idea of the measurement is comparable to the "lumped system analysis" where the temperature of a body is monitored after a sudden change of its ambient temperature. Although the lumped system analysis is not applicable for the capillary tube bundle reaction bed, a sudden temperature change of the water inlet temperature (T_{in}) can be used as step function at the beginning of the experiment and the reaction bed temperature as a function of time can be monitored. In this case, the reaction bed temperature T_{RB} is calculated as the average temperature between water in- and outlet and a normalized temperature T_{norm} is used according to equation (3-6):

$$T_{norm} = \frac{T_{RB}(t) - T_{in}}{T_{RB,initial} - T_{in}} \qquad (3\text{-}6)$$

with the reaction bed temperature as a function of time $T_{RB}(t)$, the initial reaction bed temperature $T_{RB,initial}$ and the water inlet temperature $T_{in.}$

Based on this assumption, the characteristic time of the isolated heat transfer process τ_{ht} (no chemical reaction) can be estimated using the following equation:

$$g(t) = e^{\frac{-t}{\tau_{ht}}} \qquad (3\text{-}7)$$

Figure 3-13 shows the experimental results for three different water flow rates (2, 3.5, and 5 l/min) and the adapted exponential equation g(t) for each measurement. Even though the experimental data does not fit precisely to the applied exponential equation, it is shown, that the characteristic time of the heat transfer process depends clearly on the flow rate of the coolant. Whereas the characteristic time for a water flow rate of 2 l/min is around 6 s, it is reduced to 4 and 2.5 s for flow rates of 3.5 and 5 l/min, respectively.

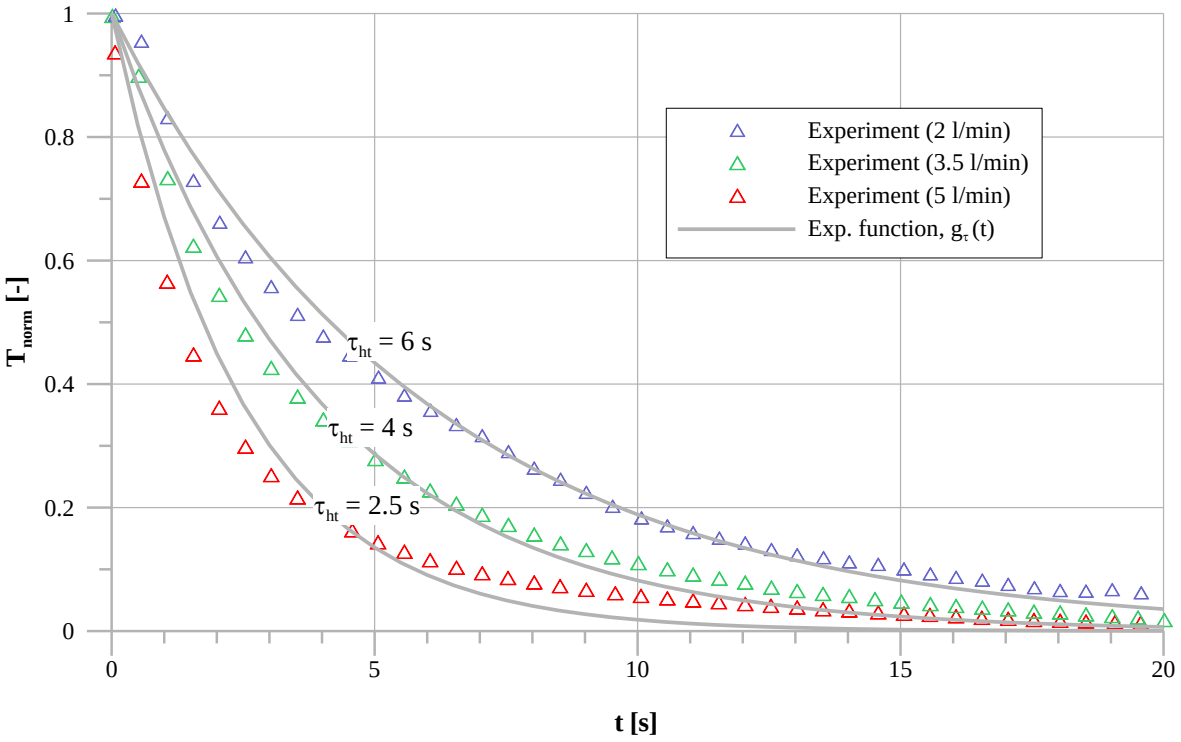

Figure 3-13: Heat transfer process for different flow rates (without chemical reaction)

In comparison to the characteristic times of intrinsic reaction kinetics of the investigated metal hydrides, the isolated heat transfer process of the reaction bed (no chemical reaction) is clearly faster. However, if the chemical reaction is taken into account (e.g. hydrogen absorption), the heat generated by the exothermal reaction has to be removed in order to keep the system away from chemical equilibrium (see chapter 1.2.2). Assuming a sufficiently fast chemical reaction, an improved heat transfer (e.g. due to a higher water flow rate) leads to a faster chemical reaction and consequently to faster reaction bed dynamics.

3.2.3 Absorption experiments

$LmNi_{4.91}Sn_{0.15}$

The used metal hydride mass in the capillary tube bundle reaction bed is 948 g of $LmNi_{4.91}Sn_{0.15}$. In Figure 3-14 the results of absorption experiments for different water flow rates (2, 3.5, 5 l/min) are shown.

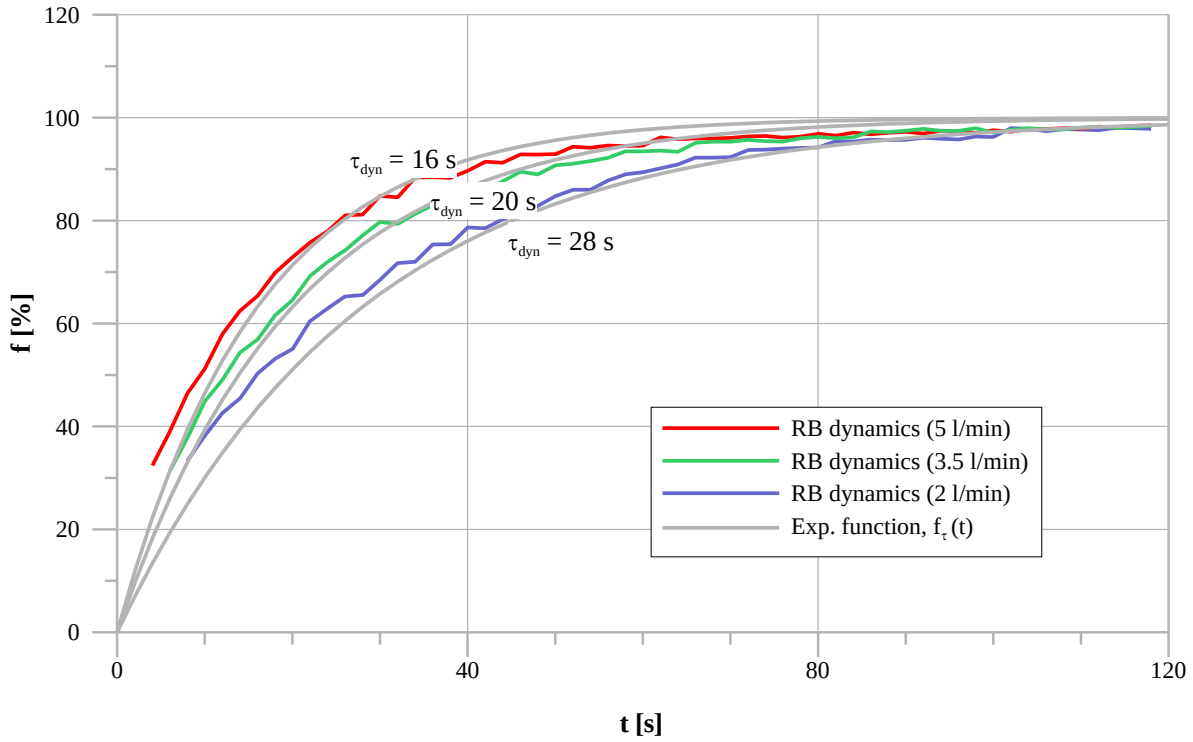

Figure 3-14: Absorption dynamics of the capillary tube bundle reaction bed with $LmNi_{4.91}Sn_{0.15}$ (p_{H2} = 11.2 bar)

All measurements were performed with a water inlet temperature of 28 °C and an identical hydrogen pressure of 11.2 bar (corresponding to the end of the plateau region). Comparable to the isolated heat transfer experiments (see Figure 3-13) an increased water flow rate reduces the characteristic time of the reaction bed dynamics. Whereas the characteristic time τ_{dyn} for the reaction with a water flow rate of 2 l/min is around 28 s, it is reduced to 20 and 16 s for flow rates of 3.5 and 5 l/min, respectively. Therefore, it can be concluded that the reaction bed dynamics is heat transfer dominated and the intrinsic reaction kinetics of $LmNi_{4.91}Sn_{0.15}$ is fast enough.

However, comparing the characteristic time of the reaction bed dynamics in Figure 3-14 (16 – 28 s) with the characteristic time of the intrinsic reaction kinetics of $LmNi_{4.91}Sn_{0.15}$ in Figure 3-5 at 28 °C (58 s), the intrinsic reaction kinetics is slower. This behavior has so far not been observed for metal hydride reaction beds. The intrinsic reaction kinetics was assumed to be clearly faster than the reaction bed dynamics and their influence on the reaction bed dynamics to be negligible.

An explanation for the fast reaction bed dynamics with the slow metal hydride $LmNi_{4.91}Sn_{0.15}$ can be seen in Figure 3-15 where different reaction bed dynamics (for different flow rates) are directly compared with the intrinsic reaction kinetics at identical initial metal hydride temperatures.

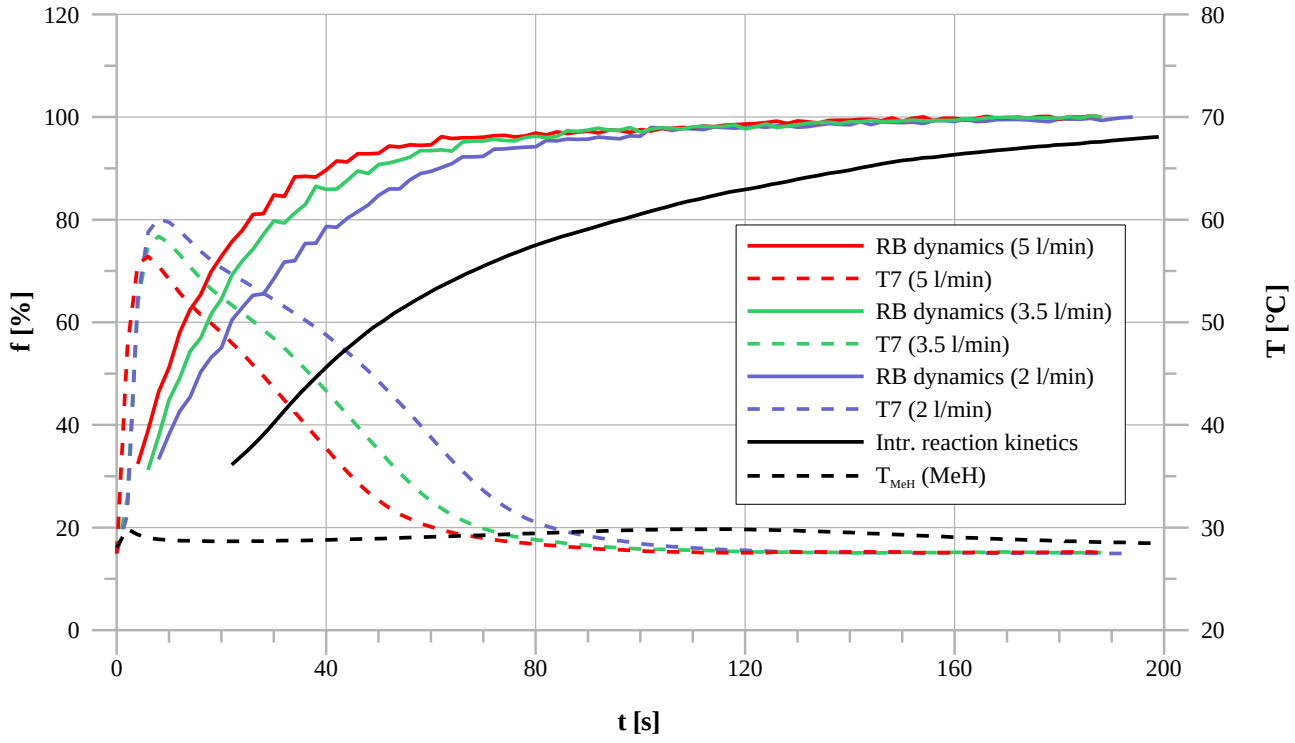

Figure 3-15: Comparison of intrinsic reaction kinetics and absorption dynamics of $LmNi_{4.91}Sn_{0.15}$ (p_{H2} = 11.2 bar)

The metal hydride temperature developments for all measurements are drawn as dashed lines and correspond to the right y-axis. As the intrinsic measurement was done at quasi-isothermal conditions (< 2 K), the temperature is constantly between 28 and 30 °C. However, the metal hydride temperature in the capillary tube bundle reaches between 55 and 60 °C at the beginning of the reaction. Based on the Arrhenius law, the higher metal hydride temperature accelerates the intrinsic reaction kinetics which is necessary to reach faster reaction bed dynamics. Taking the intrinsic reaction kinetics measurement of $LmNi_{4.19}Sn_{0.15}$ for different metal hydride temperatures into account (see Figure 3-5), the characteristic time at 40 °C is already shorter (8 s) than the characteristic time of the reaction bed dynamics with the highest water flow rate of 5 l/min (16 s).

$Ti_{0.99}Zr_{0.01}V_{0.43}Fe_{0.09}Cr_{0.05}Mn_{1.5}$

The sample mass of $Ti_{0.99}Zr_{0.01}V_{0.43}Fe_{0.09}Cr_{0.05}Mn_{1.5}$ in the capillary tube bundle reaction bed is 800 g due to the lower density (6.3 kg/m^3) of the AB_2 type alloy in comparison to $LmNi_{4.91}Sn_{0.15}$ (8.1 kg/m^3, 948 g). In order to be comparable with the PCI measurement data (see Figure 3-3), the absorption experiments were performed with a water inlet temperature of 20 °C.

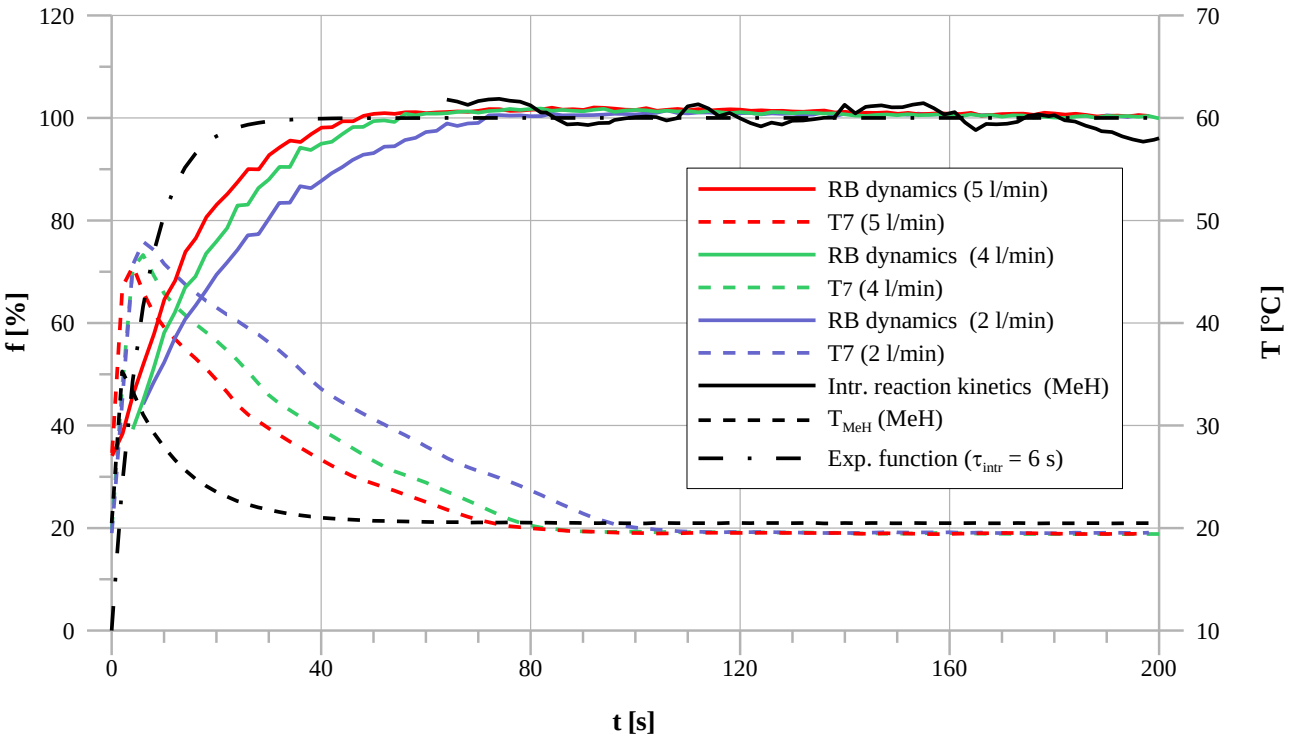

Figure 3-16: Comparison of intrinsic reaction kinetics and absorption dynamics of $Ti_{0.99}Zr_{0.01}V_{0.43}Fe_{0.09}Cr_{0.05}Mn_{1.5}$ (p_{H2} = 46 bar)

Figure 3-16 demonstrates that the intrinsic reaction kinetics of the AB_2 alloy is clearly faster than the dynamics of the capillary tube bundle reaction bed with the same metal hydride (adapted exponential function). The metal hydride temperature development during the measurement (dashed black curve) indicates that the intrinsic absorption is already completed after 30 s.

The metal hydride temperature development during the measurements is comparable to the one with the AB_5 alloy (Figure 3-15). Due to a smaller heat flux, the temperature increase of the metal hydride (T_{MeH}) is higher for a lower water flow rate (45 °C in comparison to 48 °C). However, the underlying principle is different but important for metal hydride sorption systems: Whereas the metal hydride temperature increase is necessary for $LmNi_{4.91}Sn_{0.15}$ to increase its intrinsic reaction kinetics and consequently the dynamics of the reaction bed, the intrinsic reaction kinetics of $T_{0.99}Zr_{0.01}V_{0.43}Fe_{0.09}Cr_{0.05}Mn_{1.5}$ is already fast enough (see Figure 1-8). As this increase of the metal hydride temperature is not possible during endothermic desorption experiments, the differences of the intrinsic reaction kinetics between the AB_5 and the AB_2 alloy are more crucial for the desorption dynamics of the capillary tube bundle reaction bed.

3.2.1 Desorption experiments

$LmNi_{4.91}Sn_{0.15}$

In Figure 3-17, the desorption dynamics of $LmNi_{4.91}Sn_{0.15}$ with the capillary tube bundle reaction bed are shown. Due to the higher heat flux (see chapter 3.2.2), the characteristic time of the desorption process is reduce from 56 s with a water flow rate of 2 l/min to 46 s with a flow rate of 3.5 l/min. However, an increase of the water flow rate to 5 l/min does not affect the characteristic time of the desorption dynamics.

Based on the heat and mass transfer measurements and calculations above (see chapter 3.2.1 and chapter 3.2.2), the general dependency of the capillary tube bundle reaction bed dynamics on the heat transfer process is demonstrated. Additionally, the measured absorption dynamics of the reaction bed show a clear dependency on the water flow rate. However, the desorption dynamics of $LmNi_{4.91}Sn_{0.15}$ in the same reaction bed seems to reach a limitation that is independent of the water flow rate as an increase from 3.5 l/min to 5 l/min does not affect the desorption dynamics of the reaction bed.

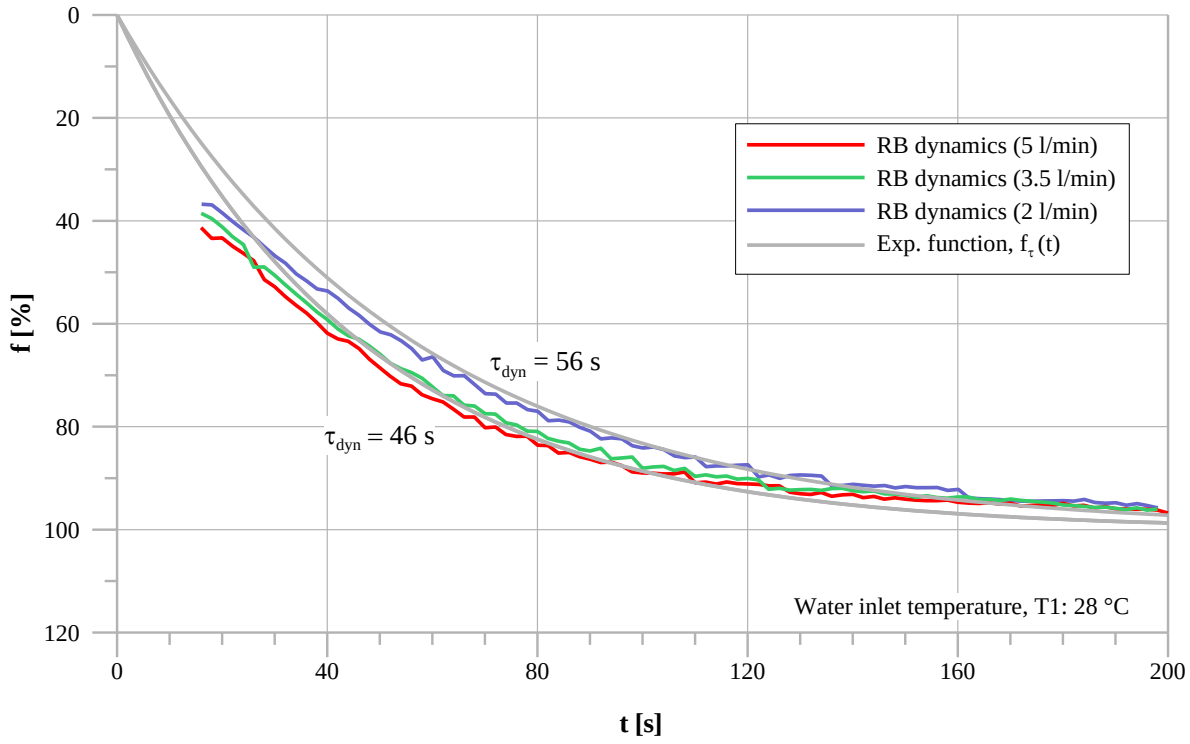

Figure 3-17: Desorption dynamics of the capillary tube bundle reaction bed with $LmNi_{4.91}Sn_{0.15}$ (into vacuum)

In Figure 3-18, the intrinsic desorption kinetics of $LmNi_{4.91}Sn_{0.15}$ is added (black line). Although, the intrinsic measurements were performed with a different reaction bed and on a different measurement set-up, the development of the reacted fraction is similar to the desorption dynamics of the capillary tube bundle reaction bed. Therefore, it can be reasonably concluded that the limitation of the desorption dynamics is due to the slow intrinsic reaction kinetics of the AB_5 alloy.

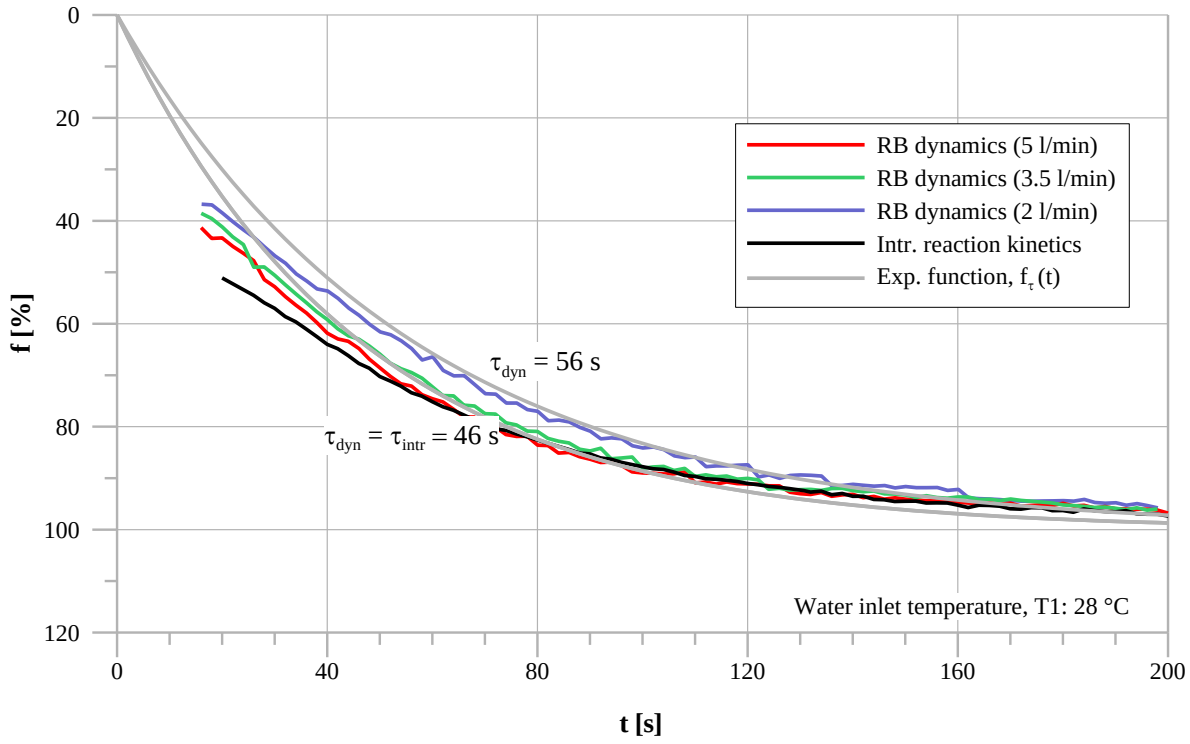

Figure 3-18: Comparison of intrinsic reaction kinetics and desorption dynamics of $LmNi_{4.91}Sn_{0.15}$ (into vacuum)

$Ti_{0.99}Zr_{0.01}V_{0.43}Fe_{0.09}Cr_{0.05}Mn_{1.5}$

In Figure 3-19, the desorption dynamics of the capillary tube bundle reaction bed are compared with the intrinisc desorption measurements of $T_{0.99}Zr_{0.01}V_{0.43}Fe_{0.09}Cr_{0.05}Mn_{1.5}$ at the same initial metal hydride temperature ($T_{MeH,initial}$ = 20 °C). As the charateristic time of the intrinisc desorption kinetics is with 28 s clearly faster, the desorption dynamics of the capillary tube bundle reaction bed depends on the heat transfer only.

The characteristic time of the desorption dynamics is reduced from 44 s with a water flow rate of 3.5 l/min to 38 s with a flow rate of 5 l/min. Therefore, a limitation of the rection bed dynamics due to the intrinisc reaction kinetics can be excluded for $T_{0.99}Zr_{0.01}V_{0.43}Fe_{0.09}Cr_{0.05}Mn_{1.5}$.

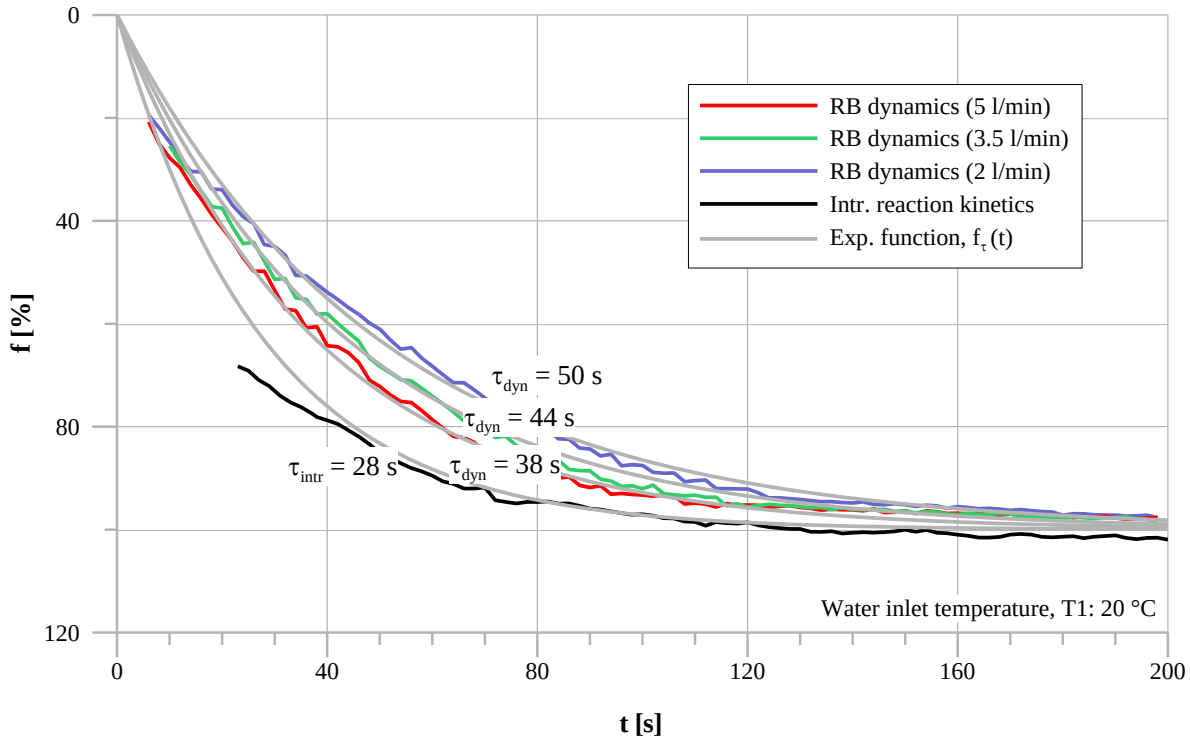

Figure 3-19: Comparison of intrinsic reaction kinetics and desorption dynamics with the AB_2 alloy (p1 = 10 bar)

3.2.2 Conclusions and final choice of metal hydride combination

Based on the results of the experimental analysis above, it is demonstrated that fast metal hydride sorption systems can be limited by the intrinsic desorption kinetics of the applied alloys. As the desorption kinetics depends on the reaction temperature, the most critical operation point is the generation of the cooling effect (desorption at the lowest temperature). The experimental results for $LmNi_{4.91}Sn_{0.15}$ shown in this chapter were based on a water inlet temperature of 28 °C. A lower temperature was not possible due to the limitation of the test bench. However, based on the Arrhenius law, it can be concluded that for reasonable cooling temperatures (< 15 °C) the intrinsic desorption kinetics is even slower. A further reduction of the half-cycle time (increase of specific power) is therefore not possible by the optimisation of the reaction bed (heat and mass transfer) but only by the application of faster metal hydrides. Therefore, a faster metal hydride (e.g. $T_{0.99}Zr_{0.01}V_{0.43}Fe_{0.09}Cr_{0.05}Mn_{1.5}$) operating at low temperatures (high-pressure alloy) is necessary in order to increase the specific power of the sorption cooling system.

Based on the experiments of individual reaction bed dynamics and the intrinsic reaction kinetics measurements, four conclusions concerning the metal hydride based sorption system can be drawn:

1. As the lowest metal hydride temperature is reached during the desorption of the high cooling half-cycle, the intrinsic reaction kinetics of the used alloy at this temperature could limit the performance of the complete system if the alloy is not carefully chosen [85].

2. The generally faster AB_2 alloys (e. g. $T_{0.99}Zr_{0.01}V_{0.43}Fe_{0.09}Cr_{0.05}Mn_{1.5}$) are therefore more applicable in fast sorption systems with necessary desorption at low temperatures as AB_5 alloys (e. g. $LmNi_{4.91}Sn_{0.15}$).

3. Based on the fast absorption dynamics of the reaction bed with $LmNi_{4.91}Sn_{0.15}$, it can be reasonably assumed that the intrinsic reaction kinetics are sufficiently fast for the low-pressure side of fast sorption systems (desorption at high temperatures, e. g. T_{Heat} = 130 °C).

4. A further improvement of the reaction bed dynamics of the capillary tube bundle reaction bed can only be achieved by improving the heat transfer to/from the metal hydride as the hydrogen distribution is sufficiently fast.

3.3 Coupled reaction beds experiments (sorption system)

All sorption system experiments were carried out applying the test bench described in chapter 2.1.2. The used metal hydride masses inside the capillary tube bundle reaction bed are 948 g of $LmNi_{4.91}Sn_{0.15}$ and 800 g of $Ti_{0.99}Zr_{0.01}V_{0.43}Fe_{0.09}Cr_{0.05}Mn_{1.5}$. Although a complete sorption system for continuous cold output consists of two identical reaction bed pairs, one reaction bed pair is sufficient to investigate reaction bed dynamics, choice of metal hydrides and corresponding temperature and pressure boundary conditions. Therefore, the experimental set-up was designed as a batch system (no continuous cold output). In the following, the coupled metal hydride sorption system is investigated with different varied parameters, like water flow rates and temperature boundary conditions.

3.3.1 Van't Hoff diagram of chosen metal hydrides

Due to the very fast intrinsic desorption kinetics at low temperatures, the AB_2 alloy $Ti_{0.99}Zr_{0.01}V_{0.43}Fe_{0.09}Cr_{0.05}Mn_{1.5}$ was chosen for the high-pressure side and $LmNi_{4.91}Sn_{0.15}$ is used as metal hydride B for the low-pressure side of the sorption system (see chapter 3.1.1). Based on the assumption that the intrinsic reaction kinetics depends on the reaction temperature and obeys Arrhenius law (see chapter 1.2.1), it can be reasonable assumed that the desorption kinetics of $LmNi_{4.91}Sn_{0.15}$ at 130 °C is sufficiently fast and does not limit the regeneration half-cycle of the sorption system.

In Figure 3-20, the van't Hoff plots of both chosen alloys are shown. The fully drawn lines represent the absorption, whereas the dashed lines correspond to the equilibrium pressures for the desorption. In order to visualize the plateau slope, three lines of each reaction are shown, for 25 %, 50 % and 75 % of the maximum storage capacity, respectively.

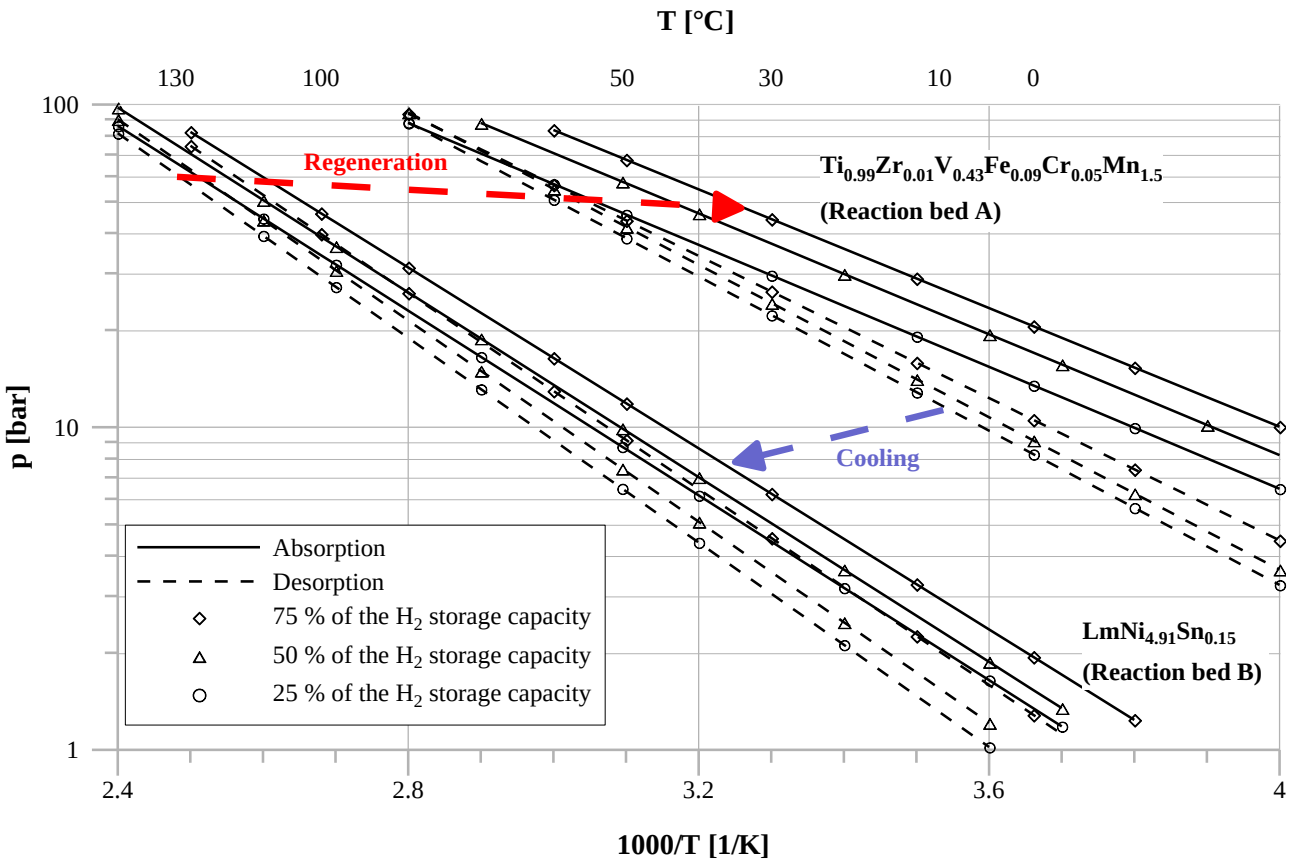

Figure 3-20: Van't Hoff plots of coupled metal hydrides ($Ti_{0.99}Zr_{0.01}V_{0.43}Fe_{0.09}Cr_{0.05}Mn_{1.5}$ and $LmNi_{4.91}Sn_{0.15}$)

The dashed blue arrow signifies the cooling half-cycle. The pressure difference between the desorption pressure of $Ti_{0.99}Zr_{0.01}V_{0.43}Fe_{0.09}Cr_{0.05}Mn_{1.5}$ at 10 °C and the absorption pressure of $LmNi_{4.91}Sn_{0.15}$ at 35 °C is sufficient, also towards the end of the half-cycle (approximately 5 bar). The necessary heating temperature to regenerate this metal hydride combination at 35 °C ambient temperature is around 130 °C (red dashed arrow).

3.3.2 Cooling half-cycle experiments

The experiments of the cooling half-cycle are comparable to the individual reaction bed experiments described in chapter 3.2. The main difference is the direct coupling of the hydrogen absorption and desorption processes in the respective reaction beds. At the beginning of each experiment, reaction bed A (high-pressure) is fully loaded with hydrogen and consequently reaction bed B is uncharged. The closed hydrogen valve (V3, Figure 2-3) separates both reaction beds. As soon as the valve is opened, a hydrogen flow is established between the desorption in reaction bed A and the absorption in reaction bed B.

Influence of the water flow rate on the hydrogen exchange rate

Based on the measurement procedure described above the influence of the water flow rate (identical for both beds) is shown in Figure 3-22. The fully drawn lines correspond to the measured hydrogen flow rate φ (MFM H_2) on the left y-axis. The dashed lines represent the accumulated exchanged hydrogen n_{H2} that is approximated according to equation (3-8):

$$n_{H_2} = \int \varphi \, dt \qquad (3\text{-}8)$$

based on the measured hydrogen flow rate φ (measurement interval $\Delta t = 2$ s). The total amount of hydrogen exchanged within the cooling half-cycle experiments is around 3.92 mol.

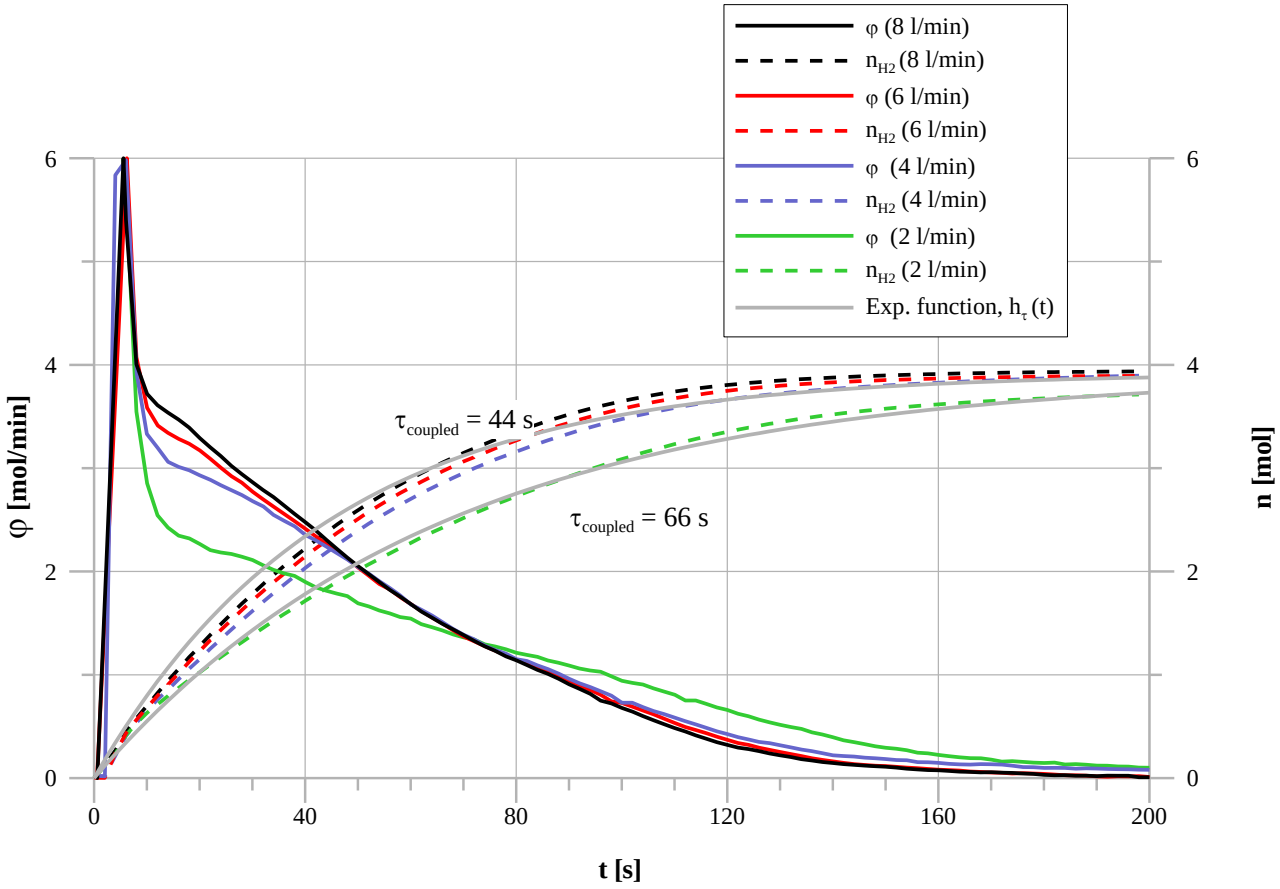

Figure 3-21: Hydrogen exchange rate for different water flow rates (T1 = 10 °C, T3 = 35°C)

The high hydrogen flow rate at the beginning of the experiment is due to the pressure balance of the hydrogen pressure as soon as the hydrogen valve is opened. Comparable to the individual reaction bed experiments, the hydrogen exchange rate depends on the water flow rate. The largest difference is observed between a water flow rate of 2 l/min and 4 l/min. A further increase leads only to a small influence during the first 40 s of the measurement. Consequently, the characteristic time $\tau_{coupled}$ of the coupled reaction process depends on the water flow rate and is reduced from 66 s for a flow rate of 2 l/min to around 44 s for higher flow rates. The exponential function h(t) is calculated according to equation (3-9):

$$h(t) = 3.92 \cdot (1 - e^{\frac{-t}{\tau_{coupled}}}) \qquad (3\text{-}9)$$

As the influence of the water flow rate on the characteristic time $\tau_{coupled}$ is only clearly visible for an increase from 2 to 4 l/min, a water flow rate of 4 l/min was set as standard flow rate for all experiments with the coupled reaction bed system.

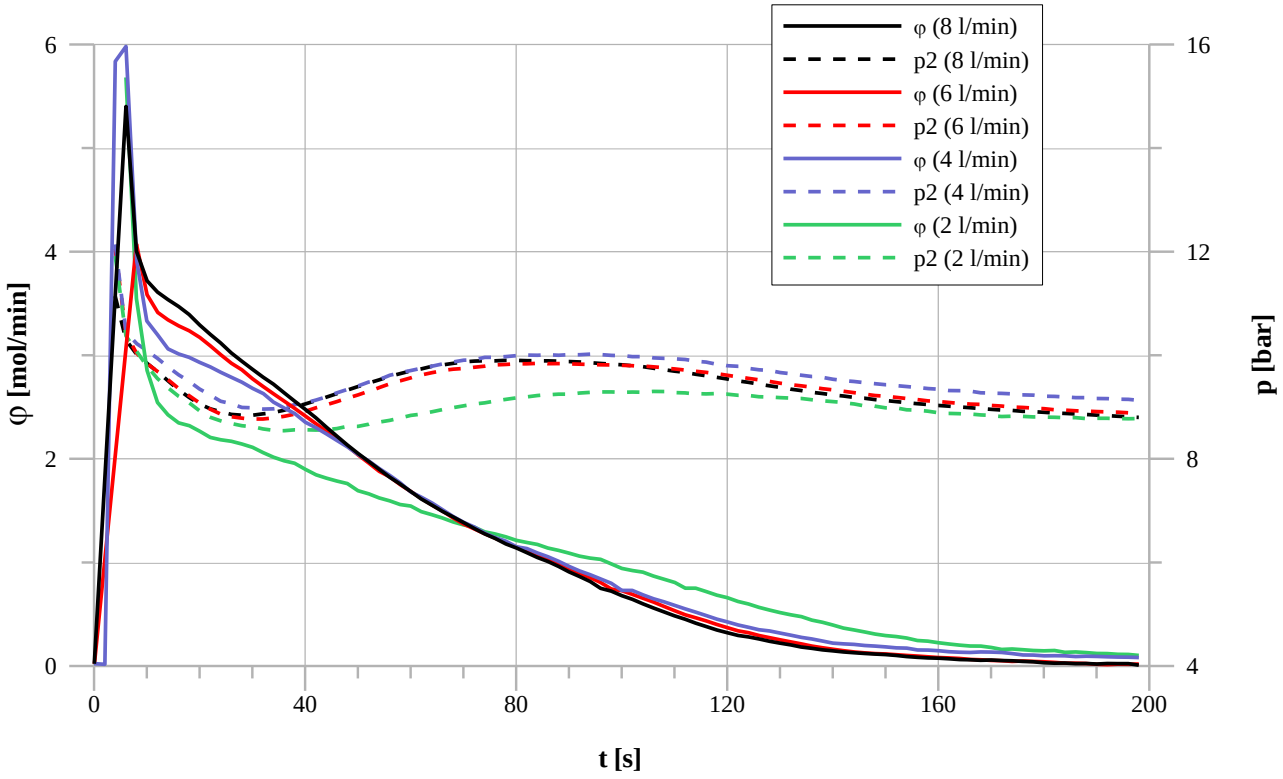

Figure 3-22: Influence of water flow rate on hydrogen exchange rate (T1 = 10 °C, T3 = 35 °C)

In Figure 3-22, the system pressure (p2) development during the experiment is shown for different water flow rates. The tendency of the system pressure is similar for all flow rates: it decreases during the first 30 s and increase afterwards until a peak is reached after 80-120 s. In general, the system pressure increases if the desorption is faster than the respective absorption in the coupled reaction bed. Therefore, the measured hydrogen pressure progressions indicate different reaction dynamics of the coupled reaction beds. The pressure increase after 40 s for all flow rates is due to a faster desorption of reaction bed A ($Ti_{0.99}Zr_{0.01}V_{0.43}Fe_{0.09}Cr_{0.05}Mn_{1.5}$). As the pressure increase is reduced for a water flow rate of 2 l/min, it can be concluded that the reduced hydrogen flow rate in Figure 3-21 is caused by a slower desorption in reaction bed A.

Comparison of the generated thermal power in reaction bed A and B

In order to avoid systematic measurement errors, the generated power is compared for different available measurement paths in Figure 3-23. The experimental set-up for coupled reaction beds consists of an hydrogen part, including the mass flow meter for hydrogen (MFM H_2), and two water heat exchanger cycles to measure the heat rejection or uptake of the respective reaction bed (thick lines in Figure 2-3).

The hydrogen flow rate φ is measured within the hydrogen connection from desorption in A and absorption in B. The corresponding thermal power P_{H2} depends on the respective reaction enthalpy ΔH of the metal hydride (see chapter 3.1.1) and is calculated according to equation (3-10):

$$P_{H2} = \left| \frac{\varphi}{60} \cdot \Delta H \right| \qquad (3\text{-}10)$$

Due to the different reaction enthalpies of the metal hydrides, the necessary thermal energy to release a specific amount of hydrogen from alloy A is less than the rejected heat of the absorption of the same amount of hydrogen in alloy B. Therefore, the ‘measured’ hydrogen powers P_{H2} based on the hydrogen exchange rate are different. The thermal power P_{water} is calculated from the heat balance of the water side according to equation (3-11):

$$P_{water} = \left| \dot{V} \cdot \rho_{water} \cdot c_p \cdot (T_{in} - T_{out}) \right| \qquad (3\text{-}11)$$

with the water flow rate $\dot{V}$, the water density ρ_{water}, the specific heat of water c_p and the temperature difference between water in- and outlet (T1-T2 and T3-T4, respectively).

Neglecting the small time shift, the thermal power based on the water side P_{water} as well as the thermal power based on the hydrogen flow rate P_{H2} are concurrent for both reaction beds (see Figure 3-23). The hydrogen power value is slightly lower than the respective measured thermal power, as the hydrogen exchange peak at the beginning is compensated during the complete reaction.

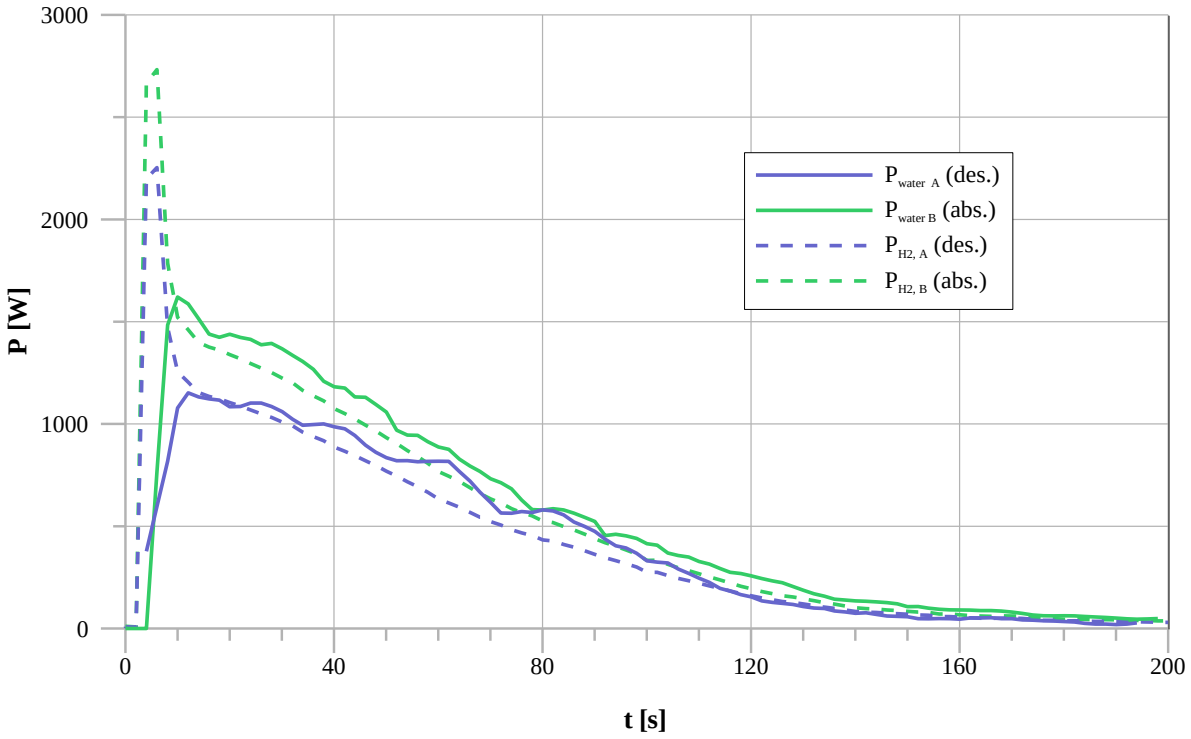

Figure 3-23: Power comparison during hydrogen exchange experiment (T_{des} = 15 °C, T_{abs} = 35 °C)

Variation of the inlet temperature to the desorbing reaction bed A

In Figure 3-24 the influence of the water inlet temperature to the desorbing reaction bed A on the hydrogen flow rate and pressure is shown. The water inlet temperature T1 into reaction bed A corresponds to the cooling temperature T_{Cool} of a sorption cooling system. The inlet temperature to the absorbing reaction bed B (T3) was set to 33 °C and the water flow rate for both sides was 4 l/min. The hydrogen flow rate φ, indicating the maximum amount of achievable cooling power (see equation (3-10)), corresponds to the left y-axis, whereas the measured system pressure p2 is shown on the right y-axis.

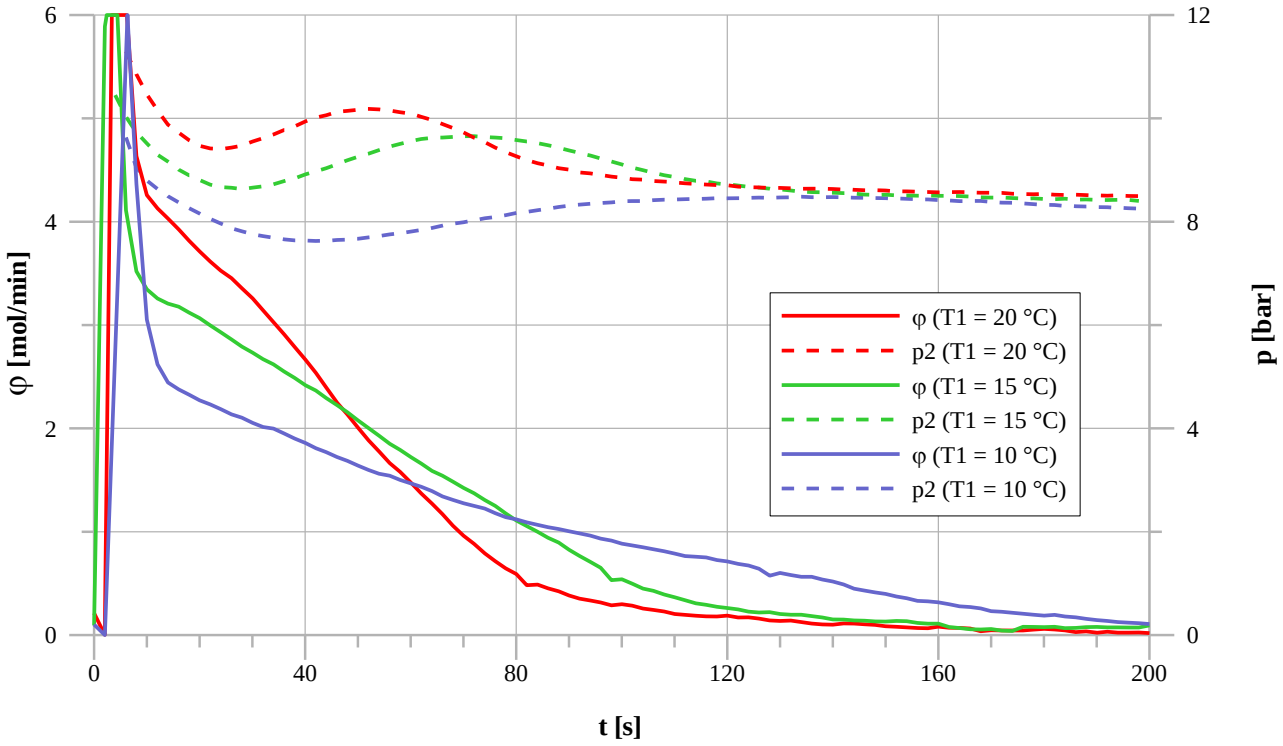

Figure 3-24: Variation of inlet water temperature to the desorbing reaction bed A (Water inlet temperature to coupled reaction bed (T3) = 33 °C)

A higher water inlet temperature to reaction bed B (T1) results in a higher hydrogen flow rate between both reaction beds. As the hydrogen pressure is directly linked to the equilibrium temperature of the respective alloy (see van't Hoff plot description in chapter 1.2.1), a higher pressure corresponds to a higher metal hydride temperature and leads to a higher temperature difference between metal hydride and cooling fluid. Therefore, the heat flux during absorption is increased which is visible due to the pressure progression plots (dashed lines): The measured hydrogen pressure increases after 20 s and the magnitude of this pressure increase is proportional to the water inlet temperature to reaction bed A.

A lower cooling temperature of the sorption systems (comparable to the water inlet temperature to reaction bed A) leads to a reduced pressure difference between both alloys, which results in a reduced hydrogen flow rate and consequently in a reduced cooling power.

3.3.3 Cycling experiments of coupled metal hydride reaction beds

In comparison to the cooling half-cycle experiments, the cycling experiments consist of a series of complete hydrogen exchange cycles. Due to different preload situations of the reaction beds, the sorption system reaches its equilibrium only after a distinct 'run-in' period. All experimental results shown in this chapter have been measured after this initial phase. The half-cycle time was adjusted manually before the measurement and is controlled by the data acquisition unit. The time between the automatically switching of the electromagnetic valves EMV 1-4 (see Figure 2-3) was set to 100 s and the heating temperature T_{Heat} (water inlet temperature to reaction bed B during regeneration) was fixed to 130 °C.

Cycling experiment with T_{Heat} = 130 °C, T_{Amb} = 28 °C and T_{Cool} = 20 °C

In Figure 3-25 the in- and outlet temperatures (see Figure 2-3, T1- T4) for four complete cycles are shown. The temperatures of the respective heat exchangers were adjusted to T_{Heat} = 130 °C, T_{Amb} = 28 °C and T_{Cool} = 20 °C. This corresponds to the easiest boundary condition for the sorption system, as the cooling temperature is rather high and the ambient temperature rather low. The blue lines correspond to the high pressure reaction bed A which is cycled between ambient T_{Amb} and cooling temperature T_{Cool} and the corresponding temperatures in reaction bed B are shown as red lines. In Figure 3-26, the hydrogen pressure development and the accumulated exchanged hydrogen during the same cycling experiment are shown. Additionally, exponential functions with the characteristic time values for the regeneration ($\tau_{coupled,\ reg}$ = 40 s) and for the cooling half-cycle ($\tau_{coupled,\ cool}$ = 40 s) are drawn as grey lines for the first cycle.

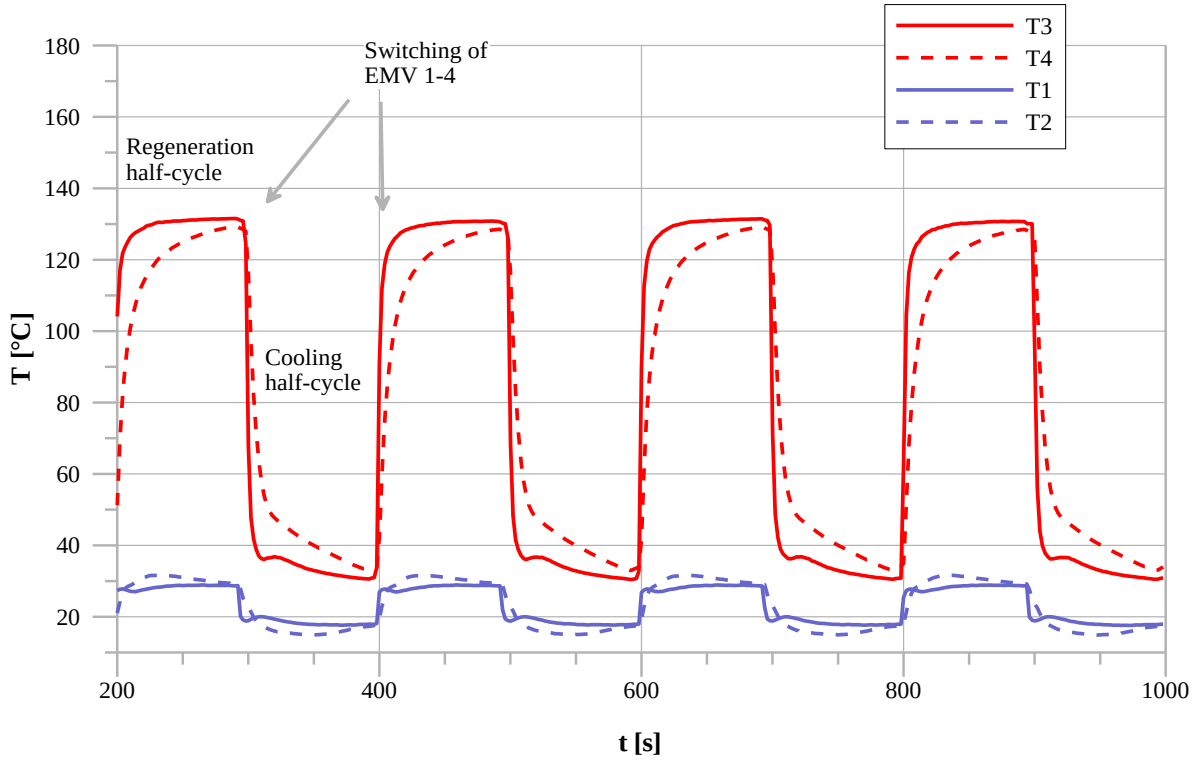

Figure 3-25: In- and outlet temperature progression during the cycling experiment

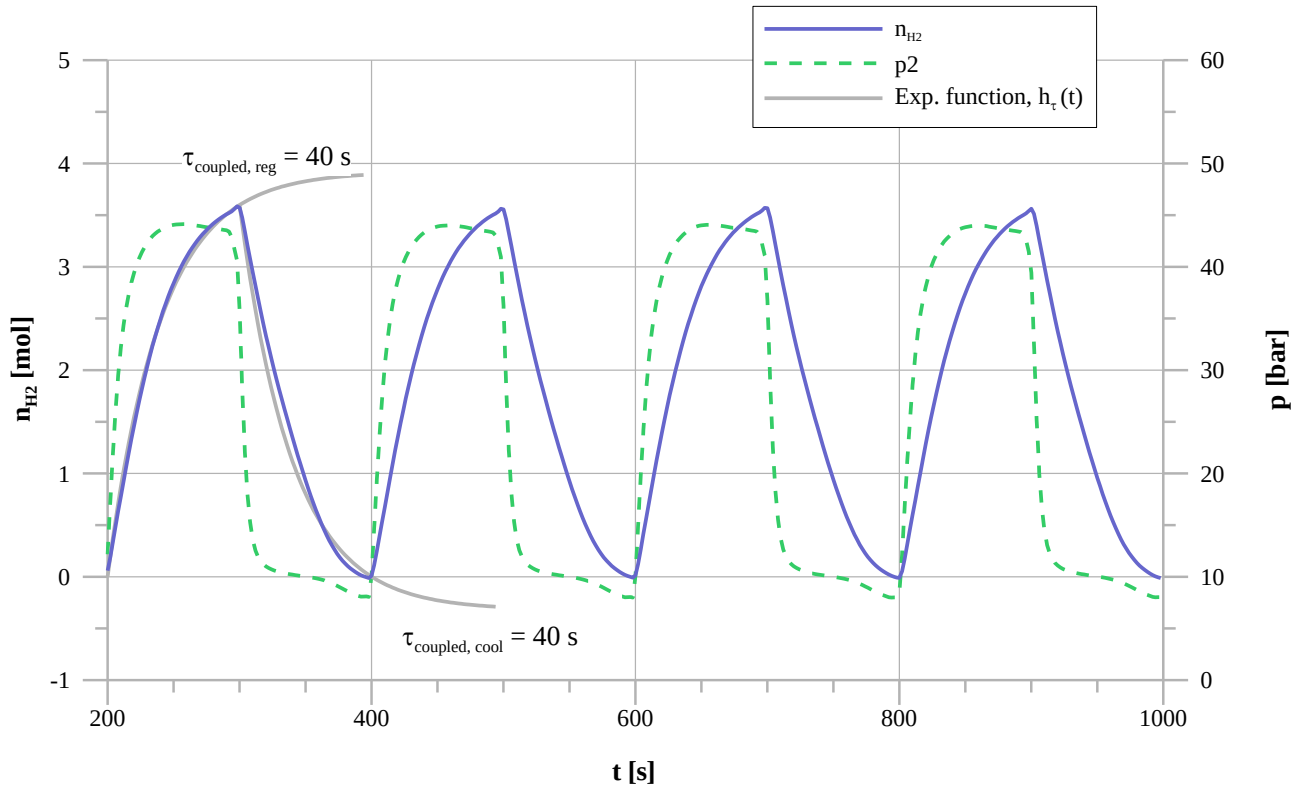

Figure 3-26: Pressure and hydrogen exchange during the cycling experiment

Towards the end of the regeneration half-cycle, the temperature of reaction bed A is around ambient temperature. Therefore, a fraction of the available reaction enthalpy at the beginning of the cooling half-cycle is required to cool down the thermal masses of the reaction bed and the cooling effect starts slightly after the actual switching of the half-cycle (dashed blue line, Figure 3-25). After this short period, the endothermic reaction cools the water current. Due to the higher temperature difference between cooling and regeneration half-cycle, this effect is even more obvious for the hot reaction bed (red line) and the necessary amount of thermal energy to reach the temperature level of the following half-cycle is higher. Therefore, the thermal masses, especially the parasitic thermal masses like pressure vessel, heat exchanger surface or filter tube should be minimized in order to maximize the efficiency of the system.

The total amount of exchanged hydrogen n_{H2} within 100 s (half-cycle time) for these temperature boundary conditions (T_{Heat} = 130 °C, T_{Amb} = 28 °C and T_{Cool} = 20 °C) is 3.6 mol. Based on the desorption enthalpy of the metal hydride in reaction bed A, the corresponding amount of thermal energy is around 81.4 kJ. As the half-cycle time was adjusted to 100 s, the average cooling power is approximately 814 W. It is the maximal achievable value (without thermal losses) as a temperature change of thermal masses also leads to a hydrogen exchange. Due to the exponential behavior of the hydrogen exchange, 63.2 % (2.28 mol) of the maximum exchangeable amount of hydrogen is already consumed after the first 40 s ($\tau_{coupled}$). During the following 40 s the amount of exchanged hydrogen is already reduced to around 0.84 mol. Therefore, the generated cooling power calculated by the measured mass flow rate of hydrogen and the respective reaction enthalpy of the metal hydride is decreasing during the half-cycle (see Figure 3-27, green dashed line).

In order to be able to change the alloys in the reaction bed, two constructions made of massive brass for the distribution of water at the in- and outlet are necessary (see Figure 2-4). Whereas the alloy mass is around 900 g and the reaction bed itself weighs around 2 kg, the massive brass in- and outlets weigh together addionally 2 kg. These components are not necessary for possible technical applications but reduce the efficiency of the test bench due to the almost doubled thermal mass of the reaction bed. Their impact is shown in Figure 3-27, where the thermal power measured in the water current $P_{water\ A}$ is compared with the calculated hydrogen power $P_{H2,A}$. Positive values correspond to the cooling half-cycle, whereas negative values represent the regeneration half-cycle.

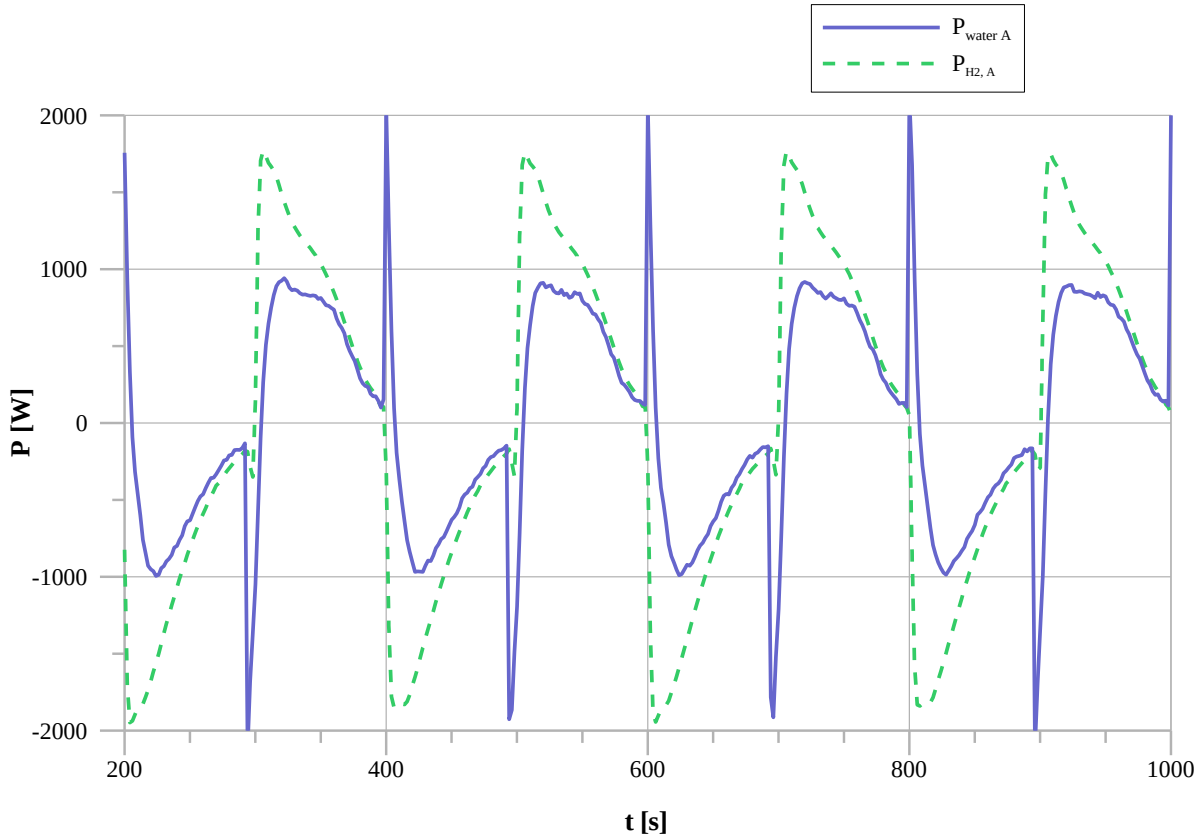

Figure 3-27: Cooling power based on hydrogen exchange rate (calculated) and measured from the water flow (thermal)

Even though the temperature conditions are favourable, the effective cooling power measured in the water flow $P_{water\ A}$ (average value = 510 W) is clearly lower than the average value of the hydrogen power $P_{H2,\ A}$ without thermal masses (average value = 890 W).

Variation of the cooling temperature (T_{Cool})

In Figure 3-28, the influence of the cooling temperature (water inlet temperature to reaction bed A during cooling half-cycle) on the thermal power of the sorption system $P_{water\ A}$ (reaction bed A, fully drawn line) and on the calculated hydrogen power $P_{H2,\ A}$ is shown (dashed line). The heating temperature as well as the ambient temperature were kept constant to T_{Heat} = 130 °C and T_{Amb} = 28 °C. The half-cycle time of the sorption system was set to 120 s.

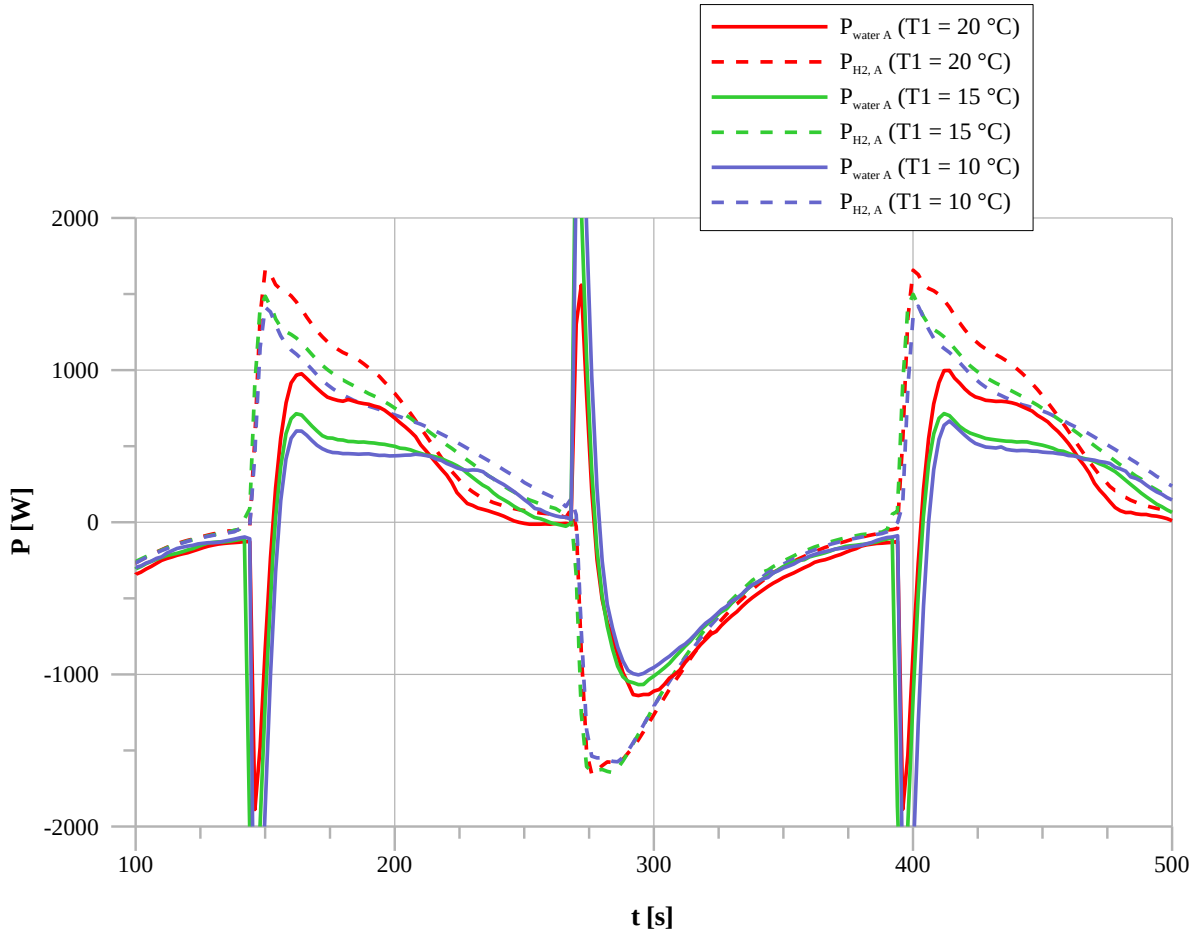

Figure 3-28: Variation of the cooling temperature – effect on thermal power ($P_{water\,A}$) and hydrogen power ($P_{H2,\,A}$)

As the heating temperature of the coupled reaction bed B is not changed and the cooling temperature only influences the cooling half-cycle, the regeneration half-cycles (negative values) are comparable. The main difference during the cooling half-cycle is the higher measured thermal power P_{water} for a cooling temperature of 20 °C in comparison to the lower cooling temperatures of 15 °C and 10 °C. The reason is due to the thermal masses described earlier. With an increasing temperature difference during regeneration and cooling half-cycle, the fraction of exchanged hydrogen necessary to change the temperature of the reaction bed itself increases. Therefore, less hydrogen is available to generate the cooling effect. Additionally, the total amount of exchanged hydrogen n_{H2} decreases with decreasing cooling temperature (see Figure 3-29).

The small difference in the measured thermal power between T_{Cool} = 15 °C and T_{Cool} = 10 °C is due to the instable inlet temperature to reaction bed A (T1) during the cooling half-cycle. Additionally, the set point of 10 °C is not reached. Therefore, the progressions of the water outlet temperature T2

shown in Figure 3-29 are almost similar for both measurements. These effects are due to the applied thermostat that is not able to balance the high heat loads properly during the regeneration and cooling mode for high temperature differences.

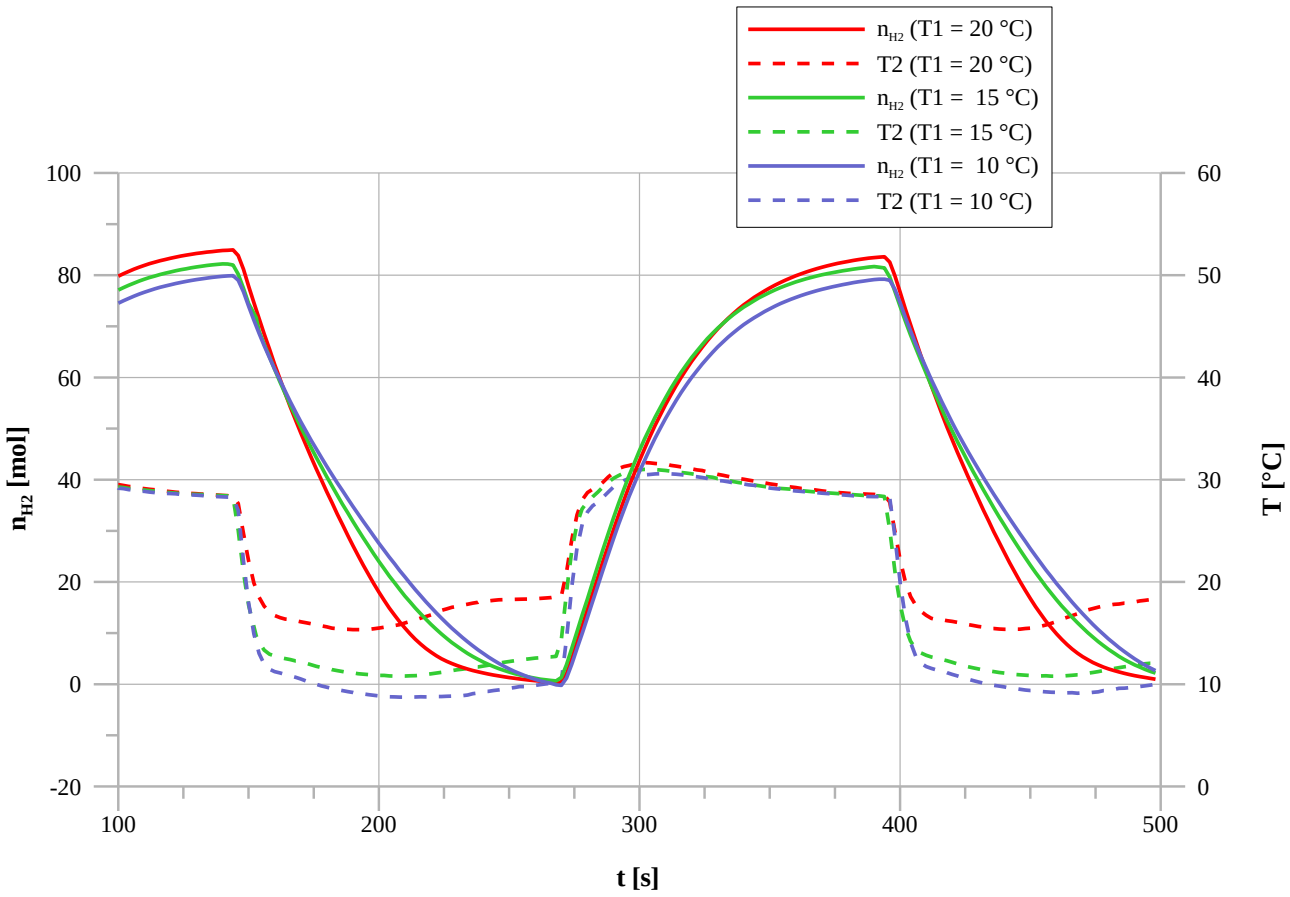

Figure 3-29: Variation of the cooling temperature – effect on hydrogen exchange

Variation of the ambient temperature (T_{Amb})

The ambient temperature (T_{Amb}) is the most critical boundary condition for thermally driven sorption systems as it affects the regeneration as well as the cooling half-cycle. An increased ambient temperature increases the corresponding equilibrium pressure of the absorbing metal hydride and consequently the system pressure p2 during both half-cycles (see dashed lines in Figure 3-30). The half-cycle time of the sorption system was set to 120 s.

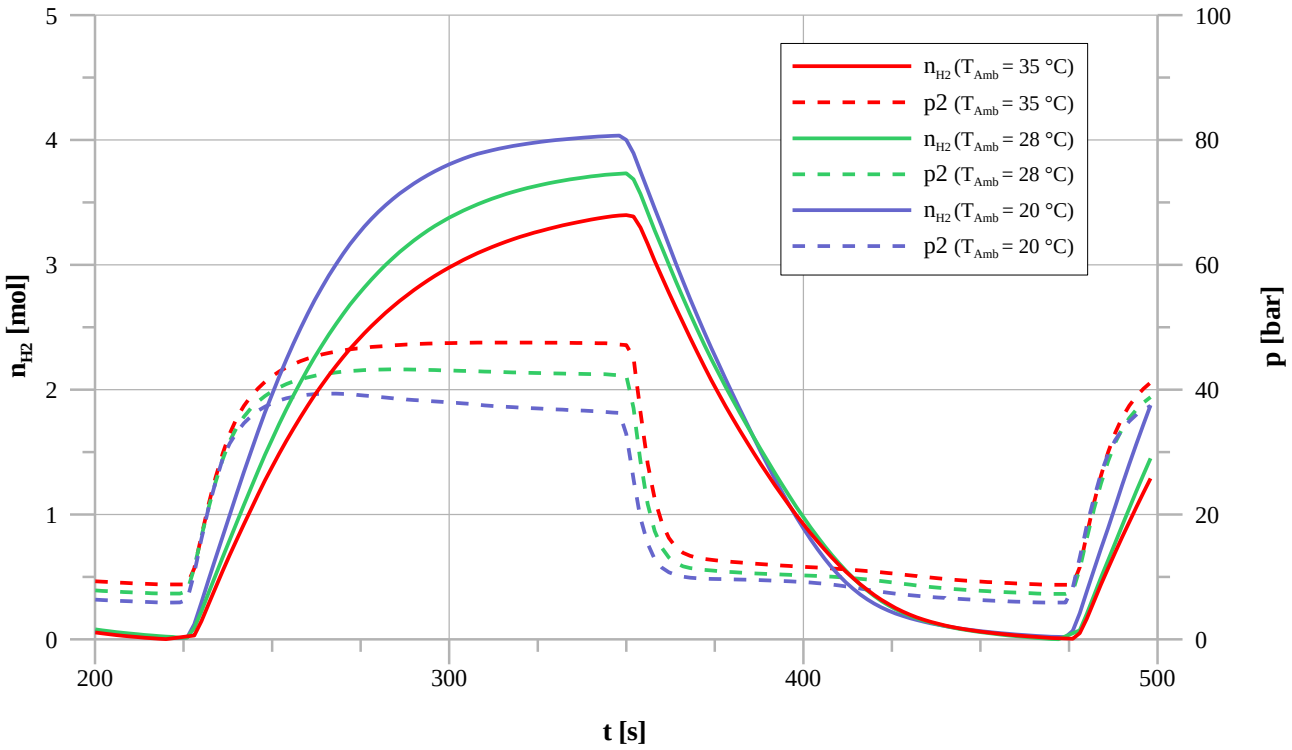

Figure 3-30: Hydrogen exchange and pressure development for different ambient temperatures

As the heating and the cooling temperature were fixed to T_{Heat} = 130 °C and T_{Cool} = 20 °C, respectively, the available desorption pressures are identical for all measurements. Therefore, the exchanged amount of hydrogen n_{H2} shown in Figure 3-30 as fully drawn lines depends clearly on the ambient temperature (T_{Amb}). Around 4 mol of hydrogen are exchanged for an ambient temperature of 20 °C, whereas only 3.8 and 3.4 mol are exchanged for T_{Amb} = 28 °C and 35 °C, respectively.

In Figure 3-31 and Figure 3-32, the respective system pressure progressions (p2) are shown for one half-cycle (T_{Amb} => T1 or T3, respectively) and compared to the corresponding van't Hoff plots of the absorbing alloy (non-logarithmic scale). Although, the desorbing alloy generates the thermally driven compression of hydrogen during the regeneration half-cycle, the system pressure p2 at the end of the regeneration phase corresponds to the absorption pressure of metal hydride A with a load situation of around 75 % of the maximum storage capacity (see non-logarithmic van't Hoff plots in Figure 3-31). However, the load situation of metal hydride A at the end of the regeneration half-cycle decreases with increasing ambient temperature T_{Amb}. Whereas the metal hydride is charged to more than 75 % of the maximum hydrogen storage capacity for a water inlet temperature of T1 = 20 °C, the load situation is reduced to 70 % at the end of the regeneration half-cycle for T1 = 35 °C.

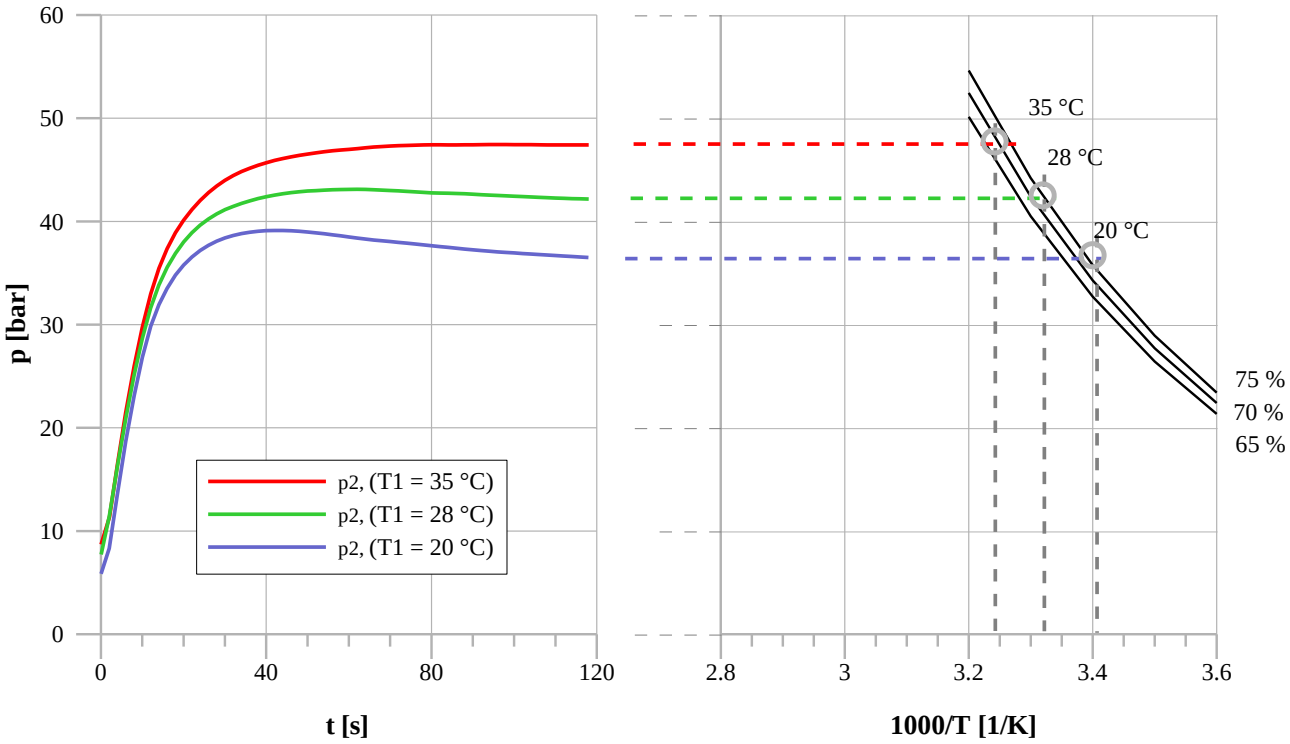

Figure 3-31: Pressure progression during regeneration half-cycle for different ambient temperatures – absorption in reaction bed A (T3 = 130 °C)

Figure 3-32 displays the progression of the system pressure p2 during the respective cooling half-cycle (T1 = 20 °C). A comparison with the van't Hoff plot absorption lines of metal hydride B shows a comparable dependency of the hydrogen load situation on the ambient temperature. The metal hydride B is charged to less than 85 % for T3 = 35 °C, whereas a load situation of almost 90 % of the maximum storage capacity is reached for a water inlet temperature of 20 °C.

Taking the used metal hydride masses and the maximum storage capacity of the respective alloys into account, 5 % of the maximum storage capacity corresponds to around 0.31 mol (calculated for $LmNi_{4.91}Sn_{0.15}$) and additional 0.32 mol of hydrogen calculated for $T_{0.99}Zr_{0.01}V_{0.43}Fe_{0.09}Cr_{0.05}Mn_{1.5}$. Therefore, the exchangeable amount of hydrogen based on the van't Hoff plots is reduced by around 0.63 mol for an ambient temperature increase from 20 °C to 35 °C. This value agrees to the value derived from the mass flow meter (MFM H_2) shown in Figure 3-30.

The cooling capability of the sorption system depends therefore considerably on the ambient temperature as the reduced amount of exchangeable hydrogen corresponds to the desorption heat of metal hydride A that is not available to generate the cooling effect.

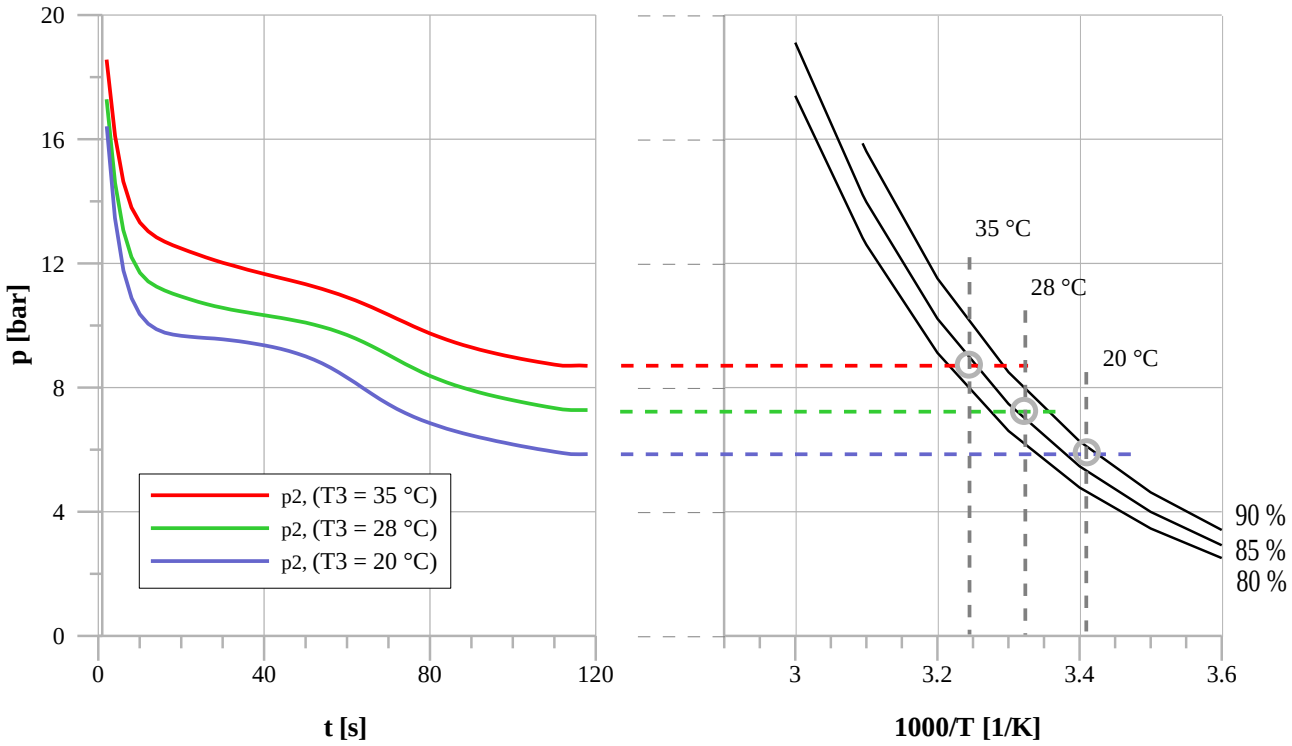

Figure 3-32: Pressure progression during cooling half-cycle for different ambient temperatures – absorption in reaction bed B (T1 = 20 °C)

3.4 Automotive cooling systems

3.4.1 The closed cooling system design – for waste heat utilisation

The basic component of the thermally driven system is a reaction bed pair with two different metal hydrides. One single pair is able to generate a cooling effect as long as hydrogen is available in the desorbing metal hydride reaction bed. Afterwards a regeneration half-cycle is necessary, to recharge it. In order to achieve a continuous cooling effect, the thermally driven sorption system operates with two reaction bed couples simultaneously. As long as the first reaction bed couple is in cooling mode, the second one is regenerating. A schematic principle of a complete automotive cooling system based on metal hydride is shown in Figure 1-17. The following estimations for the applicability of the system for automotive cooling are based on the experimental results obtained from the test-bench for coupled reaction beds (see chapter 3.3.3).

The achievable cooling power

As the reaction beds were designed to enable the exchange of metal hydrides, the in- and outlets are removeable. Therefore, a massive brass construction for the distribution of the heat carrier was necessary which increases the thermal mass of the system. Whereas the alloy mass is around 900 g and the reaction bed itself is around 1.7 kg, the massive brass in- and outlets weigh together addionally 2 kg.

The achievable specific cooling power results given in Table 3-3 are based on the experimental results presented in chapter 3.3.3. They are calculated without the additional thermal capacities of the in- and outlets as they are not representative for a possible application. For a given reaction bed geometry, the achievable cooling power depends on the ambient temperature and on the desired cooling temperature. The main reason for the reduced cooling power at higher temperature differences is due to the reduced amount of exchangeable hydrogen. Additionally, the fraction of hydrogen necessary to cool down the passive mass of the reaction bed and the metal hydride reduces the available hydrogen for the generation of the cooling effect.

Table 3-3: Achievable specific cooling power of the thermally driven system (related to the desorbing metal hydride)

Ambient temperature	28 °C	35 °C	43 °C
Cooling temperature 20 °C	780 W/kg	535 W/kg	320 W/kg
Cooling temperature 15 °C	**640 W/kg**	395 W/kg	180 W/kg
Cooling temperature 10 °C	520 W/kg	275 W/kg	60 W/kg

Based on the guidelines of the ‘TOPMACS’ project, a cooling temperature of 15 °C and an ambient temperature of 28 °C were chosen as reference [4]. Additionally, the necessary cooling power for a first prototype was determined to 2 kW. The achievable specific cooling power of around 640 W/kg (related to the desorbing metal hydride) leads to a total metal hydride mass of around 12.5 kg for the thermally driven system. In comparison to the state of the art metal hydride based cooling

system (see chapter 1.2.4), the specific power of the sorption system presented in this work is more than tripled which leads to the clearly reduced necessary mass of metal hydride. A linear up-scaling of the reaction bed masses gives the total weight of the hydrogen part of the system, which is around 40 kg.

Without the hydrogen valve and the in- and outlet construction, the volume of the tested reaction bed is around 0.6 l. The total volume of the hydrogen side for a cooling power of 2 kW can therefore be estimated to around 10 l [86]. However, due to the four (minimum three) water cycles, the volume constraints of the water side of the sorption system are not negligible and increase the volume of the complete system clearly (see Figure 1-17).

3.4.1 The open cooling system design – for H_2-driven cars

A second operation principle of a metal hydride based cooling system is conceptually proposed in this work and described in the following.

Hydrogen is seen as possible future energy carrier, especially for vehicles (e. g. fuel cell driven cars). Besides the chemical storing method in e.g. metal hydrides, two physical techniques, liquefaction and compression, are mainly used to increase the energy density of the hydrogen tank. Due to the low specific storage capacity of currently available metal hydrides, the physical storing techniques seem more promising. However, the amount of energy necessary to liquefy or to compress hydrogen is high. The energy consumption due the compression of hydrogen (800 bar) is around 15.5 % of its lower heating value (LHV) and the liquefaction of hydrogen consumes between 21 % and 35 % of its LHV [87].

The cooling system principle based on metal hydrides that is able to reutilize the compression work onboard to generate a cooling effect is schematically shown in Figure 3-33. In comparison to the above described closed system (hydrogen exchange between two metal hydrides), the new proposed system is an open process. As long as two hydrogen pressure levels (p_{Reg} and p_{Cool}) are available (e. g. between hydrogen storage tank and fuel cell), the metal hydride (A) can be integrated and utilize this pressure difference. The cooling half-cycle is achieved during the desorption of hydrogen at the pressure of the hydrogen consuming unit, e.g. fuel cell (p_{Cool}).

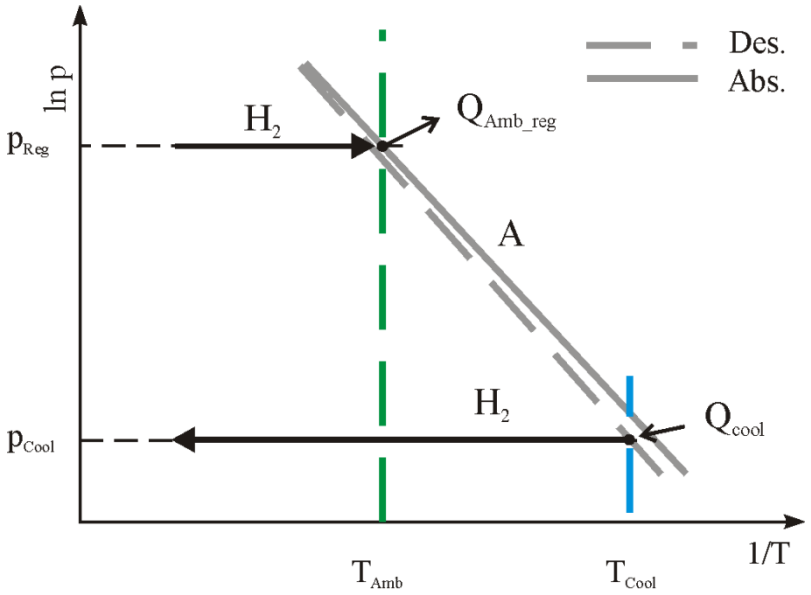

Figure 3-33: Van't Hoff diagram of open sorption cooling system (idealized)

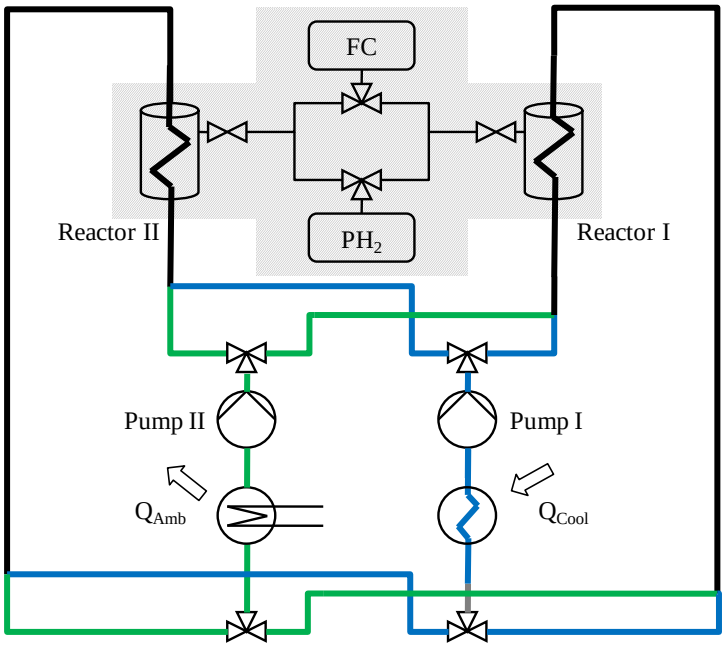

Figure 3-34: Schematic principle of the pressure-driven sorption system including all major secondary components

Instead of a thermally driven compression, the pressure difference between tank and consumer is used to regenerate the metal hydride. The schematic principle of this system is shown in Figure

3-34. The cooling effect ($Q_{Cool,}$ blue) is generated during the desorption of hydrogen and the absorption heat during regeneration is released to the ambient (Q_{Amb}, green). As for a continuous cold output only two reaction beds are necessary, the amount of secondary components is in comparison to the closed system clearly reduced.

Based on the experimental results of the reaction bed dynamics and the intrinsic reaction kinetics measurements of the different metal hydrides, $T_{0.99}Zr_{0.01}V_{0.43}Fe_{0.09}Cr_{0.05}Mn_{1.5}$ is more suitable for an application in the open cooling system. The measurement results shown below were obtained with the capillary tube bundle reaction bed and a metal hydride mass of 800 g. The measured cooling and regeneration half-cycles are shown in Figure 3-35 and Figure 3-36, respectively.

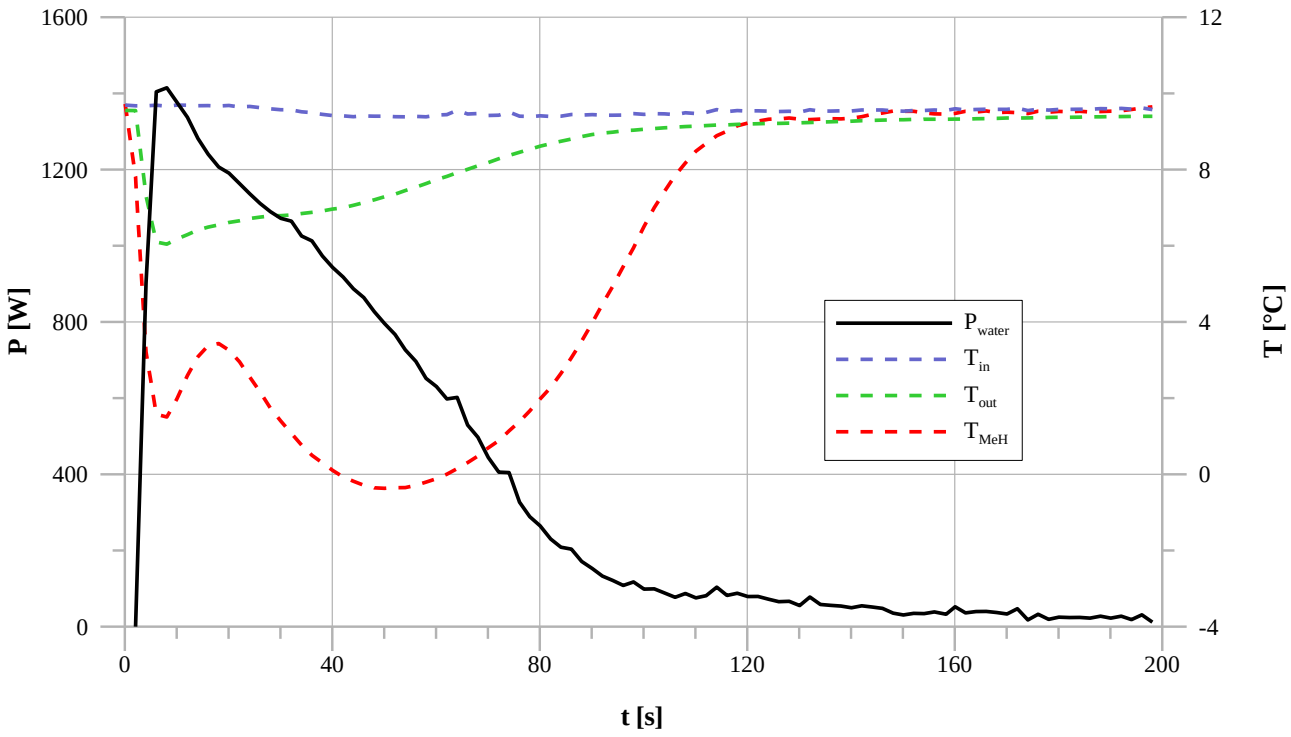

Figure 3-35: Measured cooling half-cycle for T_{in} = 10 °C with $p_{H2} \approx 5$ bar

The thermal power P_{water} corresponding to the left y-axis is drawn in black and the respective temperatures (right y-axis) are drawn with dashed lines. The desorption pressure during the cooling half-cycle experiment (see Figure 3-35) was set to 5 bar. With an inlet temperature of around 10 °C, a peak cooling power of around 1,400 W is achieved. The average cooling power is 800 W and the necessary half-cycle time is around 100 s.

The system pressure during the regeneration half-cycle (absorption, see Figure 3-36) was adjusted to 50 bar. For an inlet temperature of 35 °C, the time necessary to charge the metal hydride completely is comparable to the time for the desorption process (~ 100 s). Due to the very fast reaction at the beginning of the experiment, the maximum thermal power during regeneration is about 2,700 W.

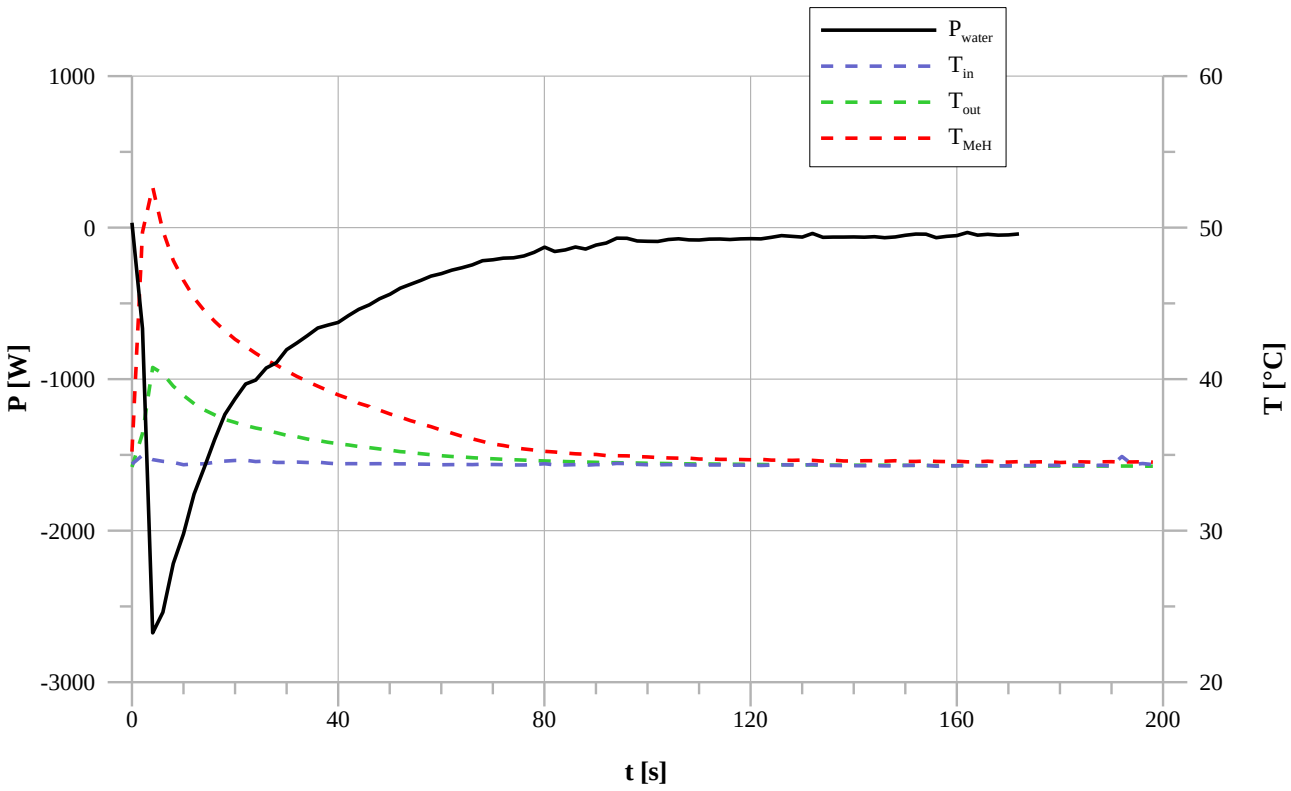

Figure 3-36: Measured regeneration half-cycle for T_{in} = 35 °C and $p_{H2} \approx$ 50 bar

Both experiments show the possibility to operate an open system between 5 bar and 50 bar hydrogen pressure. The respective achievable cooling temperature is clearly below 10 °C and the regeneration at 35 °C ambient temperature is demonstrated in Figure 3-36. As the temperature and pressure boundary conditions of the cooling system depend on the implemented alloy, the system principle can be adapted to the hydrogen consuming unit, e.g. fuel cell by modifying the alloy composition (see PCI measurements in chapter 3.1.1). Therefore, an adapted system is able to reach a maximum of reacted hydrogen fraction and consequently a high efficiency.

Necessary hydrogen flow rate

Due to the coupling of the open sorption system to a hydrogen consuming unit (e.g. fuel cell), the cooling effect is only generated as long as hydrogen is consumed. This dependency is comparable to conventional air-conditioning systems that are mechanically coupled to the engine. However, the generated cooling power of the open sorption system depends directly on the consumed hydrogen flow rate and consequently on the generated electrical power of the fuel cell.

Based on the desorption enthalpy of the applied metal hydride (22.6 kJ/mol), the caloric value of hydrogen ($Q_{caloric}$, 242 kJ/mol) and an average net efficiency (η_{FC}) of the fuel cell system of around 40 %, the ratio R_c of the generated cooling effect (Q_{Cool}) to the generated electrical energy of the fuel cell system ($Q_{electrical}$) can be calculated:

$$R_c = \frac{Q_{Cool}}{Q_{caloric} \cdot \eta_{RFC}} = \frac{Q_{Cool}}{Q_{electrical}} = 0.23 \qquad (3\text{-}12)$$

Neglecting the losses due to the heat capacities (operation temperatures between T_{Amb} and T_{Cool}), the open sorption system (using $Ti_{0.99}Zr_{0.01}V_{0.43}Fe_{0.09}Cr_{0.05}Mn_{1.5}$) is able to generate a cooling power that corresponds to around 23 % of the respective electrical power generated by the fuel cell. In other words, an electrical power demand of around 8.6 kW is sufficient to reach the average cooling power defined in the TOPMACS project (2 kW, see chapter 1.2.4). If the electrical power demand is higher, a by-pass solution (direct connection between tank and fuel cell) can be used to supply the additional hydrogen flow rate.

Weight and volume constraints

Due to the simple system set-up consisting of only two reaction beds, the complete system can be very compact and lightweight. The weight of the reaction bed used for the experiments described above is around 2.5 kg, including 800 g of metal hydride. A linear up-scaling to an average cooling power of 2 kW leads to a total weight of the hydrogen part of around 12.5 kg. The volume of this part can be estimated to around 3 l (not including the hydrogen valve and connections). Therefore, the weight and volume constraints of the open sorption system based on metal hydrides should not hinder an automotive application.

4 Summary and outlook

The state of the art of automotive refrigeration systems is mechanically driven and therefore, a cooling demand directly increases the fuel consumption along with the CO_2 emissions of the vehicle. Due to the low efficiency of internal combustion engines, a decoupling of cooling demand and fuel consumption by utilising waste heat as driving energy for the cooling systems seems to be reasonable. Additionally, the constant loss of climate-damaging working fluid of conventional systems contributes to the necessity to work on new, effective cooling technologies.

In the frame of this work, the metal hydride sorption system technology was therefore investigated for an application in automotive cooling. The comparison of so far realized thermally driven sorption systems with the practical cooling load in the vehicle identified the necessary amount of metal hydride as crucial obstacle for an automotive application. As the metal hydride mass is directly linked to the specific thermal power of the reaction bed and the corresponding necessary hydrogen exchange time, the underlying issue of this work was the optimisation of the reaction bed dynamics.

Beside the intrinsic reaction kinetics measurements of the alloys ($LmNi_{4.91}Sn_{0.15}$ and $Ti_{0.99}Zr_{0.01}V_{0.43}Fe_{0.09}Cr_{0.05}Mn_{1.5}$), an experimental analysis of limiting factors of the reaction bed dynamics was performed in order to understand underlying coherences of fast metal hydride reaction beds. Hereby, the intrinsic desorption kinetics at low temperatures (cooling temperature) was identified as possible limiting factor for metal hydride sorption systems. The endothermic reaction tends to decrease the alloy temperature and, according to the Arrhenius law, its intrinsic reaction kinetics. However, as the exothermic absorption tends to increase the temperature of the alloy along with its intrinsic reaction kinetics, the heat transfer dominated reaction bed dynamics can reach faster absorption rates than intrinsic reaction kinetics at constant absorption temperature. Both coherences have been demonstrated experimentally for $LmNi_{4.91}Sn_{0.15}$.

Therefore, a faster (intrinsic reaction kinetics) metal hydride ($Ti_{0.99}Zr_{0.01}V_{0.43}Fe_{0.09}Cr_{0.05}Mn_{1.5}$) was chosen to work at the high-pressure side of the sorption system in order to exclude a performance limitation due to intrinsic processes at low temperatures. The most interesting result concerning the coupled metal hydrides is the reduced half-cycle time from around 600 s of the so far realized systems to around 100-120 s. This value is reached due to the combination of the large heat transfer surface of the capillary tube bundle reaction bed and the fast intrinsic desorption kinetics of the high-pressure alloy $Ti_{0.99}Zr_{0.01}V_{0.43}Fe_{0.09}Cr_{0.05}Mn_{1.5.}$ As the specific cooling power is directly linked to the half-cycle time, the weight and volume constraints of the metal hydride part of the sorption system have been clearly improved. However, due to the generally complex water side (minimum

three heat exchanger loops) of thermally driven sorption systems, the weight and volume constraints of the complete system are high, even if standard automotive components are applied.

A reduction of the system complexity and consequently of its volume and weight can be achieved with a pressure-driven, open operating metal hydride cooling system which is proposed conceptually in this work. In future hydrogen fueled vehicles, the potential energy of compressed hydrogen can be used as driving energy for the metal hydride cooling system if it is integrated in-between the high-pressure hydrogen tank and the hydrogen consumer, e.g. fuel cell.

The reutilisation of compression energy offers the possibility to increase the overall efficiency of hydrogen driven cars and the former drawback of the physical hydrogen storing technique, its high energy consumption, seems partly compensable with the proposed metal hydride cooling system. The experimental investigations in this work on individual reaction beds show its automotive applicability concerning the volume and weight constraints.

However, the open metal hydride cooling system proposed conceptually within this work should be experimentally realized in order to investigate its application potential.

5 Literature

1. E. Rebhan (Hrsg.): Energiehandbuch – Gewinnung, Wandlung und Nutzung von Energie, Springer, Berlin, Heidelberg, New York, 2002

2. M. Rudolph, U. Wagner: Energieanwendungstechnik – Wege und Techniken zur effizienteren Energienutzung, Springer, Berlin, Heidelberg, 2008

3. P. Heyl und J. Fröhlich: Heizen und Kühlen mit CO_2 Klimaanlagen, in D. Schlenz (Hrsg.): PKW-Klimatisierung II – Klimakonzepte, Regelungsstrategien und Entwicklungsmethoden heute und in Zukunft, expert, Renningen-Malmsheim, 2002

4. Thermally Operated Mobile Air-Conditioning Systems (TOPMACS), European Commission, Brussels, EU-Contract TST4-CT-2005-012471 (Final report under preparation)

5. T. Onoda and T. Gueret: Fuel Efficient Road Vehicle Non-Engine Components – Potential Savings and Policy Recommendations, IEA Information Paper, OECD/IEA, 2007

6. S. Barbusse and L. Gagnepain: Automobile Air-conditioning – Its Energy and environmental Impact – Data and References, Agence de l'Environment et de la Maîtrise de l'Energie (ADEME), 2003

7. M. Wanner: Untersuchung des Langzeitverhaltens der thermodynamischen Stabilität von Metallhydriden, Dissertation, Universität Stuttgart, 2001

8. H. Rau und J. Rau: Chemische Gleichgewichtsthermodynamik, Vieweg, Braunschweig, Wiesbaden, 1995

9. G. Friedlmeier: Charakterisierung von Hochtemperatur-Metallhydriden auf Magnesium-Basis, Dissertation, Universität Stuttgart, 1997

10. J.H.N. van Vucht, F.A. Kuijpers B. Larsen and A.S. Pedersen: Reversible room-temperature absorption of large quantities of hydrogen by intermetallic compounds, Philips Research Reports 25, 133-141 (1970)

11. H.-P. Klein: Betriebsverhalten einer zweistufigen Metallhydrid-Sorptionsanlage zur Kälteerzeugung, Dissertation, Universität Stuttgart, 2007

12. M. Ron: The normalized pressure dependence method for the evaluation of kinetic rates of metal hydride formation/decomposition, J. Alloy Compd. 283, 178-191 (1999)

13. H. Buchner: Energiespeicherung in Metallhydriden, Springer, Wien, New York, 1982

14. A. Züttel: Metallhydride – Einführung, Vorlesungsmanuskript, Physik Department, Universität Fribourg, Schweiz, 2001

15. G. Friedlmeier, M. Schaaf and M. Groll: How to measure pressure-concentration-isotherms representative for technical applications, Z. Phys. Chem. 183, 185-195 (1994)

16. E.A. Kumar, M. Prakash Maiya and S. Srinivasa Murthy: Influence of transient operating conditions on pressure-concentration-isotherms and storage characteristics of hydriding alloys, Int. J. Hydrogen Energy 32, 2382-2389 (2007)

17. F. Laurencelle and J. Goyette: Simulation of heat transfer in a metal hydride reactor with aluminum foam, Int. J. Hydrogen Energy 32, 2957-2964 (2007)

18. M. Gambini, M. Manno and M. Vellini: Numerical analysis and performance assessment of metal hydride-based hydrogen storage systems, Int. J. Hydrogen Energy 33, 6178-6187 (2008)

19. G. Blumenthal, D. Linke und S. Vieth: Chemie – Grundwissen für Ingenieure, Teubner, Wiesbaden, 2006

20. C. Gommel: Messungen zur Kinetik der Wasserstoffaufnahme von $LaNi_{4.7}Al_{0.3}$ und Mg(Ni) und Modellrechnungen zu Reaktionskinetik von Hydridspeichermaterialien, Diplomarbeit, IKE, Universität Stuttgart, 1993

21. C. Borkhart: Experimente und Modellrechnung zur physikalischen Reaktionskinetik der Wasserstoffdesorption von Metallhydriden, Diplomarbeit, IKE, Universität Stuttgart, 1994

22. C.S. Wang, X.H. Wang, Y.Q. Lei, C.P. Chen and Q.D. Wang: The hydriding kinetics of $MlNi_5$ - I. Development of the model, Int. J. Hydrogen Energy 21, 471-478 (1996)

23. X.H. Wang, C.S. Wang, C.P. Chen, Y.Q. Lei and Q.D. Wang: The hydriding kinetics of $MlNi_5$-II. Experimental results, Int. J. Hydrogen Energy 21, 479-484 (1996)

24. U. Mayer, M. Groll and W. Supper: Heat and mass transfer in metal hydride reaction beds: Experimental and theoretical results, J. Less-Common Met. 131, 235-244 (1987)

25. F. Yang, X. Meng, J. Deng, Y. Wang and Z. Zhang: Identifying heat and mass transfer characteristics of metal hydride reactor during absorption – Parameter analysis and numerical study, Int. J. Hydrogen Energy 33, 1014-1022 (2008)

26. A. Jemni and S. Ben Nasrallah: Study of two-dimensional heat and mass transfer during absorption in a metal-hydrogen reactor, Int. J. Hydrogen Energy 20, 43-52 (1995)

27. M. Groll: Solid sorption machines for CFC-free generation of heat and cold (an overview), 1st ISHMT-ASME Heat and Mass Transfer Conf., January 5-7, Bombay, 1994

28. A. Isselhorst: Heat and mass transfer in coupled hydride reaction beds, J. Alloy Compd. 231, 871-879 (1995)

29. G. Mohan, M. Prakash Maiya and S. Srinivasa Murthy: Performance simulation of metal hydride hydrogen storage device with embedded filters and heat exchanger tubes, Int. J. Hydrogen Energy 32, 4978-4987 (2007)

30. M.D. Mat and Y. Kaplan: Numerical study of hydrogen absorption in an Lm-Ni_5 hydride reactor, Int. J. Hydrogen Energy 26, 957-963 (2001)

31. Z. Dehouche, W. de Jong, E. Willers, A. Isselhorst and M. Groll: Modelling and Simulation of Heating/Air Conditioning Systems using the Multi-Hydride-Thermal-Wave concept, Applied Thermal Engineering 18, 457-480 (1998)

32. M. Ram Gopal and S. Srinivasa Murthy: Prediction of Metal Hydride Heat Transformer Performance Based on Heat Transfer and Reaction Kinetics, Ind. Eng. Chem. Res. 34, 2305-2313 (1995)

33. E. Hahne and J. Kallweit: Thermal conductivity of metal hydride materials for storage of hydrogen: experimental investigation, Int. J. Hydrogen Energy, 107-114 (1998)

34. Y. Asakuma, S. Miyauchi, T. Yamamoto, H. Aoki and T. Miura: Homogenization method for effective thermal conductivity of metal hydride bed, Int. J. Hydrogen Energy 29, 209-216 (2004)

35. D.-W. Sun and S.-J. Deng: Theoretical descriptions and experimental measurements on the effective thermal conductivity in metal hydride powder beds, J. Less-common met. 160, 387-395 (1990)

36. D.-W. Sun and S.-J. Deng: A theoretical model predicting the effective thermal conductivity in powdered metal hydride beds, Int. J. Hydrogen Energy 14, 331-336 (1990)

37. J. Kapischke and J. Hapke: Measurement of the effective thermal conductivity of a metal hydride bed with chemical reaction, Exp. Them. Fluid Sci 9, 337-344 (1994)

38. J. Kapischke and J. Hapke: Measurement of the effective thermal conductivity of a Mg-MgH_2 packed bed with oscillating heating, Exp. Them. Fluid Sci 17, 347-355 (1998)

39. M. Groll: Reaction beds for dry sorption machines, Heat Recovery Systems and CHP 13, 341-346 (1993)

40. R. Werner: Experimentelle Untersuchung eines zweistufigen Metallhydrid-Wärmetransformators, Fortschritt-Berichte VDI, Reihe 19, Nr. 37, VDI, Düsseldorf, 1993

41. E. Willers: Multi-Hydrid-Sorptionsanlage zur kombinierten Heizung und Kühlung, Dissertation, Universität Stuttgart, 2002

42. R. Werner and M. Groll: Two-stage metal hydride heat transformer laboratory model: results of reaction bed tests, J. Less-Common Met. 172-174, 1122-1129 (1991)

43. M. Groll, W. Supper, U. Mayer and O. Brost: Heat and mass transfer limitations in metal hydride reaction beds, Int. J. Hydrogen Energy 12, 89-97 (1987)

44. A. Isselhorst and M. Groll: Two-stage metal hydride heat transformer laboratory model, J. Alloy. Compd. 231, 888-894 (1995)

45. M. Nagel: Untersuchung des Betriebsverhaltens einer periodisch mit Metallhydriden arbeitenden Kältemaschine, VDI Fortschritt-Berichte, Reihe 19, Nr. 37, VDI, Düsseldorf, 1989

46. S.-G. Lee, Y.-K. Kim and J.-Y. Lee: Operating Characteristics of metal hydride heat pump using Zr-based Laves phases, Int. J. Hydrogen Energy 20, 77-85 (1995)

47. A. Isselhorst: Dynamik gekoppelter Metallhydrid-Reaktionsbetten, Dissertation, Universität Stuttgart, 1993

48. M. Groll and H.-P. Klein: Metal hydride technology with special emphasis on thermodynamic machines, 16th National Heat and Mass Transfer Conf. / 5th ISHMT-ASME Heat and Mass Transfer Conf., January 1-5, Kalkutta, 2002

49. M. Groll, A. Isselhorst and M. Wierse: Metal hydride devices for environmentally clean energy technology, Int. J. Hydrogen Energy 19, 507-515 (1994)

50. A. R. Sanchez, H.-P. Klein and M. Groll: Expanded graphite as heat transfer matrix in metal hydride beds, Int. J. Hydrogen Energy 28, 515-527 (2003)

51. D. Bielz: Zyklustests und Analyse von Sorptionsreaktoren mit Graphitmatrix-Metallhydridpellets, Diplomarbeit, IKE, Universität Stuttgart, 1999

52. H.-P. Klein and M. Groll: Heat transfer characteristics of expanded graphite matrices in metal hydride beds, Int. J. Hydrogen Energy 29, 1503-1511 (2004)

53. K.J. Kim, B .Montoya, A. Razani and K.-H. Lee: Metal hydride compacts of improved thermal conductivity, Int. J. Hydrogen Energy 26, 609-613 (2001)

54. K.J. Kim K.T. Feldman Jr., G. Lloyd, A. Razani and K.L. Shanahan: Performance of high power metal hydride reactors, Int. J. Hydrogen Energy 23, 355-362 (1998)

55. K.J. Kim, G.M. Lloyd, K.T. Feldman Jr. and A. Razani: Thermal analysis of the $Ca_{0.4}Mm_{0.6}Ni_5$ metal-hydride reactor, Applied Thermal Engineering 18, 1325-1336 (1998)

56. M. Ram Gopal and S. Srinivasa Murthy: Experiments on a metal hydride cooling system working with ZrMnFe/$MmNi_{4.5}Al_{0.5}$ pair, Int. J. Refrigeration 22, 137-149 (1999)

57. F. Qin, J. Chen, M. Lu, Z. Chen, Y. Zhou and K. Yang: Development of a metal hydride refrigeration system as an exhaust gas-driven automobile air conditioner, Renew Energy 32, 2034-2052 (2007)

58. J. Ni and H. Liu, Experimental research on refrigeration characteristics of a metal hydride heat pump in auto air-conditioning, Int. J. Hydrogen Energy 32, 2567-2572 (2007)

59. B.H. Kang, C.W. Park and C.S. Lee: Dynamic behavior of heat and hydrogen transfer in a metal hydride cooling system, Int. J. Hydrogen Energy 21, 769-774 (1996)

60. S. Mellouli, F. Askri, H. Dhaou, A. Jemni and S.B. Nasrallah: A novel design of a heat exchanger for metal-hydrogen reactor, Int. J. Hydrogen Energy 32, 3501-3507 (2007)

61. E. Willers and M. Groll: Evaluation of metal hydride machines for heat pumping and cooling applications, Int. J. Refrigeration 22, 47-58 (1999)

62. E. Willers: Berechnung des Wärme- und Stofftransports innerhalb einer Metallhydrid-Kältemaschine so wie deren Auslegung als Omnibusklimaanlage, Diplomarbeit, IKE, Universität Stuttgart, 1993

63. T. Imoto, T. Yonesaki, S. Fujitani, I. Yonezu, N. Hiro, K. Nasako and T. Saito: Development of an F-Class refrigeration system using hydrogen-absorbing alloys, Int. J. Hydrogen Energy, 451-455 (1996)

64. E. Willers and M. Groll: The two-stage metal hydride heat transformer, Int. J. Hydrogen Energy 24, 269-276 (1999)

65. E. Willers, M. Wanner and M. Groll: A multi-hydride thermal wave device for simultaneous heating and cooling, J. Alloy Compd. 293-295, 915-918 (1999)

66. A.S. Chernikov, L.A. Izhvanov, A.I. Solovey, V.P. Frolov and Y.I. Shanin: An installation for water cooling based on a metal hydride heat pump, J. Alloy Compd. 330-332, 907-910 (2002)

67. H.-P. Klein and M. Groll: Development of a two-stage metal hydride system as topping cycle in cascading sorption systems for cold generation, Applied Thermal Engineering 22, 631-639 (2002)

68. M. Linder: Charakterisierung von Metallhydriden zur Auslegung einer wärmegetriebenen Sorptionskälteanlage, Diplomarbeit, IKE, Universität Stuttgart, 2006

69. M. Groll and A. Isselhorst: Metal hydride machines for generation of heat and cold, Symposium on Solid Sorption Refrigeration, November 18-20, Paris, 1992

70. H.-P. Klein, E. Willers and M. Groll: Thermally driven high-performance sorption heat pumps, Int. Proc. Symp. on Energy Engineering in the 21st century, January 9-13, Hongkong, 2000

71. H.L. Talom and A. Beyene: Heat recovery from automotive engine, Applied Thermal Engineering 29, 439-444 (2008)

72. Y. Fu: Investigation on hydrogen storage properties of Mg-based nanostructured composites, Dissertation, Universität Stuttgart, 2008

73. R. Noveva: Theoretische und experimentelle Untersuchung moderner Metallhydride zur Wasserstoffspeicherung, Diplomarbeit, IKE, Universität Stuttgart, 2008

74. J. Payá, M. Linder, E. Laurien, J.M. Corberán: Mathematical models for the P-C-T characterization of hydrogen absorbing alloys, J. Alloy Compd. 484, 190-195 (2009)

75. P. Muthukumar, M. Linder, R. Mertz, E. Laurien: Measurement of thermodynamic properties of some hydrogen absorbing alloys, Int. J. Hydrogen Energy 34, 1873-1879 (2009)

76. A. Satheesh, P. Muthukumar, M. Linder, R. Mertz, E. Laurien: Reaction Kinetics Studies on $LmNi_{4.91}Sn_{0.15}$ Hydride, Hydrogen and Hydrogen Storage – Methods and Materials, January 3-6, Bangalore, 2009

77. W. Supper, M. Groll and U. Mayer: Reaction kinetics in metal hydride reaction beds with improved heat and mass transfer, J. Less-Common Met. 104, 279-286 (1984)

78. E. Anil Kumar, M. Prakash Maiya and S. Srinivasa Murthy: Influence of aluminum content on the dynamic characteristics of mischmetal based hydrogen storage alloys, J. Alloys Compd. 470, 157-162 (2009)

79. M. Martin, C. Gommel, C. Borkhart and E. Fromm: Absorption and desorption kinetics of hydrogen storage alloys, J. Alloys Comp. 238, 193-201 (1996)

80. T. Forde, J.P. Maehlen, V.A. Yartys, M.V. Lototsky and H. Uchida: Influence of intrinsic hydrogenation/dehydrogenation kinetics on the dynamic behaviour of metal hydrides: A semi-empirical model and its verification, Int. J. Hydrogen Energy 32, 1041-1049 (2007)

81. F. Cuevas, B. Villeroy, E. Leroy, P. Olier and M. Latroche: Relationship between microstructure and hydrogenation properties of Ti0.85Zr0.15Mn1.5V0.5 alloy, J. Alloys Comp. 446-447, 218-223 (2007)

82. K. Hertwig, L. Martens: Chemische Verfahrenstechnik – Berechnung, Auslegung und Betrieb chemischer Reaktoren, Oldenburg, München, Wien, 2007

83. U. Mayer: Untersuchung des Wärme- und Stofftransports in Metallhydrid-Reaktionsbetten, Dissertation, Universität Stuttgart, 1987

84. T.M. Brown, J. Brouwer, G.S. Samuelsen, F.H. Holcomb and J. King: Accurate simplified dynamic model of a metal hydride tank, Int. J. Hydrogen Energy 33, 5596-5605 (2008)

85. M. Linder, E. Laurien: Thermally driven sorption machine for fast hydrogen exchange, Hydrogen and Hydrogen Storage – Methods and Materials, January 3-6, Bangalore, 2009

86. J. Payá, M. Linder, E. Laurien, J.M. Corberán: Dynamic model and experimental results of a thermally driven metal hydride cooling system, Int. J. Hydrogen Energy 34, 3173-3184 (2009)

87. J.O. Jensen, A.P. Vestbo, Q. Li and N.J. Bjerrum: The energy efficiency of onboard hydrogen storage, J. Alloys Comp. 446-447, 723-728 (2007)

Appendix - Uncertainty analysis

Directly measured data

The error margins of directly measured data (e.g. temperature, flow rate or pressure) as well as descriptions of the respective measurement test benches and procedures can be found in chapter 2.1.

Time dependency of measured data

The measurement interval was set to 2 s for all experiments, which is sufficient for the respective measurement sensors. However, the measurement delay time during the kinetics measurements is due to fast pressure equalisations (e. g. due to opening of hydrogen valve, compare kinetics measurements in chapter 3.1.2) and cannot be avoided with the available set-ups. Therefore, only data measured after this time span have been used in the respective diagrams.

Calculated data – Storage capacity

The storage capacity was measured on two different test benches: The PCI test bench and the test bench for individual reaction bed measurements. Additionally, two different measurement procedures have been performed: The PCI and the kinetics measurement.

The set-up for PCI and kinetics measurements was already available at IKE. Several authors give detailed descriptions of the hydrogen uptake calculation procedure as well as the achievable accuracies of this type of measurement system [7, 9, 15 and 72]. However, as the accuracy of the system depends on measurement conditions like sample mass and absolute hydrogen pressure, the uncertainties can be given for 'typical measurement conditions', only. In this work, the PCI measurement of both alloys can be seen as reference, as the measurement conditions correspond to the 'typical measurement conditions' described by Friedlmeier [9]. The uncertainties of the measured storage capacities are therefore less than ± 5 % of the maximum hydrogen uptake.

In Table A-1, the results of the measured storage capacity (for the three measurement procedures) as well as the deviation from the PCI measurement (in brackets) are given. Due to the high pressure and the small sample mass of the intrinsic kinetics measurement, the maximum difference occurs for $Ti_{0.99}Zr_{0.01}V_{0.43}Fe_{0.09}Cr_{0.05}Mn_{1.5}$ with around 11 %.

Table A-1: Comparison of different storage capacity measurements

Metal hydride	PCI measurement (reference)	Intrinsic kinetics measurement	Reaction bed dynamics m.
$LmNi_{4.91}Sn_{0.15}$ (27 °C, 11 bar)	1.29 ± 0.06	1.28 (< 1 %)	1.24 (< 4 %)
$Ti_{0.99}Zr_{0.01}V_{0.43}Fe_{0.09}Cr_{0.05}Mn_{1.5}$ (20 °C, 47 bar)	1.67 ± 0.08	1.48 (~ 11 %)	1.61 (< 4 %)

Calculated data – cooling power

The cooling power is calculated by a caloric measurement set-up consisting of a flow meter and one resistance thermometer at the in- and outlet of the reaction bed, respectively. Therefore, the uncertainty of this measurement depends on the uncertainty of the flow meter, the uncertainty of the temperature difference measurement and the uncertainty of the water properties (specific heat and density).

Test bench for individual reaction bed measurements

The water temperature during all measurements was between 5 °C and 45 °C. Within this range, the deviations of the water properties (ρ = 998.3 kg/m^3, c_p = 4.183 kJ/(kgK) for 20 °C) are less than 1 %. The deviation of the water flow rate is ± 2.5 % F.S. (corresponding to ± 0.31 l/min). Additionally, the maximum difference between the two temperature sensors (inlet and outlet) has been determined to ± 0.1 K. For a water flow rate of 3.5 l/min and a representative thermal power of 800 W, the error margin is ± 40 W (or around ± 5 %).

Test bench for coupled reaction beds

The water temperature during all measurements was between 5 °C and 45 °C (reaction bed A). The deviation of the water flow rate is ± 0.3 % F.S. (corresponding to ± 0.045 l/min) and the maximum difference between the two temperature sensors (inlet and outlet) has been determined to 0.2 K. The

deviation of the water properties is identical to the test bench for individual reaction bed experiments. For a water flow rate of 4 l/min and a representative cooling power of 640 W, the error margin is ± 26 W (or around ± 4 %).

The test bench for coupled reaction beds was additionally equipped with a mass flow meter for hydrogen between the two reaction beds. Therefore an additional independent measurement principle is available for comparison (determination of systematic errors). As the reaction enthalpy of the metal hydride can be deduced from PCI measurements, the hydrogen flow rate corresponds to a thermal power generation P_{H2} (or demand). In Figure A-1, the comparison of both measurement principles ($P_{caloric}$ and P_{H2}) is shown. The measurement was performed for given temperatures in order to avoid the influence of thermal masses. Neglecting the small time shift, the thermal energy (based on the water side) as well as the chemical energy (based on the hydrogen flow rate) are concurrent for both reaction beds. The hydrogen power value is slightly lower than the respective measured thermal power, as the hydrogen exchange peak at the beginning is compensated during the complete reaction.

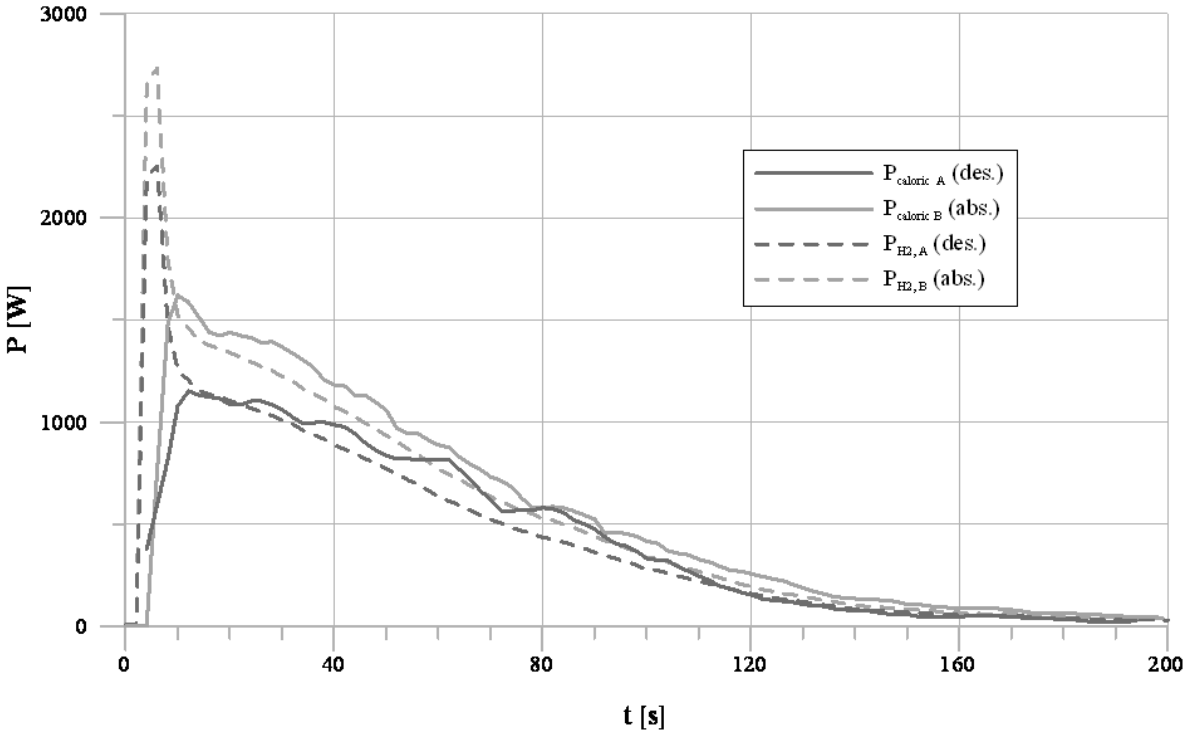

Figure A-1: Comparison of thermal power measurement between two measurement paths